CFD Modeling of Hot Spot Identification and Mitigation in a PEM Fuel Cell

Submitted in partial fulfilment of the requirements for the award of the degree of

DOCTOR OF PHILOSOPHY

IN

CHEMICAL ENGINEERING

By

RAMAKANT GADHEWAL

(Roll No. 716165)

Under the supervision of

Dr. Venu Vinod Ananthula

Dr. Venkata Suresh Patnaikuni

DEPARTMENT OF CHEMICAL ENGINEERING
NATIONAL INSTITUTE OF TECHNOLOGY WARANGAL
WARANGAL – 506004, TELANGANA INDIA.

JULY 2022

APPROVAL SHEET

This thesis work entitled **"CFD Modeling of Hot Spot Identification and Mitigation in a PEM Fuel Cell"** by **Mr. Ramakant Gadhewal** is approved for the degree of Doctor of Philosophy.

Examiners

Supervisor

Prof. VENU VINOD ANANTHULA

Co-supervisor

Prof. VENKATA SURESH PATNAIKUNI

Chairman (Program Coordinator)

Prof. SRINATH SURANANI

Date: _____ Place:

DECLARATION

This is to certify that the work presented in the thesis entitled **"CFD Modeling of Hot Spot Identification and Mitigation in a PEM Fuel Cell"** is a bonafide work done by me under the supervision of Prof. Venu Vinod Ananthula, Prof. Venkata Suresh Patnaikuni and was not submitted elsewhere for the award of any degree.

I declare that this written submission represents my ideas in my own words and where others' ideas or words have been included; I have adequately cited and referenced the original sources. I also declare that I have adhered to all principles of academic honesty and integrity and have not misrepresented or fabricated or falsified any idea/data/fact/source in my submission. I understand that any violation of the above will be a cause for disciplinary action by the Institute and can also evoke penal action from the sources which have thus not been properly cited or from whom proper permission has not been taken when needed.

RAMAKANT GADHEWAL

Roll No.716165

Date: 21-07-2022

NATIONAL INSTITUTE OF TECHNOLOGY WARANGAL
WARANGAL – 506004, TELANGANA INDIA.

CERTIFICATE

This is to certify that the thesis entitled **"CFD Modeling of Hot Spot Identification and Mitigation in a PEM Fuel Cell"** is being submitted by **Mr. RAMAKANT GADHEWAL (Roll No. 716165)** for the award of the degree of **Doctor of Philosophy (Ph.D.)** in **Chemical Engineering** to the National Institute of Technology, Warangal, India is a record of the bonafide research work carried out by him under my supervision. The thesis has fulfilled the requirements according to the regulations of this Institute and, in my opinion, has reached the standard for the submission. The results embodied in the thesis have not been submitted to any other University or Institute for the award of any degree or diploma.

Prof. Venu Vinod Ananthula
Professor
Supervisor
Department of Chemical Engineering
National Institute of Technology
Warangal 506004, Telangana State, India

Prof. Venkata Suresh Patnaikuni
Professor
Co-Supervisor
Department of Chemical Engineering
National Institute of Technology
Warangal 506004, Telangana State, India

Acknowledgements

I take this opportunity to express my sincere gratitude to my respected supervisors, ***Prof. Venu Vinod Ananthula*** and ***Prof. Venkata Suresh Patnaikuni***, Department of Chemical Engineering, National Institute of Technology, Warangal, India, for giving me an opportunity to pursue doctoral thesis work under his esteemed supervision. His outstanding guidance, constant support, patience, motivation, and immense knowledge significantly helped me in all the time of research and writing of this thesis. I could not have imagined having a better advisor and mentor for my Ph.D. study.

I am grateful to ***Prof. N.V. Ramana Rao***, Director, NIT Warangal, for providing me institute fellowship for completing the Ph.D. I am thankful to ***Dr. Srinath Suranani***, Head of the Department of Chemical Engineering, for providing the necessary facilities in the department and for his valuable suggestions. I am also grateful to earlier HODs, ***Prof. Shirish H Sonawane***, ***Prof. A.Sarat Babu***, and ***Prof. K. Anand Kishor.***

I would like to express my sincere gratitude to all my Doctoral Scrutiny Committee members ***Dr. S. Vidyasagar, Dr. G.Uday Bhaskar Babu***, Department of Chemical Engineering and ***Dr. G. Naga Srinivasulu,*** Department of Mechanical Engineering, for their valuable time, patience, attention, insightful comments and helpful pieces of advice during the review presentation of this research work.

I would like to express heartfelt thanks to ***Dr. T. Sunil Kumar***, Associate Professor, Department of Chemical Engineering, **Indian Institute of Technology**, Tirupati, for his guidance, support, and encouragement.

I wish to express my profound thanks to the entire Faculty, scholars, Non-teaching staff, and all others in the chemical Engineering Department and in the Institute who directly and indirectly helped me during my research work at NIT Warangal.

I wish to express sincere thanks to my beloved friend and lab mates, ***Mr. Rahul Gaikwad***, and ***Mr. Shailesh Singh Shikarwar,*** for their constant encouragement and help acquired during my research period at NIT Warangal.

My sincere thanks to my fellow scholars, ***Dr. Sheik Abdul Gaffer,*** and ***Snigdha saha*** for their timely help and support in completing my research work.

I would like to express my profound to my family members: my wife, ***Mrs. Navratan,*** and my son, ***Moksh***, my mother, ***Mrs. Krishna,*** and other members of my family for their support and continuous encouragement throughout my years of study and through the process of researching and writing this thesis.

Also, I take this opportunity to thank all my relatives, friends, teachers, and well-wishers who are part of this journey directly and indirectly. Thank You.

Ramakant Gadhewal

ABSTRACT

Hot spot formation is one of the most critical factors contributing to the membrane layer deterioration and, hence, fuel cell performance degradation. When local hot spot patches develop, the long-term endurance of a Proton Exchange Membrane Fuel Cell (PEMFC) catalyst and membrane layer is dramatically reduced. In this work, a simulation study is carried out on a 3D geometry of the cathode side of a single-cell, PEM fuel cell since the cathode reaction is the limiting step. The oxygen and nitrogen mass fraction in the inlet feed on the cathode side are varied as well as the total feed flow rate consisting of traces of water vapor. The worst-case scenario of no-cooling i.e., with an insulated bipolar plate is assumed to test the maximum thermal effect on the membrane. The flow, heat, and mass transfer multiphysics phenomena in the gas diffusion layer and catalyst scaffold layer were simulated using a simplified geometry in COMSOL Multiphysics software. The electrochemical reaction of oxygen reacting with hydrogen is considered instantaneous reaction at the catalyst surface. It is optimized for the purpose of determining the optimum oxygen mass fraction in feed and net feed flow rate that gives long life thermally and low operating cost of a PEMFC.

In this numerical study, it has been shown that a hot spot would be formed close to the entrance of the PEM fuel cell cathode side near the membrane layer. COMSOL Multiphysics was used to conduct time-dependent simulations on a 2D model of the cathode portion of the PEM fuel cell. The start-up dynamics show that hot spot build-up and its extent are time taking processes. Two strategies are proposed to mitigate hot spots - first, introducing bumps in the reactive gas flow channel and, secondly, supplying a higher fraction of nitrogen relative to oxygen on the cathode side of the straight flow channels. Parametric studies on both techniques were conducted by varying the size of the bump, the amplitude of the cyclic nitrogen gas composition, and the Pt catalyst fractional coverage. Both strategies significantly decrease hot spot temperature, which affects the membrane layer endurance. Finally, an approach that combines the two proposed techniques is also analysed.

The thermal model has been further extended to cathode side with more rigorous 3-D reconstructed porous gas diffusion layer for better prediction of hot spot temperatures. The effect of different geometric shapes of the flow channel on the hot spot mitigation is also studied

by considering bumped, diverging, converging, wavy, variable wave-A and variable wave-B type channels. Among the different shapes of the channels considered, diverging channel has been found to be effective with respect to mitigation of hot spots by reducing the maximum temperature as well as pressure drop offered. The effect of oscillatory flow inlet of nitrogen and oxygen at the inlet on the mitigation of hot spot temperature is also studied on the conventional flow channel along with the above-mentioned shapes of the flow channels. The oscillatory nitrogen gas supply strategy significantly reduces the local hot spot temperature in different flow channel designs.

This study establishes the importance of hot spot identification and its mitigation for extending the durability of the membrane and membrane electrode assembly of the PEM fuel cell.

Table of Contents

Page No

List of Figures

List of Tables

Nomenclature

C_P	Species molar heat capacity (J $mol^{-1}K^{-1}$)
D_i^F	Mass diffusion coefficient for species i (m^2s^{-1})
D_i^T	Thermal diffusion coefficient (m^2s^{-1})
$D_{O_2}^F$	Fick's diffusivity of oxygen gas (m^2s^{-1})
$D_{N_2}^F$	Fick's diffusivity of nitrogen gas (m^2s^{-1})
$D_{H_2o}^F$	Fick's diffusivity of water vapor (m^2s^{-1})
ΔH_R	Heat of the reaction of water vapor formation (J mol^{-1})
I	Identity matrix (Dimensionless)
j_i	Mass flux of each species (kg $m^{-2}s^{-1}$)
j_{O2}	Oxygen mass flux (kg m^{-2} s^{-1})
k	Thermal conductivity (W $m^{-1}K^{-1}$)
M_n	Average molecular weight (kg $kmol^{-1}$)
M_i	Molecular weight of each species (kg $kmol^{-1}$)
$M_{w,i}$	Molecular weight of each species (kg $kmol^{-1}$)
N_i	Total flux of species 'i' (mol $m^{-2}s^{-1}$)
P	Pressure field (Pa)
q_w	Heat source at catalyst wall surface (W m^{-2})
R	Universal gas constant (J $kmol^{-1}K^{-1}$)
R_i	Reaction rate of each species in bulk (kg $m^{-3}s^{-1}$)
T	Operating temperature (K)
u	Velocity vector field (m s^{-1})
ω_i	Mass fraction of the i^{th} component
x_i	Mass fraction of species i
y_i	Mole fraction of species i

Greek & Other Symbols

δ	Amplitude of cyclic supply of the oxygen and nitrogen
ε	Fractional coverage of the platinum catalyst
∇	Gradient or divergence operator (m^{-1})

μ Dynamic viscosity (Pa. s)

ρ Gas mixture density (kg m^{-3})

Abbreviations

AFC Alkaline Fuel Cell

CFD Computational fluid dynamics

CL Catalyst layer

DMFC Direct Methanol Fuel Cell

FEM Finite volume methods

F Faraday constant, C/kmol

GDL Gas diffusion layer

LBM Lattice Boltzmann method

MCFC Molten Carbonate Fuel Cell

MEA Membrane electrode assembly

MW Molecular weight

PAFC Phosphoric acid fuel cells

PEM Polymer electrolyte membrane

SOFC Solid Oxide Fuel Cell

T Operating Temperature, K

Chapter 1

Introduction

Chapter-1

Introduction

According to projections, the planet's population is expected to expand by 2 billion in the next 30 years, from 7.7 billion today to 9.7 billion around the year 2050. By 2027, India will be expected to exceed China's population, making it the most populated nation on the planet [1]. Because of its population expansion and economic development, it is expected that India's share of the world's primary energy consumption will almost double by 2040 compared to current levels. India's net CO_2 emissions are expected to more than double by 2040 to 5 GT, increasing its proportion of global CO_2 emissions from 7 % in 2019 to 14 % in 2040 and becoming India the world's second-biggest source of CO_2 emissions by 2040 [2]. In 2021, global CO_2 emissions will increase by roughly 5%, nearing the 2018-2019 high. Carbon dioxide emissions surged by 60% in slightly over two generations, from 22.70 billion metric tons in 1990 to 36.44 billion metric tons in 2021. Carbon dioxide is a major contributor to global climate change and is a significant source of greenhouse gas emissions. The rise in CO_2 emissions and other greenhouse gases during the industrial revolution raised the global mean temperature by around 0.8 °C compared to pre-industrial levels [3].

Many countries have enacted strict emission caps and carbon-neutral targets on their way to combating global warming and depleting the world's fossil fuel supply. In the battle against climate change, some scientists believe hydrogen-powered fuel cells might be an alternative to fossil fuels. According to fuel cell technology experts, the high-power density, high energy conversion efficiency, and low operating temperature of Proton Exchange Membrane Fuel Cells (PEMFCs) make PEMFCs one of today's most appealing technologies. These fuel cells may also be used as a stationary power source [4].

1.1 Fuel cell

By definition, a fuel cell is an electrochemical device that can convert the chemical energy of the fuels (i.e., hydrogen and oxygen) into electrical energy. It is employed in the generation of electrical energy. The process is very efficient, with some occurrences attaining thermodynamic efficiencies of more than 80% in certain circumstances [5]. Using waste heat to increase overall

efficiency can be very beneficial. In a PEM fuel cell, oxygen acts as an oxidant on the cathode, while hydrogen is fuel at the anode. The reactant gases are fed into various compartments separated by a solid electrolyte, a polymer membrane. The compartments may include catalyst material on electrodes connected to an external circuit that will, for example, contain an electric motor, bulb etc. The hydrogen supplied decomposes into hydrogen ions (protons) and electrons (Oxidation reaction, Eq. 1.1) at the anode and the oxygen combines with the protons and the electrons to form water at the cathode (reduction reaction, Eq. 1.2). The polymer membrane can conduct protons, but it is impervious to the reactant gases. These two half-cell reactions occur due to the separation, which prevents the reactants from reacting with regular combustion. When electrons are transferred from the internal circuit to the external circuit, a current is generated that can be used to power the device. Protons (hydrogen ions) must be transferred across the membrane to complete the process. Figure 1.1 illustrates the flow of work through the whole process.

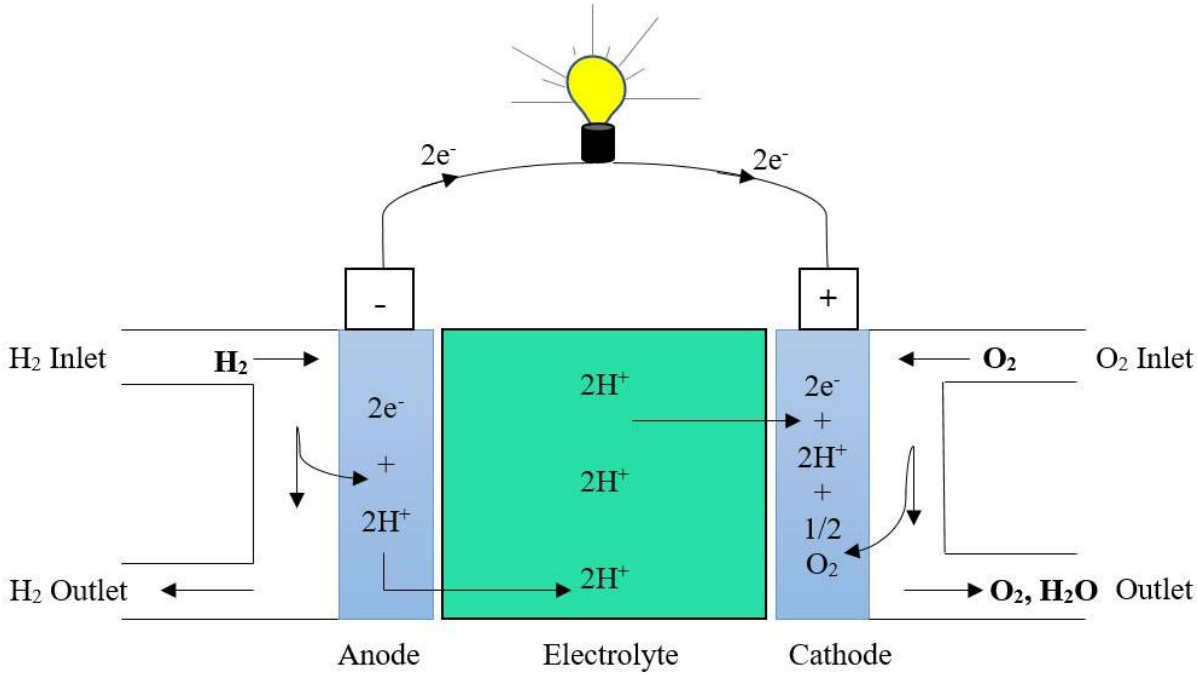

Figure 1.1 Schematic of PEM fuel cell.

The electrochemical reactions that occur in a typical PEM fuel cell are:

Anode side half-reaction

$$H_2(g) \longrightarrow 2H^+(aq) + 2e^- \qquad E_o = 0\ V \qquad [1.1]$$

Cathode side half-reaction

$$\frac{1}{2}O_2(g)+2H^+(aq)+2e^- \longrightarrow O_2 \qquad E_0=1.229\ V \qquad [1.2]$$

Overall electrochemical reaction:

$$H_2(g)+\frac{1}{2}O_2(g)\longrightarrow H_2O(liq)+Electricity+Heat \qquad E_0=1.229\ V \qquad [1.3]$$

1.2 Types of fuel cells

Table 1.1 presents the six primary types of fuel cells. They operate at various temperatures, have varying tolerances for contaminants in the fuel, and have distinct performance characteristics. The fuel cells are named after the respective electrolytes, including alkaline, polymer, phosphoric acid, molten carbonate and solid oxide. Furthermore, direct fuel cells, which electrochemically transform (liquid) fuels such as methanol, ethanol, or hydrazine at the anode, are termed after the fuel; for example, direct methanol fuel cells or direct hydrazine fuel cells.

Table 1. 1 Different types of fuel cells [6].

Cell types	**AFCs**	**PEMFCs**	**DMFCs**	**PAFCs**	**MCFCs**	**SOFCs**
Common Electrolytes	KOH_{aq}	Cation exchange membrane	Cation exchange membrane	Con. phosphoric acid	Alkaline Metal carbonate	Y-stabilized ZrO_2
Ions in the electrolyte	OH^-	H^+	H^+	H^+	CO_3^{2-}	O^{2-}
Operating Temperature	60 to 80°C	60 to100°C	60 to 100°C	180 to 220°C	600 to 660°C	700 to 1000°C
Fuels	H_2 (CO_2 free)	H_2 (CO<50 ppm)	CH_3OH	H_2 (CO<1%)	H_2, CO, (CH_4)	H_2, CO, (CH_4)
Application fields	Military, Space	Transportation cogeneration, and maritime	Transportation, portable power	Distributed generation	Auxiliary power, naval, Distributed generation, Electric utility,	

1.2.1 Polymer Electrolyte Membrane Fuel Cells (PEMFCs)

The proton exchange membrane fuel cell (also known as polymer electrolyte membrane fuel cell, PEMFC or solid polymer fuel cell, SPFC) is lightweight and compact in addition to having a high-power density. PEM fuel cells comprise three major components: an anode with a negative charge,

a cathode with a positive charge, and a solid electrolyte (i.e., the membrane layer) between the two electrodes. In order for PEM fuel cells to work properly, hydrogen gas must be supplied on the anode side, and oxygen gas must be provided on the cathode side of the fuel cells. Proton ions are transferred from the anode side to the cathode side electrode via the electrolyte membrane, and electrons are transported through an external circuit, which is represented by the charge, resulting in electricity being generated. In fuel cells, a solid membrane is used to separate the fuel and oxidant compartments from one another. This allows for efficient ion transport while also maintaining charge balance in the fuel cell.

These fuel cells operate at temperatures below 100 °C and have a production efficiency of around 50% when employed. They may get a start-up fast due to the low operating temperature. These cells offer a wide range of applications and are used in small and medium-sized automobiles and stationary systems. PEMFCs may generate anything from a few 0.001MW to 10 MW [6].

1.2.2 Alkaline Fuel Cells (AFCs)

An electrolyte is a solution of aqueous alkali potassium hydroxide contained in a matrix. This cell also runs on hydrogen gas and pure oxygen (or oxygen present in air). These fuel cells have an operating temperature range of between 150 to 200 °C. Alkaline fuel cells have a power range of 300 W to 5000 W. Their working temperature is restricted to 80 °C to 90 °C at atmospheric pressure, with a yield of 50% at this temperature. However, when running under pressure and with a highly concentrated electrolyte, this temperature may be raised to 250 °C. The National Aeronautics and Space Administration has implemented alkaline fuel cells (AFCs) on space missions because they can attain a power production efficiency of up to 70% [7].

1.2.3 Phosphoric acid fuel cells (PAFCs)

The ortho-phosphoric acid used as an electrolyte in the PAFCs allows them to operate at temperatures of up to 200 °C, which is very high. Carbon monoxide (CO) poisons the platinum in the catalyst when it is exposed to low temperatures. The temperatures at which they function range from 150 to 300 °C. During the operation, the temperature ranges between 180 °C and 210 °C. If the electrolyte is exposed to low temperatures, it becomes a poor conductor and solidifies at 40 °C. PAFC cell technology is the most advanced in terms of research and commercialization. Indeed, permanent installations with capacities of up to 50 MW have been established. These PAFCs were tested for local municipal power generation on a limited scale and for remote-site power

generation. The phosphoric acid fuel cells (PAFCs) have a power production efficiency of 40% and can produce up to 100 kW of electricity [8].

1.2.4 Molten carbonate fuel cells (MCFCs)

When MCFC cells (such as those used in SOFC cells) operate at a high enough temperature, carbon monoxide (CO) may be used as a fuel. This is one of the cells distinguishing properties. This cell functioning is more complex than the processes used in PEMFCs, AFCs, or PAFCs. Ionic conduction is the passage of carbonate ions from the anode to the cathode via an electrolyte of molten carbonates, which guarantees that carbonate ions migrate from the anode to the cathode. It is important to note that carbon monoxide is a poison for cells that operate at low and medium temperatures. This is a possibility as a consequence of the hydrocarbon reforming procedure [7].

At the anode, it is possible that two electrochemical reactions may occur. The first is the main reaction, which is responsible for converting the energy contained in hydrogen into electrical energy. A second reaction may occur when carbon monoxide (CO) is present in the fuel (as opposed to when pure hydrogen is supplied to a fuel cell), and this second electrochemical reaction is beneficial to the fuel cell since it may create electricity.

Air conditioning, for example, is a common stationary use for MCFCs. In the United States, a 2 MW natural gas mini-plant that has been in operation for over 4,000 hours is an example of what may be achieved from 500 kW to 10 megawatts (MW), electricity is available with an efficiency of 55% [7].

1.2.5 Solid oxide fuel cells (SOFCs)

Solid oxide fuel cells (SOFCs) are used in large, high-capacity power facilities, such as those used in manufacturing in the industrial sector. Solid oxide cells are typically composed of a solid ceramic component that contains solid zirconium oxide and a trace of yttria, which replaces the liquid electrolyte in the system. Solid oxide cells can be used in a variety of applications. These solid oxide fuel cells have an operating temperature of up to 1,000 °C. When cogeneration is used and the output power reaches 100 kW, their efficiency may approach 60 to 85%. The temperature ranges between 800 °C and 1,000 °C during operation. Ionic conductivity is very high in ceramics at this temperature because of its composition. SOFCs are mostly used in stationary applications; however, due to their ability to work on a wide range of fuels, some automotive manufacturers

believe that these fuel cells may be used in automobiles in the future. Solid oxide fuel cells can generate between 1 kW and 10 MW of power. These fuel cells are also impervious to trace amounts of sulphur impurity in the fuel [8].

1.2.6 Direct methanol fuel cells (DMFCs)

Because of the huge potential for small applications of fuel cells, there has been considerable interest in developing a fuel cell that can only operate on methanol. Direct methanol fuel cells (DMFCs) generate electricity using the same polymer membrane as PEM fuel cells to convert methanol into energy.

DMFCs use methanol as their fuel rather than hydrogen as their fuel. Methanol is used as a fuel, and it passes through the anode, where it is broken down into protons, electrons, water, and carbon dioxide. Methanol has many benefits, including that it is readily accessible worldwide and may be quickly converted from hydrocarbon or biomass.

Even though its energy density is just one-fifth that of hydrogen per unit weight, it offers more than four times as much energy per volume as hydrogen in the presence of 250 atm of pressure.

1.3 Components of PEM fuel cells

PEM fuel cells comprise many components built from various materials, all of which work together to generate electricity. PEM fuel cells are used to generate electricity. The membrane electrode assembly (MEA) is the heart of the PEM fuel cells and is composed of a membrane and catalyst layers on either side of the membrane. The cell also contains gas diffusion layers, bipolar plates, current collectors, and endplates on both sides of the MEA.

1.3.1 Polymer Electrode Membrane (PEM)

It is often constructed of a polyperfluoro sulfonic acid with a polytetrafluorethylene (PTFE) backbone, which transmits exclusively positively charged ions and blocks the passage of electrons. Since it creates a potential difference between the anode and the cathode, the PEM is the most important component of the fuel cell. This potential difference works as a driving factor for electrons to flow externally between anode and cathode.

1.3.2 Electrolyte (Membrane) Layers

The electrolyte layer is at the heart of a fuel cell (also known as an electrolytic polymer membrane). Protons are drawn into the membrane, permitting them to move through while retaining their proton state. The electrons travel via the outer circuit to reach the other half of the fuel cell. The hydrogen protons pass through the electrolyte layer and reach the cathode electrode, where they combine with the oxygen and the electrons to form water. Because the membrane is an interlink polymer, it must possess the following characteristics: it must be a strong ionic conductor and acts as an electronic insulator. It must be impermeable to gas, and it must be mechanically and chemically stable [6].

1.3.3 Catalytic Layers (CLs)

The anode and cathode half-cell reactions in the fuel cell take place at the catalyst layers (CLs), of the anode and the cathode electrodes. The hydrogen is split into electrons and protons at the anode side electrode. Hydrogen ions, electrons and oxygen recombine at the cathode, resulting in the formation of liquid water. It is necessary to use a catalyst if the working temperature is kept low (frequently T<100 °C) since the electrochemical reactions are sluggish at low temperatures. Despite other available alternatives, platinum is still the most frequently used catalyst on both anode and cathode electrodes in PEMFCs.

1.3.4 Gas Diffusion Layers (GDLs)

GDLs are fibrous porous media that serve two primary purposes: ensure a uniform distribution of reactive gasses on the electrode surfaces and transport electrons to and from the outer electrical circuit. The GDLs contain a fibrous porous structure made of thin carbon fibers and are generally made hydrophobic by suitable coating with PTFE. The width of these fibers is within 250 to 400 microns and the size of the aperture or holes is between 4 and 50 microns. Another important function of the gas diffusion layers is facilitating the evacuation of any water molecules from the catalyst layer to the channel, which would otherwise restrict the electrochemical reaction from happening [7].

1.3.5 Bipolar plates (BPs)

Bipolar plates, constructed of graphite or metal, assign the fuel and oxidant to the fuel cell cells equally. They also conduct the electrons between the GDLs and current collectors. When it comes to single-cell fuel cells, there is no bipolar plate; instead, there is a single-sided plate that allows electrons to pass through the cell. In fuel cells with more than one cell, there is at least one bipolar

plate (in which flow control patterns are present on both sides of the plate) to regulate fuel/oxidant flow. When used in fuel cells, bipolar plates perform various tasks such as distributing fuel and oxidant inside each cell; isolating and separating cells; collecting the electric current generated; evacuating the water from each cell; humidifying the gasses, and chilling each cell individually. Bipolar plates also contain channels that enable reactants (fuel and oxidant) to flow through either side of the plate. They are located on opposing sides of the bipolar plate, forming the anode and cathode compartments. The reactive gas flow channels may be designed in various ways; they can be straightforward, serpentine, parallel, comb-like, or equally distributed, as shown in Figure 1.2.

1.3.6 Gaskets

The addition of gaskets to the edge of the MEAs in a fuel cell to avoid leakage of gases is necessary when MEAs are sandwiched between two bipolar plates. These gaskets are typically composed of rubbery polymers that are flexible.

1.3.7 Current collectors (CCs)

Copper is widely utilized in current collectors because of its superior electron conductivity. Electrons generated on the anode travel via the catalyst layer, GDL and bipolar plates before arriving at the current collectors. On the other hand, electrons go from the current collectors to the catalyst layer through the cathode's bipolar plates and GDL. Externally attached current collectors on the anode and cathode sides complete the circuit and help with the flow of electrons from the anode to the cathode.

1.3.8 End Plates

End plates, which are located at the back end of both the anode and cathode sides, help to keep all of the fuel cell components in place. Because of its excellent heat conductivity, aluminium is frequently used to construct these plates. These plates aid in dissipating waste heat generated during fuel cell operation to the environment.

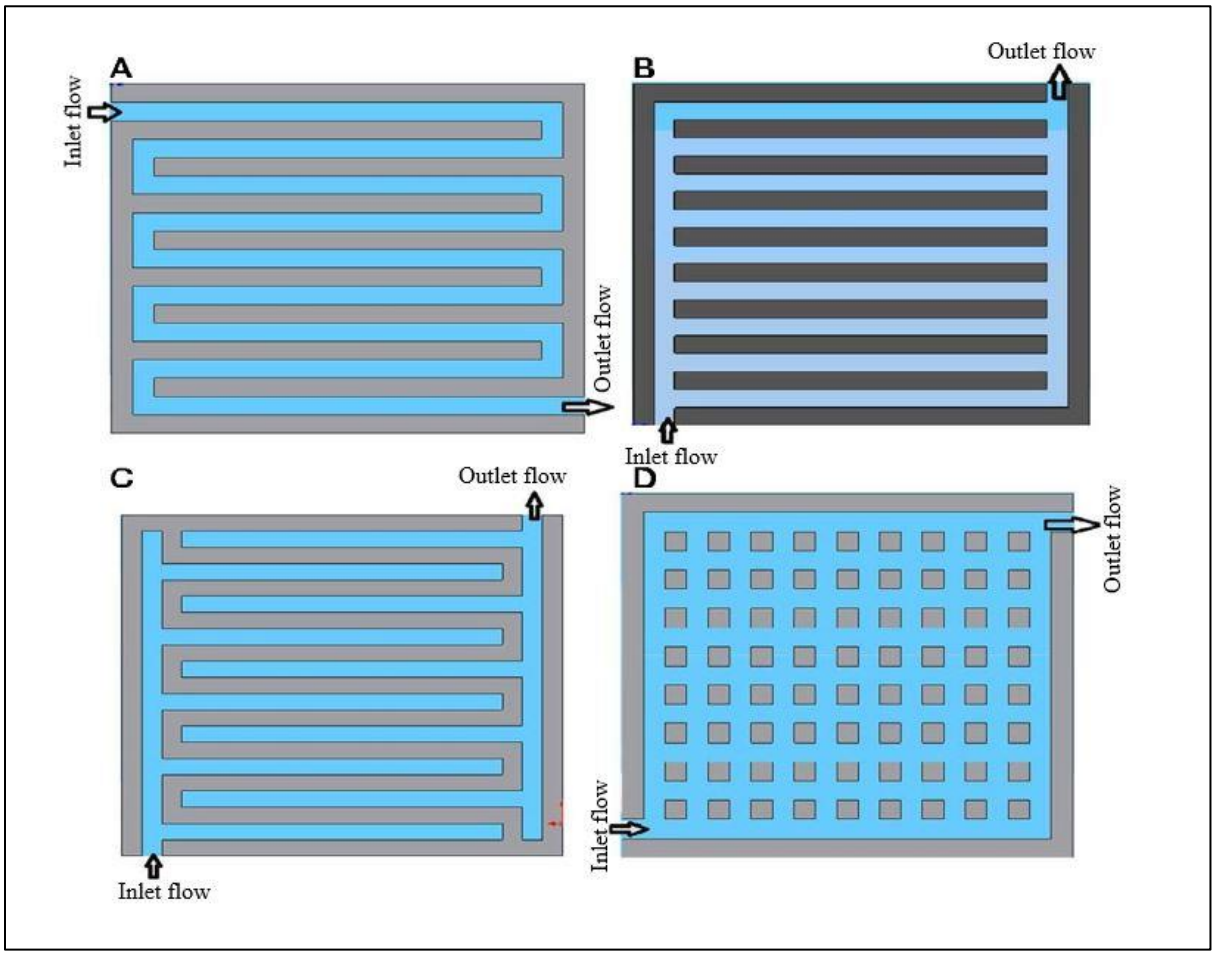

Figure 1. 2 Standard bipolar plate designs [9] (a) Serpentine; (b) Parallel; (c) Interdigitated; (d) Pin

1.4 Performance of PEM fuel cells (Polarization losses and IV curve)

Operating factors such as applied load, temperature and reactant flow rates affect a single fuel cell output voltage. The polarization curve, which depicts the behavior of voltage versus current density, is the standard criterion for fuel cell performance. Even though the theoretical potential of a single PEM fuel cell is 1.229 V, the open-circuit voltage (OCV) dips to a lower value during the actual fuel cell operation owing to thermodynamic limitations. The deviation from this reference condition is because of the unavoidable "losses". The polarization curve depicts the decrease in output voltage with current density. Polarization curves are commonly acquired using a galvanostatic / potentiostat, which pulls the current while measuring the cell output voltage. Figure 1.3 depicts a typical polarization curve.

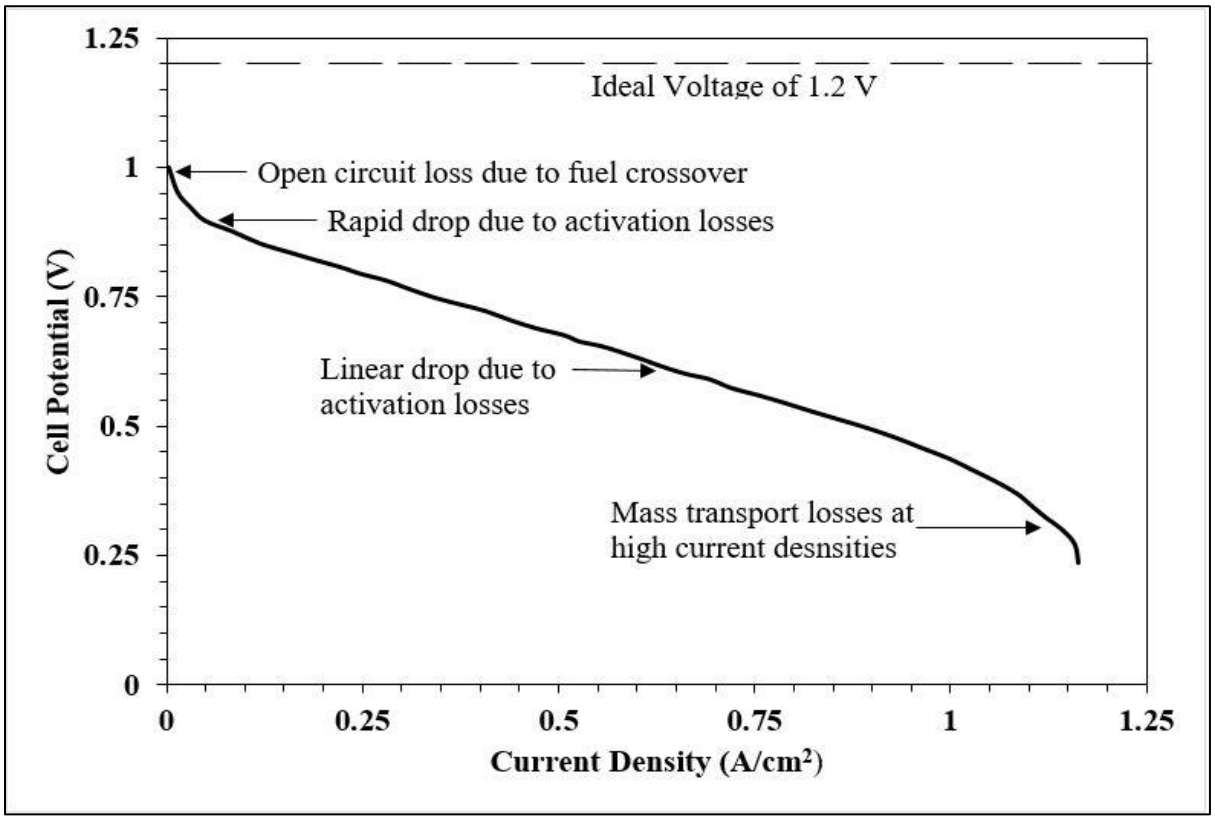

Figure 1. 3 Typical polarization curve of PEM fuel cells [10].

On the polarization curve of the fuel cell, there are often three separate visible zones.

- In the first zone, the activation polarization of the cell is responsible for the decline in cell potential in the lower current density area.
- In the second zone, the fuel cell potential decreases linearly with output current due to the fuel cell's ohmic losses in the moderate current density region.
- In the third zone, due to the concentration polarization in the high current density or low-voltage zone, the decrease in potential is more dramatic.

1.4.1 Activation Polarization

The voltage overpotential necessary to overcome the activation barrier and allow the electrochemical reaction to occur on the catalyst surface is called activation polarization. As the gaseous reactants, solid catalysts, protons and electrons must into contact with each other, the

reactions entail intricate three-phase difficulties. Voltage loss occurs on both the anode and cathode sides; however, oxygen reduction causes significantly greater overpotential due to slower electrode kinetics than hydrogen oxidation. The total activation overpotential amounts to about 0.1 to 0.2 V, which results in lowering the OCV to less than 1 V. Activation polarization predominates at low current densities [11].

1.4.2 Ohmic Polarization

Conductors have an inherent characteristic that resists the movement of charged particles, resulting in a decrease in cell voltage. This phenomenon is known as "ohmic polarization," and it is made up of two resistances. The first is electrical resistance (R_{elec}), and the second is ionic resistance (R_{ionic}). The electrical resistance (R_{elec}) develops due to electron flow resistance in cell components. Catalysts, gas diffusion, bipolar plates, interface contacts, and terminal connections contribute to electrical resistance. Ionic resistance (R_{ionic}) is caused primarily by resistance to proton transport across the membrane. This overpotential essentially linearly raises with voltage and is more prevalent in the moderate voltage range. The material quality mainly determines the ohmic losses [11].

1.4.3 Concentration Polarization

To operate a fuel cell efficiently, reactants must be continuously supplied to generate power, and the product must be continuously removed. The concentration of reactants and products on the catalyst surface controls fuel conversion to products. Concentration polarization occurs when the reactant concentration at the catalyst surface is not restored as quickly as it is used owing to mass transport limitations. As a consequence, the output voltage drops. Diffusion is the dominant mode of mass transport in fuel cell electrodes. Mass transport in fuel cell electrodes should be enhanced to reduce concentration loss. One of the most effective approaches is to improve the flow field shape. The concentration losses are highly dependent on the cell's operating parameters. If there are any punctures in the membrane layers or leaks in the assembly, the output voltage may be reduced owing to fuel crossover and an electric short-circuit [11].

1.5 Thermal management of PEM fuel cells

Thermal management is another critical issue to be taken care along with water management in the operation of PEM fuel cells. High temperature is one of the key causes of performance degradation and membrane failure of the proton exchange membrane fuel cells. The hot spot is

generally defined as localized high temperature region resulting from the thermal effect of the instantaneous electrochemical reaction on the catalyst layer, which does not entirely dissipate the heat into the surrounding area. Nonuniform reactants distribution within the fuel cell is the predominant cause of local hot spot generation throughout the operation. When fuel cells are in operation, the local hot spot and erratic temperature distribution may cause severe deterioration of the membrane and catalyst layers. However, because of the catalyst layer's high heat release rate and low thermal conductivity, dynamic scenarios such as acceleration, deceleration, and overload running, which are common in heavy truck operation (for instance), can still result in local hotspots in the catalyst layer, which can reach dozens of degrees higher than the coolant temperature. The emerging hot spots accelerate membrane deterioration, Pt aggregation, and carbon corrosion [12, 13]. Furthermore, pinholes in the membrane may occur, accelerating hydrogen crossing from the anode to the cathode. Permeated hydrogen catalytically combusts at the cathode, accelerating membrane breakdown and eventually leading to PEMFC failure. Furthermore, unequal temperature distribution at each location in the PEMFC causes several issues, such as membrane impairment and cell breakdown owing to thermal stress [14, 15]. As a result, heat transport inside the PEMFCs should be investigated to provide adequate thermal management and durable PEMFC functioning.

1.6 Motivation for the present study

Despite significant advancements in PEM fuel cell technology over the past few decades, commercialization of the technology at a low cost and with excellent performance for a longer lifespan is yet to be realized. The two most significant issues affecting the performance of low-temperature PEM fuel cells are inadequate water and thermal managements. These two are in fact linked and the improper thermal management may lead to dehydration of the membrane and/or flooding of the cell. Hence, a better understanding of the transient heat transport phenomena in the PEM fuel during its start-up and operation would help in identifying the formation of hot spots and their ill effects on the cell performance. Although several theoretical and experimental studies are available on the aspects related to water and thermal management as discussed in the Chapter 2, a very few studies were focused on transient studies showing hot spot formation and their purging through different channel configurations. This served as motivation for the current study and accordingly the thesis objectives were formulated after thorough review of the relevant literature.

1.7 Outline of the thesis

Chapter 1 explains the fundamental theory, types, working principles, and significant losses in a fuel cell. It also includes the challenges in the present field.

Chapter 2 presents thorough literature review on the existing theoretical models of PEM fuel cells. It depicts the current state of research in 1D, 2D, and 3D modeling of cathode side of the cell and also full-scale fuel cell. This chapter concludes by addressing specific gaps in the literature and developing the objectives and scope, which have driven the formulation and execution of the current research activity.

Chapter 3 presents the problem definition and comprehensive modeling methods. This chapter describes the governing equations that were solved, the boundary conditions that were employed, the simulation approach that was used, as well as the validation.

The results obtained from the present work are detailed and discussed in Chapters 4, 5, 6, and 7. Chapter 4 demonstrates the optimal supply and usage of pure oxygen in relation to the different inflow mass factions and inlet velocity. A comprehensive single-cell parametric examination for the computation of performance factors. Chapter 5 compares the fuel cell performance factor simulation findings obtained with a single-cell straight channel flow field to those obtained with a bumping channel. This chapter also includes a local hot spot formation and parametric examination of the flow field design using 2D simulations. Mitigation strategies of local hot spot are discussed. In chapter 6, hot spot identification and purging using 3D simulations by reconstructing the randomized 3-D gas diffusion layer (carbon paper) into the single cell cathode model are presented. In Chapter 7, further investigation on hot spot mitigation using alternate flow channel topologies is done.

Finally, Chapter 8 presents the overall conclusions drawn from the present study and the scope for future work.

Chapter 2

Literature review

Chapter- 2

Literature review

Replacement of fossil-fuel-powered engines by PEM fuel cells is imperative. PEM fuel cells are generally assembled in a stack to generate a high voltage for heavy vehicles. The basic principles of PEMFCs functioning are well established and shown to be dependable. Governments across the globe are actively encouraging and subsidizing the use of PEMFCs in a broad range of power production applications. Future market competition may require further optimization of the hydrogen fuel and oxidant used to prolong the lifespan of PEMFCs, especially the membrane, to maintain or improve their performance. However, the conversion or usage of hydrogen and oxygen may differ based on the design form of the fuel cell. Several studies including modelling and experimental were carried out over the past three to four decades on the performance enhancement and cost reduction, which can be witnessed by the large number of review articles published in the literature [16-22]. Some of the important literature pertaining to 1-D, 2-D and 3-D modelling of PEM fuel cells using cathode side alone and full-scale cell level, are reviewed in this chapter.

2.1 Studies on thermal management

It has been suggested in the literature that a low working temperature (range 60–80 °C) should be maintained since the production of water vapor is associated with the generation of heat, which may be detrimental to the membrane layers [23]. If excessive heat is generated, the membrane may be destroyed. Consequently, maintaining the resultant temperature below the threshold value for membrane layer stability is critical, resulting in high oxygen conversion and power density. The stack functioning of the PEMFC was deemed sensitive to variations in feed flow rates in a review on PEMFC because the membrane tolerates only a tiny deviation in design temperature, and hence the usage of different cooling methods was developed [24]. On the cathode side, pure oxygen was examined experimentally as a substitute for air in the subsurface, where the air is absent [25]. This chapter provides a comprehensive overview of the key publications in the literature on the various flow field layouts and modifications in isothermal and non-isothermal models. Studies on channel dimension optimization, the influence of operating circumstances on cell performance, and thermal control are also discussed. The models discussed in the next section are given chronologically and are classified based on their time and space and the relevant region of the fuel cells investigated.

2.2 Review of 1-D models

2.2.1 Studies based on cathode side modeling

Bernardi et al. [26] presented one of the earliest and most innovative 1-D and time-dependent models of PEMFCs, in which a numerical model for PEMFCs was built to explain the cathode side of the MEA and predict the cell potential, water transport, and catalyst electro-activity. A technique known as Newman's method was used to solve equations. Furthermore, this specific study gives critical information about the catalyst layer (CL) and the transport model for the portions of the electrolyte and electrodes that are not covered by the general work. This model assumes that the CLs are thin layers where the reactive gases diffuse. The electrolyte and CLs' spatial fluctuation of total overpotential in the electrolyte and CLs for various current densities were examined. The overpotential was projected to be 0.6 V, at a current density of 0.88 A/cm2, with 0.41 V representing activation overpotential and 0.19 V representing ohmic losses owing to membrane ionic resistance. The polarization behavior was compared to that reported by Ticianelli et al. [27], and the findings showed that they were in excellent agreement. Springer et al. [28] developed a 1-D constant temperature model, accounting for the losses caused by interfacial kinetics at the Pt/ionomer interface, transport of gas, limitations of ionic conductivity in the catalyst layer and gas transport in the cathode side of the PEMFCs. The governing equations were solved using Newman's method. The model predictions were compared with experimental data for various gas compositions. In order to investigate the kinetics of the ORR on a Pt/c cathode electrocatalyst, Gloaguen et al. [29] devised a non-isothermal one-dimensional model. The macro-homogeneous and the agglomeration models were used in this inquiry, which was conducted utilizing two different methodologies. The Runge-Kutta approach solved the overpotentials associated with mass transfer, ohmic resistance, and activation. The results revealed that the macro-homogeneous model could simulate the oxygen reduction reaction (ORR) but not the operation of the porous gas diffusion cathode, as was previously thought. It was determined that the agglomeration model was valid even though the active layers were assumed to be thin and devoid of PTFE. The consistency between the experimental and calculated Tafel plots showed this.

A 1-D, adiabatic model of the cathode side of the PEMFCs, was developed by Fukada [30] to evaluate the rate of ORR and water production rate in the cathode gas diffusion electrode. An important assumption was that the Pt catalyst loading would be deposited in the active layer at the

area where the ORR occurs, which turned out to be correct. The Stefan-Maxwell equation was proposed for solving the associated equations of the catalyst layer, and the results were published in the journal Science. The polarization characteristic of the PEMFC was compared to the data provided. Researchers discovered that when the agglomeration radius was more than 2 μm, the diffusion of both oxygen and hydrogen via the catalysts was significantly increased, increasing the cell's voltage and current density. The findings obtained by the model were considerably different from those obtained by Ridge et al. [31]. The relationship between cathode potential and current density was first described by Hsuen [32] using a 1-D, constant temperature model. All losses due to electrical resistance, transport limits, oxygen diffusion constraints, proton migration, electron conduction, and oxygen reduction in the catalyst layer are considered in the calculations. Parabolic and piecewise linear regression proposed two methods for predicting the catalyst layer's ionomer and catalyst potential profiles. The numerical solutions to the algebraic problems were obtained using Newton's methods. It was shown that using piecewise linear regression, the potential losses due to electron conduction and proton migration could be estimated more accurately. To further understand the PEMFC cathode catalyst layer, Jeng et al. [33] created a 1-D and constant temperature model. The governing equations were non-dimensionalized to simplify the catalyst layer phenomena and three dimensionless variables were included. The three dimensionless variables represent oxygen concentration, reaction rate, and current density. PEMFC cathode catalysts can be optimized using a 1-D and constant temperature model proposed by Song et al. [34]. The goal of this study was to increase the cathode catalyst layer's current density at a specific electrode potential. The Nafion content, platinum loading, catalyst layer thickness, and porosity were all considered. When designing the cathode catalyst layer, one or two of the four previously mentioned parameters were considered. The study found that using any of the four parameters as an optimization parameter always results in a better solution. Overall, the thickness of the catalyst layer was the most important factor in determining the catalyst layer's performance. The findings were compared to those of Qi and Kaufman [35], who had performed similar experiments.

According to Du et al. [36], a 1-D and constant temperature model for a cathode catalyst layer was developed to compare the performance of a conventional active layer with an ordered active layer in PEMFCs. The catalyst layer was modeled using the agglomeration model, which was applied to it. The equations presented in the model take into account the Tafel kinetics of ORR, proton migration, and oxygen diffusion in the electrolyte and catalyst layer. The Newton-Raphson

technique was used to solve the equations, and the C programming language was used to write the code. The results supplied by the model revealed that the performance of the PEMFC with the ordered active layer had greatly improved compared to the performance of traditional CLs with low platinum loadings, according to the model. The reduced concentration polarization of the ordered catalyst layer (which has a highly orientated structure and may be used as a substitute for the traditional active layer) is attributed to the improved performance of the ordered catalyst layer. Additionally, the precise kind of CLs used allows for a more even dispersion of oxygen throughout the surface of the catalyst layer. For the record, the modeling findings were in excellent agreement with the experimental data from the literature supplied by Brokk et al. [37] in their conclusion. For the cathode catalyst layer of a PEMFC, Gerteisen et al. [38] developed a 1-D, constant temperature model to analyze the AC impedance spectra and, therefore, the polarization curves. The agglomeration model was performed by the CLs, assuming it was composed of scattered Pt/C filled with electrolytes. The differential equations used in this model can account for the Fickian diffusion of nitrogen, oxygen, water vapors, and Tafel kinetics for the ORR, proton migration, and ohmic losses double-layer charging in the electrode. The comparison shows that the agreement between the observed and simulated polarization curves was excellent. To characterize the events at the cathode catalyst layer of the PEMFC, Liu et al. [39] created a 1-D and constant temperature model based on a constant temperature assumption. In turn, the iterative solution approach found a solution for the non-linear and connected algebraic equations under relaxation. The conventional Thomas algorithm was used to solve each stage of the iteration process. Besides that, the CLs were modeled as a distinct computational domain characterized as a macro-pseudo-homogeneous structure in which solid conductive material, catalyst, electrolyte, and empty space were all evenly distributed throughout. The model was verified using the research findings conducted by Hicker MA et al. [40], and the results showed a statistically significant-excellent agreement. According to Eikerling et al. [41], for the investigation of the cathode catalyst layer, they constructed a macro-homogeneous 1-D model under constant temperature circumstances, which included the agglomeration model. The impacts of reaction kinetics, double layer capacitance at the catalyst-electrolyte interface, proton conductivity, and oxygen transport via the gas-pore region were all considered in this investigation. The findings identified the contribution of CLs concerning the contributions of the other layers of the fuel cell and gave quantifiable information. It was determined whether or not the findings obtained by the created model were comparable to those

supplied by Lee et al. [42]. To optimize the structure of the cathode CLs in PEMFCs, Marr and Li [43] constructed a 1-D and constant temperature model. The processes of electrochemistry and mass transfer were also considered. The Runge-Kutta technique was used to solve the fourth-order set of transport equations. The ideal void fraction for attaining larger current densities was also investigated in this study. According to the research findings, greater current densities result in a reduction in the efficiency of the platinum catalyst layer. As a result, smaller platinum loadings may be more practicable at greater current densities than larger platinum loadings.

2.2.2 Studies based on modeling of both anode and cathode sides

To better understand the effects of various geometries and operating conditions on the performance of a PEM fuel cell, Rowe and Li [44] developed a 1-D, non-adiabatic model of a PEM fuel cell to be used in their research. The CLs area in both the anode and the cathode was assumed to be a mixture of the membrane, the catalyst layer, and the void space. They used the Fan and White [45] approach to solve the non-dimensionalized governing equations and get the solution. Ticiauelli and Derouin [46] study was taken into consideration, and the experimental findings obtained by the model were found to be in great agreement with those obtained by reading the literature. Based on the findings of Rowe and Li [44], they discovered two essential criteria for improving cell polarization: a high platinum loading while keeping large electro-reactive surfaces and a high porosity while increasing permeability of gas to the reactive surface, as detailed in the paper. For the PEMFC, Ramousse et al. [47] created a 1-D constant temperature model that allows them to analytically incorporate the essential processes that affect the performance of the PEMFC while considering the whole MEA and bipolar plates. Several independent explanations of heat and mass transmission processes were included in the developed model. An electrolyte was used to create a homogeneous mixture of catalyst and carbon powder, then submerged in the electrolyte.

Using a 1-D, non-adiabatic model, Hu et al. [48] evaluated the influence of various catalyst settings and operating scenarios on the performance of the PEM fuel cell on both the anode and cathode sides of the device. A thin polymer film representing the catalyst layer was created using the agglomeration model to represent the catalyst layer. The governing equations were solved with the help of COMSOL Multiphysics. In order to evaluate how different catalyst structural parameters, such as Pt-loading and agglomeration radius, affect the overall performance of a fuel cell, many experiments were conducted. According to the findings of the previous research, the shape of the

catalyst layer, in conjunction with optimal operating conditions, can significantly improve the performance of a PEM fuel cell.

Figure 2.1 shows the distribution of the 1-D models found in the literature under the categories of isothermal and non-isothermal as well as cathode side and both anode & cathode side models. It can be noted that majority (73.3 %) of the 1-D models evaluated were created under constant temperature parameters, while about one-fourth were created under non-adiabatic conditions. 1-D models of the reactant gas fluxes and concentrations were used to investigate the interaction of transport phenomena occurring at each layer of the PEM fuel cell to understand better the interplay of transport phenomena occurring at each layer of the PEM fuel cell. Furthermore, the cathode side models occupy about 80 % of the 1-D models, while 20% of the studies looked at both the anode and cathode sides, demonstrating that the electrochemical performance of PEM fuel cells was the major emphasis at the time. A further point to mention is that the majority of the research produced under 1-D consideration occurred in the early years of modeling PEM fuel cells, with an emphasis placed on improving the conditions under which ORR occurs in order to identify factors that can be used to optimize the related transport and electrochemical processes.

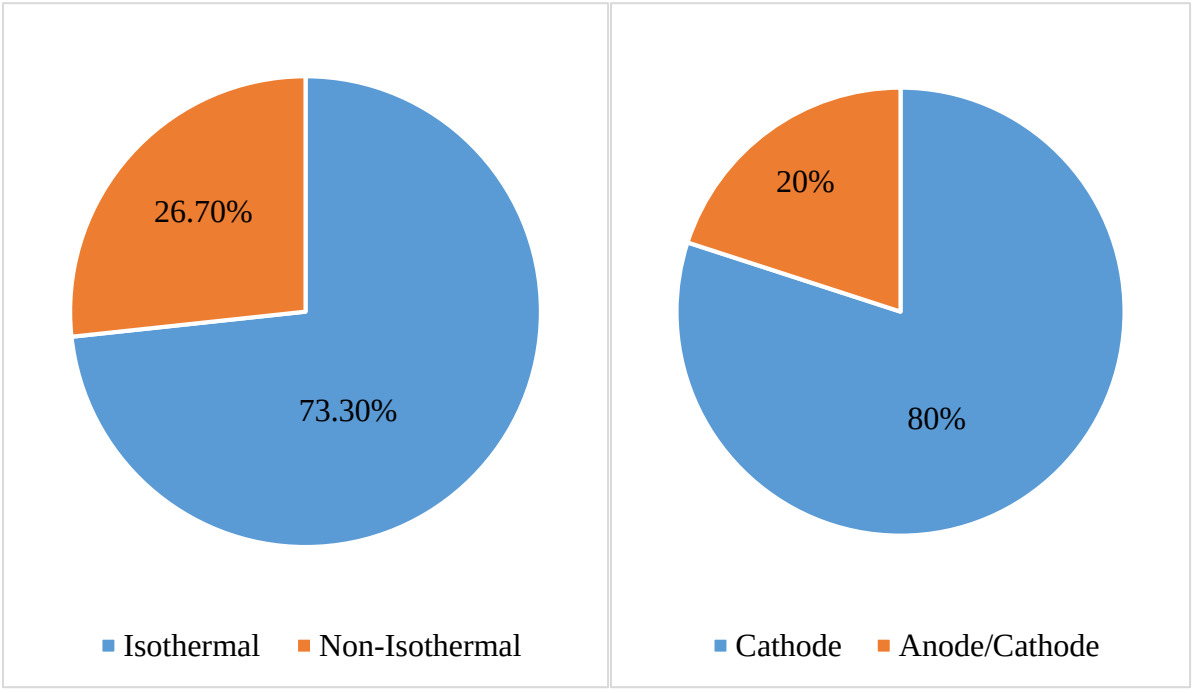

Figure 2.1 Categorization of studies based on 1-D modes [16].

2.3 Review of 2-D models

2.3.1 Studies based on the cathode side modeling

A 2-D, adiabatic model of a PEMFC's cathode side, was developed by Sun et al. [49]. The cathode catalyst layer was modeled by a sequence of catalyst agglomerates coated by a thin polymer electrolyte layer in the model. The model allowed for the mobility of an electron, an ion, and chemical species inside the catalyst layer. The model was simulated using the software FEMLAB, developed by the University of California at Berkeley. Also noted was the inaccurate assumption of constant overpotential while studying the PEMFCs functioning under real operating conditions, which may have resulted in an overestimation of the device's current density. The model also revealed that both electron transport and proton migration play a role in influencing the electrode response rate for oxygen diffusion, which is consistent with previous findings. Finally, the model investigated the performance of PEMFCs under a variety of structural conditions, including Nafion and platinum loading and distributions, among others. Acosta et al. [50] created a 2-D, non-adiabatic model using finite element analysis for the cathode side of a PEM fuel cell. The transport model was simulated using MUFTE UG. On the other hand, the catalyst layer was seen as a thin layer in which oxygen is depleted, resulting in the formation of water and heat. Finally, the model was able to precisely predict the transport processes on the cathode side of the PEM fuel cell system.

In a study by Secanell et al. [51], an adaptive finite element formulation was utilized to develop a 2-D and constant temperature cathode electrode model that considers voltage losses between the electrolyte and solid phases. The model provides an extremely versatile multivariable toolkit to optimize current densities at a given electrode potential. According to the current thinking, the catalyst layer is considered to be made up of a mixture of carbon-supported platinum, ionomer membrane electrolyte, and empty space. The results of the optimization research revealed that increasing the platinum loading in the catalyst layer and reaching a Nafion mass fraction of 20–30 weight % in the catalyst layer increased the performance of PEM fuel cells. The model results were compared to Kulikovsky et al. [52]. In examining the cathode catalyst layer of a PEMFC and assessing overall fuel cell efficiency, Kamarajugadda and Mazumder [53] developed a 2-D, constant temperature model for use in research and development. The agglomeration model was used to manage the catalyst layer, which assumed a spherical ionomer-coated carbon-platinum

agglomerate as the starting point. When it came to solving the diffusion and reaction equations, the finite volume approach came in handy. In the study, researchers discovered that agglomerates within a small radius of 200 micrometers did not affect the overall performance of a fuel cell system. On the other hand, aggregates with a large radius have been demonstrated to be essential, especially at high current densities, agglomerates with a large radius. A previous study conducted by Kamarajugadda and Mazumder [54] validated the 2-D model.

A 2-D, constant temperature model was developed by Roshandel and Ahmadi [55] to explore the effect of catalyst loading in PEMFCs at the cathode electrode. The agglomerate catalyst served as the foundation for the model. Initially, the approach for solving the model relied on the determination of cell voltage as a boundary condition, then iterated for the current and overpotential distributions. Once convergence was achieved, the iterative procedure was repeated. The fuel cells were subsequently put through their paces, and experiments confirmed the results. The experimental technique contributed to optimizing the CL and, consequently, the overall performance of the PEM fuel cells. The study findings revealed that the distribution of catalyst loading significantly impacts the amount of catalyst used.

Also considered was the use of additional catalyst loading to increase power density in areas where high reaction rates occur. This was a significant feature that was carefully investigated. Fofana et al. [56] developed a 2-D, constant temperature model that considers electrochemical processes, momentum, species, and charge conservation equations, among other things. Finite element techniques were used in COMSOL Multiphysics to numerically solve the governing equations, which were then solved numerically. Three different types of catalyst cathodes were used to assess the model's performance. Experimentation was used to verify the polarization curves, and it was discovered that the best performance was obtained using a three-Pt sputtered layer cathode.

Centibas et al. [57] developed a 2-D, constant temperature model using the spherical agglomerate approach in which the cathode catalyst layer was investigated. It was discovered that a more exact approach for determining the effective agglomerate surface area could be devised and implemented. The agglomeration model equation was modified to better correctly estimate the agglomeration surface area due to overlapping particles in the agglomeration. According to the results, the model is more accurate than earlier studies in comparison to other methods of prediction. Furthermore, the model's predictions for the optimal Pt loading, ionomer loading, and

Pt/C ratio were found to be in good agreement with the most recent experimental results reported by Secanell et al. [58].

2.3.2 Studies based on modeling of anode and cathode sides

Xing et al. [59] proposed a 2-D, non-adiabatic model for the catalyst layer that used the agglomeration model. CFD commercial package, with the help of COMSOL Multiphysics, was used to solve the transport model equations. According to the findings, heat builds inside the cathode catalyst layer underneath the channel. Furthermore, increasing the temperature of the PEM fuel cell increases overall performance owing to improved kinetics. Under the non-adiabatic model, Gurau et al. [60] studied the whole MEA as well as CLs and GCs. Their study contains all of the equations needed to describe the events at each layer, especially the catalyst layer on both the anode and cathode sides. The governing equations were solved numerically using the SIMPLE algorithm. Furthermore, electrochemical equations were used to determine the polarization curves under various operating circumstances. Singh et al. [61] created a 2-D, constant temperature model to simulate the transport phenomena in PEM fuel cells. Because the catalyst layer is considered to be much thinner than either the GDL or the membrane, the CL is regarded as a thin interface on both the anode and cathode electrodes of the cell. The PDEs were solved using the FVM, while the algebraic sets of discretized equations were solved using an iterative block methodology. The porosity of the electrode was investigated, resulting in porosity variations that substantially impacted the mass transport of reactant gases. In contrast, when compared with the experimental results given by Bernardi and Verbrugge [62], the model findings showed a high degree of consistency.

Anode and cathode CLs were investigated in a 2-D and non-adiabatic model of a PEM fuel cell created by Siegel et al. [63]. The model included species movement, electrochemical kinetics, energy transfer, current distribution, and water absorption at the anode and the cathode CLs. The differential equations for the whole structure, including the gas channel, GDL, and catalyst layer for the anode and cathode, were solved using a FEM. The agglomeration model was used to mimic the catalyst layer areas in the simulation. Furthermore, the PDEs were implemented using the CFDesign CFD solver, a computational fluid dynamics solver. The findings demonstrated that the shape of the catalyst layer had a significant impact on the performance of the fuel cell. The relative

volume fraction of catalyst pores and membrane-enclosed inside the active area were the factors that influenced the performance of the PEM fuel cell system.

Anode and cathode CLs were included in the CFD model developed by Sahraoui et al. [64]. The model was 2-D with non-adiabatic for steady-state conditions. It accounted for electrochemical, mass, and heat transport processes in the whole model of the PEM fuel cell, including the anode and cathode CLs. The FVM, which is based on the semi-implicit method for pressure-linked equations algorithm, was used to solve the set of PDEs in question. The catalyst layer was described as a volume area rather than an interface between the GDL and membrane. Furthermore, factors like temperature, pressure and the porosity of the pore structures were studied to determine how the performance and efficiency of the PEM fuel cell were impacted. The model findings for current density were compared with those of the experimental data given by Siegel [63], and they were found to be in excellent agreement.

Jung et al. [65] introduced a 2-D numerical model for PEM fuel cells that included the anode and cathode CLs under constant temperature conditions. The governing equations and boundary conditions were solved with the help of the commercial CFD software ANSYS Fluent, which is based on the FVM. The catalyst layer was created using the agglomeration model. The model's findings were compared to different experimental data from the literature, and the agreement was substantially high. Several factors, including the composition of Pt/C, Nafion, and void space in the catalyst layer, were also examined for their effect on cell polarization.

Ameri and Oroojie [66] created a 2-D, constant temperature model to examine the performance of a PEM fuel cell at different operating voltages. In addition, mass transport, velocity map of the reactive gases, current density map, and polarization curve of the reactive gases were also studied in detail. Additionally, the agglomeration model was used to describe the electrochemical processes occurring at the anode and cathode sides of the cell. The final results were obtained by solving the transport equations using the FEM in COMSOL Multiphysics to get the final results. The findings were acquired at various operating voltages to develop a strategy for increasing the performance of PEM fuel cells while also lowering the cost of the devices.

A 2-D and constant temperature model for a PEM fuel cell was developed by Xing et al. [67]. The catalyst layer was addressed using an agglomeration model in which water and ionomer occupy the void space, forming a carbon-ionomer-liquid water agglomerate, as shown in Figure 2.1. The

FVM was utilized to solve the fully coupled equations in COMSOL Multiphysics, with the numerical solution of all equations based on the finite element method. A mathematical model was also developed in which both film thickness and current density were considered to be related. Furthermore, the polarization curve for the agglomerate with a thin coating showed considerable excellent agreement with other experimental results while not overestimating the current density. Yan et al. [68] collected the empirical data used to validate their model. PEMFC models have been presented by Liu et al. [69], who suggested a 2-D and constant temperature model for the device. The model considers the electrochemical processes on the anode and cathode catalyst layers and GDLs and GCs. The equations in their study were solved using analytical methods.

Additionally, Tao et al. [70] compared the findings given by the model with those found in the existing literature and found that they were in excellent agreement. As anticipated, the oxygen concentration on the cathode side of the catalyst layer dropped as the current density increased. The concentration polarization occurred mainly on the cathode side of the catalyst layer. According to Hosseini et al. [71], they established a 2-D, non-adiabatic, and agglomerate model. CFD software was applied to solve the species transport equations. At both the anode and cathode CLs, the impact of different operating factors, such as the stoichiometric coefficient, the operating temperature, pressure, and relative humidity, on the performance of the PEM fuel cell was investigated. Rao et al. [72] compared the model findings with those obtained from various previously published techniques. Moreover, it concluded that the agglomerate model had superior accuracy.

Gurau et al. [73] developed a steady-state and constant temperature, 2-D a PEM fuel cell numerical model in which the cell was divided into three regions: an anode, a cathode, and PEM. They investigated the effects of liquid water on fuel cells under the assumption that liquid water was generated in the membrane electrode of the cell. The study found that (1) fuel cell performance improves with increased cathode and anode entry speeds and temperatures, and (2) liquid water is likely to transmit from cathode to anode in low current density, or else liquid water is likely to transmit from anode to cathode in high current density, was found to be effective. It was shown that numerical simulation of simultaneous flow, heat transfer, and electrochemical reaction, single-phase is possible for PEM fuel cells by Qi & Zhang [74]. The distribution of temperature, oxygen, and water vapor on the cathode side of the PEM fuel cell was obtained. The LBM is transient-

state, 2-D, and temperature-dependent, emphasizing the ACL with reconstructed microstructures. FVM was used to solve the macro-scale model, while LBM was used to solve the pore-scale model. The pore-scale CL modeling was then combined with a macro-scale simulation of the air channel and GDL and experimentally validated using a 3.5 cm^2 dehumidifier. The results revealed that the CL microstructure substantially impacts the air output characteristics of PEM dehumidifiers, particularly in the initial stage.

2.4 Review of 3-D models

2.4.1 Studies based on the cathode side modeling

Das et al. [75] developed a 3-D, adiabatic model of the CCLs of a PEM fuel cell, in which they employed a multi-agglomerate model to explore the activation polarization and current densities of the specific layer under investigation. The transport equations and boundary conditions were solved using the COMSOL Multiphysics software. A further investigation into three different agglomeration topologies was carried out in order to establish the oxygen transport pathways and the influence of activation polarization in the CCL. Overall, the model provided insight into the agglomerate arrangement, which was useful in designing the PEMFC and optimizing its overall performance. Das et al. [76] conducted a previous investigation that confirmed the accuracy of the 3-D model.

Obut and Alper [77] created a 3-D, non-adiabatic PEM fuel cell model. When the characteristics of the CCL were changed, the model could be used to determine the performance of the fuel cell system. The CLs were also considered spherical agglomeration models, which was another consideration. In order to study the performance of the PEM fuel cell, several cathode catalyst layer configurations were tested (e.g., the catalyst layer thickness, agglomerate size, porosity, and ionomer film thickness). The researchers employed the ANSYS Fluent CFD software to solve the governing equation. The data also indicated that the mobility of species, electrons, and protons inside the CCLs significantly influenced the performance of the PEM fuel cell in the final analysis. Chang et al. [78] utilized experimental data from their prior work to validate the 3-D model they developed.

Xie et al. [79] constructed a 3-D, non-adiabatic model of the cathode catalyst layer, and an enhanced agglomerated sub-model was generated as a result of their work. The model was created using the commercial computational fluid dynamics (CFD) tool ANSYS Fluent. Furthermore, the

model considered the influence of platinum loading on oxygen transport and, as a result, on overall fuel cell performance. The simulation produced findings that were consistent with the experimental data. Aside from that, the researchers discovered that ionomer resistance rose dramatically when Pt loadings were less than 0.1 mg/cm, which they attribute to mass transport restrictions inside the fuel cell. According to Owejan et al. [80], the generated polarization curves were then compared to experimental data to determine more accuracy.

A 3-D and time-dependent, constant temperature numerical model for simulation studies on the cathode of fuel cells was developed by Natarajan and Nguyen [81], which described gas mass transfer with a multiplexed diffusion equation and the capillary action of liquid water with Darcy's law within a porous material using Darcy's law. In order to investigate different transients of fuel cells under varying operating parameters, design parameter effects, and cathode overpotential, the results of the simulations were compared to actual data collected from field experiments.

2.4.2 Studies based on both anode and cathode sides modeling

A 3-D, non-adiabatic model of a PEMFC was developed by Berning and Djilali [82], taking into account the MEA and GCs' anode and cathode sides. The CL was implicit in being a thin interface, and the study results validated this assumption. In order to create a CFD model, the UDFs provided crucial information such as reactant concentrations, current densities, and temperatures. PEM fuel cell performance was evaluated by Berning and Djilali [83] in light of the effects of several operational parameters, including the two CLs. The thickness and porosity of gas diffusion electrodes and other geometric and material properties were considered. According to the researchers, the results proved the model's usefulness as an optimization and design tool.

Wang et al. [84] have constructed a 3-D and constant temperature model of a PEM fuel cell. Tests were conducted under varied operational conditions. Using mass, Navier-Stokes, heat, and species concentration equations, various fuel cell layers were studied. The governing equations were also solved using ANSYS Fluent. In addition, chemical reaction kinetics were related to the membrane and catalyst layer potential phase equations. The performance of the fuel cell was affected by cathode humidification and temperature, explicitly at high current densities, whereas the anode had no effect. In addition, it was found that boosting the fuel cell's operating pressure improved performance. The findings also indicated substantial-excellent agreement compared to other 3-D models in the literature.

Meng and Wang [85] used finite volume analysis to develop a 3-D and constant temperature model of PEMFCs. The conservation equations for mass, momentum, and species were intertwined with the electrochemical transport processes and equations throughout the fuel cell structure. In addition, source terms were used to account for electrochemical oxidation and reduction processes. CFD software STAR-CCM+ was used to solve the transport phenomena equations. According to the findings, catalyst layers cannot be ignored when modeling PEM fuel cells because of the ohmic losses caused by proton transport.

PEM fuel cells with straight and interdigitated gas flow channels were studied by Um and Wang [86], who developed a 3-D constant temperature model better to understand the interaction between mass transport and electrochemical kinematics. A Pt/C ionomer was mixed with an ionomer at the active CLs (anode/cathode). The finite volume approach was used to build the model, then tested using commercial computational fluid dynamics software. By enhancing water removal from the catalyst layer and the delivery of oxygen to active layers, interdigitated flow fields improved fuel cell efficiency. A 3-D and non-adiabatic model incorporating electrochemical and transport equations was provided by Ju et al. [87]. Anode and cathode compartment membranes are included in the model, as are GDLs (anode/cl) and CLs (both anode/cl). STAR-CCM+ was also used for these simulations. The simulation indicated that the thermal effect of PEM fuel cells is more significant at high current densities. A 3-D, non-adiabatic PEM fuel cell model, was constructed by Sivertsen and Djilali [88]. Dispersed heat generation from electrochemical processes in the cathode and anode catalyst layers was included in the model.

A more precise prediction of local current density was achieved thanks to the model's ability to accurately compute the ionic and electric potentials and the local overpotentials. In-house CFD package ANSYS Fluent solved the numerical model equations. The model's output was compared to Wang et al. experimental results [84]. An isothermal model developed by Chiang and Chu [89] was used to study transport processes and how they affect PEM fuel cell performance. The simulation took species, momentum, and current transfer conservation equations into account. The anode and cathode CLs were mimicked using porous media. Anode and cathode reactions were also described using electrochemical phenomena. A commercial CFD-ACE+ algorithm based on the SIMPLE approach was used to build the model, and the findings were compared to those of Um et al. [86].

Sadiq et al. [90] proposed 3-D and non-adiabatic PEMFC models. This model took into account convection and dissipative heat transfer, mass transfer, and electrode kinetics were all considered in the model. They were able to discretize and solve the governing equation using a general-purpose CFD code. They developed a precise model for computing local activation overpotentials, enhancing their calculation capabilities, and better estimating the local current density distribution. In addition, the catalyst layer was seen as a thin interface with the words "source" and "sink" included in the concept. The PEMFC's performance was investigated in various working conditions, providing insights into complex processes that are difficult to investigate experimentally.

Rismanchi and Akbari [91] created a 3-D, constant-temperature PEM fuel cell model. Mass, momentum, species, energy, and charge transfer equation used in the PEMFC design were taken into consideration in the modeling and electrochemical kinetics. The agglomeration model was used on the catalyst layer to simulate the process. As well as describing the flow and current distributions, the model may also contain information about other cell characteristics, such as voltages between the anodes and cathodes of bipolar plates, the electrolyte in general, as well as GCs and CLs. In order to numerically solve the governing equations, the FVM approach solves them.

A good agreement between the Wang and Liu [92] findings and the fuel cell's polarization curve were found, as was the polarization curve of another fuel cell under consideration. An isothermal PEM fuel cell model created by Yuan et al. [93] was used to investigate the behavior of the cell under different operating conditions, including pressure, temperature, humidity, and the stoichiometric ratio of reactant gas mixtures in the cell. On both the anode and cathode sides, the model comprises current collectors and flow channels, as well as a GDL, a CL (anode/copper), and a memory Fluent, were used to generate the model, which was built using the finite volume method. Only modest deviations between numerical predictions and actual polarization curves were found compared to previous experiments. Rizvandi and Yesilyurt [94] developed models for both sides of the PEM fuel cell. The velocity field in the channels was calculated using Navier-Stokes equations and corrected for porous media using Brinkman correction. For the diffusion and advection of gas species, Maxwell-Stefan equations were used. Anode electrochemical processes were modeled using Butler-Volmer equations, while cathode kinetics were modeled using the

agglomeration model. The governing equations were solved using COMSOL Multiphysics, a commercial finite element tool. Compared to Nandjou et al. [95], the simulation results showed a good match. PEM fuel cells with a dead-ended anode channel were studied by Peng et al. [96] in 3-D and a non-adiabatic model. Anode and cathode-side transport equations were analyzed for continuity, Navier-Stokes, heat, species, and charge. In addition, they employed the Butler-Volmer equation 3D model to build the transport equations. Comparing the current density at different fuel cell voltages validated the computational model [84]. In addition, the fuel cell's performance was assessed under various operating conditions, both with and without a purging mechanism.

To study the effects of liquid water on fuel humidification, proton exchange membranes, and porous electrodes, as well as heat generation and transmission in cells, Berning et al. [97] constructed a 3-D steady-state and non-adiabatic PEM fuel cell model. According to the results, better water management will impact PEM fuel cell efficiency by preventing proton exchange membrane dehydration or liquid water accumulation that causes overflow. Ge and Yi [98] developed a 2D and steady-state isothermal PEM fuel cell numerical model with anode and cathode to investigate the variables of different operation conditions, such as exchange membrane thickness and two entries of parallel flow or cross-flow, to determine how much water is transferred and distributed, as well as the effect of ohmic resistance on performance, in order to determine how much water is transferred and distributed. While conducting research, it was critical to study the transfer of water between the gaseous phase and the liquid phase in cathode diffusion, where the transfer of water in the exchange membrane was preceded by diffusion, convection, and electro-osmosis.

Jourdani et al. [99] used COMSOL Multiphysics to create a 3D simulation study of a PEM fuel cell based on the varied transport phenomena in the PEM fuel cell, which plays a key influence on overall cell performance. This model was built on the assumptions of an isothermal, steady-state, perfect gas, and constant density flow. According to the investigation, the performance of a PEM fuel cell is determined by the characteristics of the membrane, gas diffusion layer, catalyst, and operating parameters such as operating pressure, cell operating temperature, relative humidity, and the mass flow rate of the feed gasses, channel geometries, and stack design. The results demonstrate that a thinner membrane corresponds to a greater current density, hydrogen and oxygen consumption, and higher water generation.

Abdulla and Patnaikuni [100] compared the performance of greater active area fuel cells with enhanced cross-flow split serpentine flow fields and triple serpentine flow fields using a 3-D, two-phase computational fluid dynamic full-scale fuel cell model. In modeling fuel cells with active surfaces of 50 cm^2, 100 cm^2, 150 cm^2, and 200 cm^2, the ECSSFF design was used as the cathode channel and the parallel design as the anode channel. The performance of these cells is also compared to that of cells with a triple serpentine flow design on the cathode side. According to the findings, ECSSFF surpasses all other active locations in greater currents, lower pressure drops, and higher power generation. In cell areas ranging from 50 cm^2 to 200 cm^2, the percentage improvement in net power output generated using the ECSSFF design over the TSFF design ranges from 4.5 % to 13.5 %. As the active area of the ECSSFF design expands, the percentage loss in net power density increases, but the percentage loss in net power density almost doubles as the active area of the triple serpentine design develops. According to the findings, the ECSSFF is a potential flow field designed to investigate the development of high-area fuel cell devices for large-scale power generation.

Stack operation of the PEMFC was considered sensitive to changes in flow rate of feed, as the membrane can tolerate only a small deviation in design temperature and hence the use of various cooling technologies was suggested by Kandlikar and Lu [24]. On the cathode side, pure oxygen as a feed instead of pure air was also evaluated experimentally in the submarine context, where the air is not available [25]. Computer simulation offers a platform for inexpensive optimization of the design. Simulation of transport models in the gas diffusion layer and the catalyst layer was proposed, taking water formation on the cathode side also into consideration [101]. A study on PEM fuel cells by modeling and simulation found that water as a cooling fluid shows a higher ability than air-cooling of the bipolar plate. A 3D numerical model was also used to study the above aspects [102]. In another study on water removal in PEM fuel cells, the effect of humidity in the feed was studied by experiments [103]. An attempt was made to model the transport processes in the GDL and CL, and the effect of pore level transport properties and microscopic properties in GDL has been investigated by a stochastic model [104]. In another study, the applicability of the continuum model for momentum, heat, and mass transport in fuel cells at a microscale was analyzed and suggested to be applicable [105]. A new mass transport model was proposed to deal with both the macroscopic diffusion in GDL and Knudsen regimes in the porous catalyst layer [106].

Similarly, a model applicable to the porous catalyst layer embedded in the gas diffusion layer was proposed [107]. It has been identified that heat and mass transfer are to be coupled while modeling the phenomena in fuel cells, and the concept of reaction boundary was introduced [108]. The reaction is that of oxygen with an H+ ion on the cathode Pt catalyst layer. In a very recent study, the multi-objective optimization regarding the operating condition of isothermal temperature in the PEM fuel cell has been explored [109].

It has been suggested that the 3D simulation of complicated flow channels is difficult [110]. It was attempted to simulate the mass and heat transfer using various structures of the cathode catalyst layer [111]. Attempts were made to modify flow channels to obtain uniform temperature in GDL [112]. The GDL is modeled as a porous layer [113]. Oxygen transport was modeled by an effective diffusivity approach across the catalyst layer [114]. The entire mass and heat transport model was taken up, but the porous layer flow in the catalyst layer was considered [115]. The effect of catalyst loading was studied and found that more than 30% of the coating of the Pt is insignificant in improving the power density [116]. COMSOL was used to simulate it, but an isothermal operating condition was used [117]. OpenFOAM, an open-source CFD program that operates on the C++ framework, was also employed as an alternate tool for PEM fuel cell single and multiphase modeling purposes [118]. In another study, a simulation based on a single-phase assumption was developed [119]. Oxygen reduction is not the limiting step, as per one of the studies [120]. Water transport in the cathode side of GDL is also a bottleneck in the simulation of PEM fuel cells [121]. A 60°C temperature was recommended to be the optimum maximum for a long life of membrane in PEMFCs [122]. A complete simulation was performed, assuming a porous layer GDL [123]. Proton transport across the membrane was not found to be a limiting step in power generation by PEMFCs [124]. CFD models for fuel cell stacks were available in the literature to obtain temperature distribution, but hot spots were not reported [125]. The steady-state and dynamic simulation was carried out using MATLAB and DAE solver (differential algebraic equation) along flow direction [126]. Experiments with pure oxygen on the cathode side were carried out [127]. In another relevant work, pure oxygen should have been used on the cathode side instead of air to limit the cathodic reaction since this would have reduced the cathodic reaction. It was observed that MEA aged more quickly when fed pure oxygen, which was most likely due to corrosion of parts in the system assembly. The oxygen percentage varies as 21%, 50%, and 100%, with balance as nitrogen on the cathode side [128]. Current density increased monotonically with increasing the

inlet oxygen mass fraction. These current density values can be transformed into power density produced using the literature correlation or the polarization characteristics of PEMFCs [129].

The 3-D models created are useful for giving a more realistic and comprehensive picture of PEM fuel cells performance, taking into account both electrochemical and transport processes. As can be observed from Figure 2.2, the number of research works looking at both the cathode and anode sides of CLs has risen. There are quite a good number of works involving 3D modeling of non-isothermal PEMFC systems as well as full cell level simulations. The increased computational power has enabled solution of more complex problems involving various transport and electrochemical phenomena, allowing for the investigation of the precise spatial distribution of current density, temperature, chemical species, and current. This has allowed for more accurate conclusions about the operation and performance of PEM fuel cells to be reached.

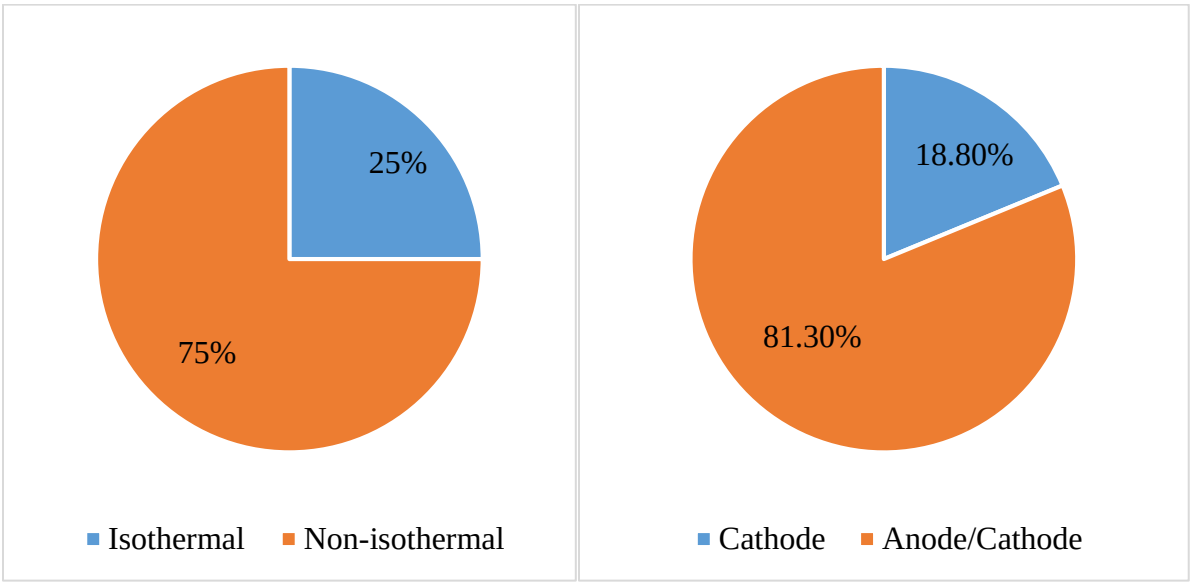

Figure 2.2 Distribution of 3-D computational models [16].

2.5 Gaps identified

From the above literature review, the following gaps are observed with regard to the formation and mitigation of hot spots, concerning the thermal stability of a PEMFC.

1. The gas diffusion layer is commonly modeled as porous media in majority of the studies instead of microscopic flow past discrete carbon fiber. The heat generated from the

electrochemical reaction at the membrane catalyst (Platinum) surface on the cathode side is not modeled as a surface heat flux. Commonly the temperature is assumed to be constant and uniform in the entire fuel cell, particularly in GDL. In reality, the temperature is not uniform in a fuel cell. Therefore, the actual model and simulation should provide detailed temperature distribution in and around the membrane so that the location of hot spots, if any, can be identified.

2. In particular, the oxygen percentage at the cathode inlet less than that of the air (21%) was not explored in the literature, which is very relevant for submarine applications. The composition of the feed inlet on the cathode side containing pure oxygen and pure nitrogen is not optimized for safe thermal operation.

3. Although many studies have been reported on numerical simulations of gas flow field channels and catalyst loading using computational fluid dynamics, the key concern pertaining to hot spot minimization is still unanswered. One of the main problems is how to find the hot spot by numerical simulation, and once detected, how to mitigate it. Not many studies are focused on this, and there is scope for developing the hot spot mitigation strategies.

4. Most of the simulation studies reported in the literature considered GDL as a simple porous zone and did not consider the 3D randomized fibrous structure while accounting for heat transfer, hot spot generation, and identification. Many numerical modeling investigations into the 3D gas diffusion layer, whether carbon fabric or paper, have solely used the isothermal condition. However, the actual porous GDL contains random arrangement of carbon fibres and show significant effect on the reactant flow and heat transfer. This is not explored in the thermal management studies reported in the literature.

5. The effect of geometric shape of the channels in a flow field on the hot spot mitigation is not explored.

The above identified gaps in the literature led to the formulation of the following objectives for the present study.

2.6 Objectives and scope of the present work

The overall aim of this study is to identify the formation of hot spots and propose strategies to mitigate their formation using computational analysis of the cathode side of the PEM fuel cell. The following are identified as the objectives of the present work.

1. To simulate the hot spot occurrence using steady state simulation of the cathode portion of PEM fuel cell.
2. To obtain the optimum mass fraction of oxygen in the feed with respect to the performance of the fuel cell.
3. To study the local hot spot mitigation on a bumped channel design using transient 2-D simulation of the cathode.
4. To study the effect of an oscillatory (cyclic) supply of oxygen and nitrogen in the inlet gas stream to the conventional straight channel on the hot spot mitigation.
5. To study the hot spot occurrence in the conventional straight channel using transient 3-D simulation of the cathode side of the cell with random porous GDL structure.
6. To study the effect of shape of the of flow field channel on the hot spot mitigation.

The above stated objectives are achieved by developing a 2-D and 3-D, single-phase, non-isothermal transient models incorporating the multi-scale, multi-physics associated with the PEM fuel cell in the CFD environment using the academic research version of COMSOL Multiphysics 4.4a. The scope of the study was limited to computational analysis of the fuel cells having different shapes of the flow channels with and without the oscillatory supply of the nitrogen gas. The detailed modeling equations and solution strategies used to simulate the cathode side of the PEMFC are described in the next chapter.

Chapter- 3

Modeling Methodology

Chapter- 3

Modeling Methodology

One of the primary objectives of the study is to optimize the supply and utilization of pure oxygen and nitrogen on the cathode side of a PEM fuel cell to improve thermal stability without taking into account the optimal temperature of the catalyst and membrane layers. The computational model is tailored to estimate the optimal oxygen mass fraction in feed and net feed flow rate, resulting in long thermal life and low operating cost. It also aims to extend the single-layer cathode side of a PEM fuel cell to identify the local hot spot patch near the reactive gas flow channel entrance. Another study aims to mitigate the local hot spot patch on the catalyst and membrane layer by introducing an oscillatory nitrogen supply in a time-dependent analysis. The effect of shape of the gas flow channel on the mitigation of the hot spots is also analysed in one of the objectives.

To perform computational analysis, the cathode-side PEM fuel cells has been appropriately modeled, including fluid flow, heat transfer, mass transfer, and the movement of concentrated species. This is done step by step, methodically in a simulation environment employing the COMSOL Multiphysics 4.4 software package and performed parameter optimization. This chapter provides a complete overview of the modeling equations and the computational domains used in the simulations.

3.1 Problem formulation and modeling equations

PEM fuel cell physics includes mass movement of species (such as hydrogen, oxygen, water, and nitrogen), heat transfer, and electrochemical reactions. Partial differential equations that explain species, energy, mass conservation, electrical charges, and momentum transfer are used to express these processes numerically. The present study employs a rigorous 2-D and 3-D computational fluid dynamics modeling technique using novel boundary conditions. Probably, the best utilization of hydrogen (fuel) and oxidants (oxygen) would be necessary to increase the lifetime of PEM fuel cells, particularly the catalyst and membrane layer. Figure 3.1 demonstrates that, in general, hydrogen is supplied by the individual pure gas storage cylinder, while oxygen is supplied by air from outside the storage cylinder (21% O_2 & 79% N_2). However, the conversion of hydrogen and

oxygen depends on many designs and operating parameters of the fuel cell. Furthermore, according to the literature, different thermal management aspects contribute to maintaining a low operating temperature (60–80°C) since the creation of water vapor is associated with high heat generation, which may injure the membrane layer [131]. The effect of a local hot spot patch on the catalyst membrane layer on cell performance will be examined and determined.

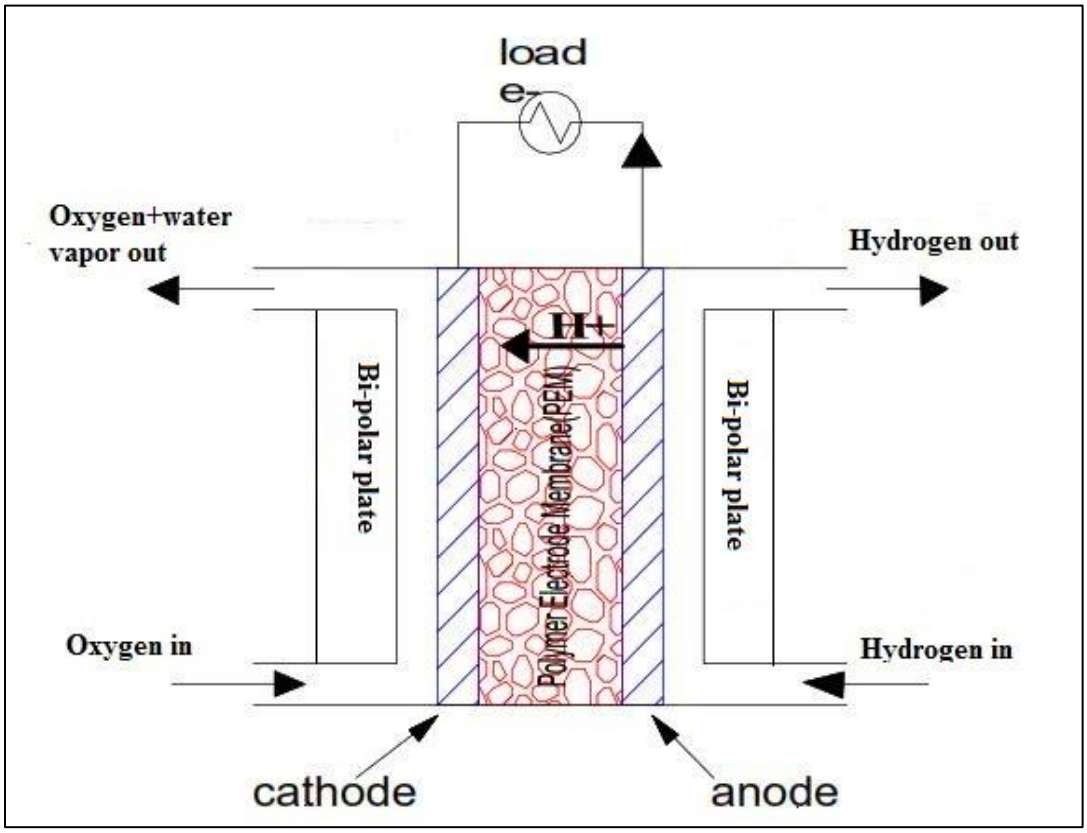

Figure 3. 1 Schematic diagram of a PEM fuel cell.

The schematic representation of a PEM fuel cells is illustrated in Figure 3.1. It features a proton exchanging membrane as the core layer is sandwiched between two catalyst layers (anode and cathode), gas diffusion layers (anode and cathode) and bipolar plates as its outside layers. As it is well-known, hydrogen is passed in pure form on the anodic side of the cell. At the anodic catalyst layer, the hydrogen is catalyzed to split into H^+ ions (protons) and electrons. The H+ ions pass through the membrane (electrolyte) to the cathode side, where oxygen combines with this proton and electrons coming through the external load and resulting in the formation of water vapor. Both of the above are electrochemical reactions, and the heterogeneous electrochemical reactions generate heat when water vapor formation takes place on the cathode side. The ΔH_R for water

formation is −286,000 J/mol of water produced. The – ve sign shows that the process is exothermic. To go into the specifics of the gas diffusion layer, it comprises carbon fabric coated with a Pt-catalyst layer. Since accurate modeling of fluid flow, heat transfer, mass transfer, and instantaneous electrochemical reaction are complicated, a simplified version is assumed, as shown schematically in Figure 3.2.

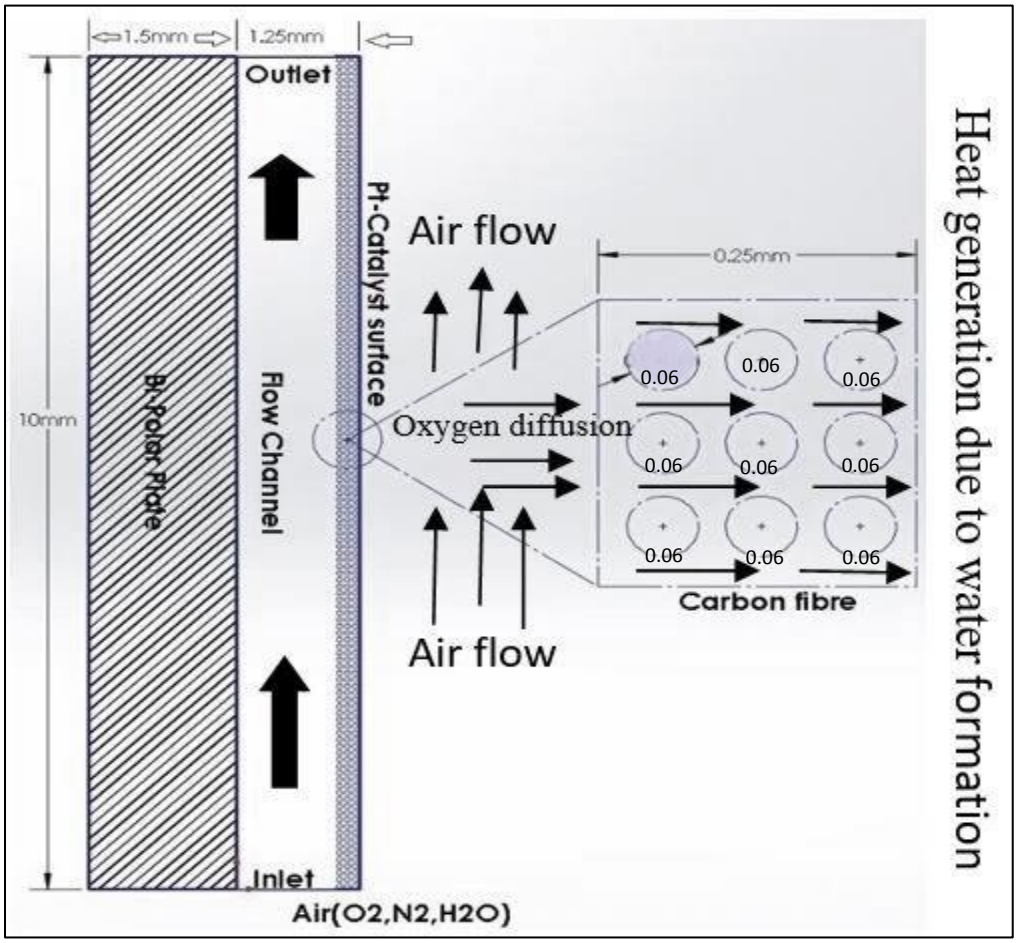

Figure 3. 2 2D schematic of the cathode section used for the present simulation study.

Only the cathode side of the PEM fuel cell is considered to simulate and predict the worst-case scenario of temperature distribution in the different parts of the cathode side of the fuel cell. The extreme side of the bipolar plate is assumed to be thermally insulated in the proposed model, whereas the other side is not. A thin layer of pt-catalyst is thought to have been applied sparingly to the catalyst surface. At this surface, the electrochemical cathode reaction of water formation occurs at this contact and the surface heat flux is generated by the ΔH_R (heat of reaction of water production). A novel geometry and boundary conditions for simulating flow, heat, concentrated

species diffusion, and instantaneous surface reactions that result in heat generation in a fluid flow system are proposed. There are several types of physics at work in this proposed model, including heat transfer in solids in a bipolar plate, heat transfer in a gas flow channel, and heat transfer in a carbon fiber manifold (gas diffusion layer). The transport of concentrated species in a gas flow channel and laminar flow through a carbon fabric is represented by an array of micron-sized solids circular, as shown in Figure 3.2, which can be referred to for a zoomed schematic of the model. The computational geometry contains cathode side of the cell consisting of bipolar plate section, single gas flow channel and three-layered gas diffusion layer represented by an array of micron-sized cylindrical solids. The dimensions of these parts are shown in Figure 3.2. A modified program that solves steady-state and transient state partial differential equations using the COMSOL Multiphysics 4.4 software simulates these transport phenomena.

3.2 Governing equations of the model

3.2.1 Model assumptions

Following are some of the assumptions considered to establish the model foundation.

1. The fluid in gas channels and diffusion layers behaves identically to an ideal gas.
2. The pressure at the outlet of the gas channels is equivalent to the pressure in the surrounding environment.
3. Fuel and electron crossover through the membrane are not considered.
4. Cell temperature is non-isothermal
5. The fluid is compressible
6. Due to the low velocity of the gasses, flow is laminar everywhere
7. The membrane is impermeable to the gases
8. The effect of gravity is ignored.
9. Water in the vapor phase is considered.

Regarding the preceding assumptions, it should be emphasized that water and heat transfer are linked, and the process in the channel is quite complicated when the gas-liquid interface is followed. Because many water transport activities, such as phase change and liquid water transit in the channel, and liquid water entering the channel from GDL, are accompanied by heat exchange. When considering the flow pattern of liquid water, it is challenging to explain heat transmission due to its complexity effectively.

3.2.2 Gas diffusion layer equations

The continuity equation (mass conservation) for laminar flow containing the temporal term is

$$\frac{\partial \rho}{\partial \mathrm{t}} + \boldsymbol{\nabla} \cdot (\rho \mathbf{u}) \quad [3.1]$$

The time-dependent Navier-Stokes equation for compressible flow describing the momentum conservation of the fluid was used for modeling with zero gravitational force.

$$\rho \frac{\partial \mathbf{u}}{\partial t} + \rho(\mathbf{u} \cdot \boldsymbol{\nabla})\mathbf{u} = \boldsymbol{\nabla} \cdot \left[-p\mathbf{I} + \mu(\boldsymbol{\nabla}\mathbf{u} + (\boldsymbol{\nabla}\mathbf{u})^T) - \frac{2}{3}\mu(\boldsymbol{\nabla} \cdot \mathbf{u})\mathbf{I}\right] \quad [3.2]$$

Density is defined as per the ideal gas law in Equation [3.3]

$$\rho = \frac{\mathrm{PM_{Avg}}}{\mathrm{RT}} \quad [3.3]$$

A transient equation that describes the heat transfer in the inlet gas flow channel: [128.129].

$$\rho \mathrm{C_P} \frac{\partial T}{\partial t} + \rho \mathrm{C_P} \mathbf{u} \cdot \boldsymbol{\nabla} T = \boldsymbol{\nabla} \cdot (k \boldsymbol{\nabla} T) \quad [3.4]$$

The transport of concentrated species (oxygen, nitrogen, and water vapor) is modeled by modified Fick's law [128], where the steady-state governing equations for each of them are represented in Eq. [3.5a-3.5c].

$$\rho \frac{\partial \omega_i}{\partial t} + \boldsymbol{\nabla} \cdot \mathbf{j}_i + \rho(\mathbf{u} \cdot \boldsymbol{\nabla})\omega_i = \mathrm{R_i} \quad [3.5a]$$

$$\mathbf{N_i} = \mathbf{j}_i + \rho \mathbf{u} \omega_i \quad [3.5b]$$

Where, the diffusive flux j_i is represented as in Equation [3.5b]

$$\underline{\mathrm{j_i}} = -\left(\rho \mathrm{D_i^F} \underline{\nabla} \mathrm{w_i} + \rho \mathrm{w_i} \mathrm{D_i^F} \frac{\nabla \mathrm{M_n}}{\mathrm{M_n}} + \mathrm{D_i^T} \frac{\nabla \mathrm{T}}{\mathrm{T}}\right) \quad [3.5c]$$

Where, concentrated species diffusion and Soret (thermal) diffusion are considered. Here the mean molecular weight M_n is given in Equation [3.5c].

$$\mathrm{M_n} = \sum_{\mathrm{i}} \left(\frac{\mathrm{w_i}}{\mathrm{M_i}}\right)^{-1} \quad [3.5c]$$

In the above equations D_i^F is the concentration-based diffusion coefficient in the above equations, and D_i^T is the thermal diffusion coefficient. The expressions for D_i^F and D_i^T are given in Equations 3.6 (a–d) for oxygen, nitrogen, and water vapor [129, 130].

$$\mathrm{D_{O_2}^F} = 3.2 \times 10^{-5} \left(\frac{\mathrm{T}}{353}\right)^{1.5} \left(\frac{100000}{\mathrm{P}}\right) \quad [3.6a]$$

$$\mathrm{D_{N_2}^F} = 3.2 \times 10^{-5} \left(\frac{\mathrm{T}}{353}\right)^{1.5} \left(\frac{100000}{\mathrm{P}}\right) \quad [3.6b]$$

$$D_{H_2O}^{F} = 7.35 \times 10^{-5} \left(\frac{T}{353}\right)^{1.5} \left(\frac{100000}{P}\right) \quad [3.6c]$$

$$D_{i}^{T} = -2.59 \times 10^{-7} T^{0.659} \left[\frac{M_{w,i}^{0.511} X_i}{\sum_{i=1}^{N} M_{w,i}^{0.511} X_i} - Y_i\right] \cdot \left[\frac{\sum_{i=1}^{N} M_{w,i}^{0.511} X_i}{\sum_{i=1}^{N} M_{w,i}^{0.489} X_i}\right] \quad [3.6d]$$

3.2.3 Bipolar plate

The heat transfer in the bipolar plate of Figure 3.2 is modeled by unsteady-state heat conduction in the solid's equation (Laplace Equation) which

$$\rho C_p \frac{\partial T}{\partial t} + \rho C_p \mathbf{u} \cdot \boldsymbol{\nabla} T = \boldsymbol{\nabla} \cdot (k \boldsymbol{\nabla} T) \quad [3.7]$$

3.2.4 Carbon fibre manifold

The heat conduction in the carbon fiber manifold of Figure 3.2 is also modeled by unsteady-state heat conduction in the solid's equation (Laplace Equation), which is

$$\rho C_p \frac{\partial T}{\partial t} + \rho C_p \mathbf{u} \cdot \boldsymbol{\nabla} T = \boldsymbol{\nabla} \cdot (k \boldsymbol{\nabla} T) \quad [3.8]$$

3.3 Boundary conditions

The above presented partial differential equations are the governing equations. In order to solve the entire problem, appropriate boundary conditions are required. The boundary condition shown in Figure 3.2 will be used as a novel approach in the ensuing investigation, described in detail below. The feed is assigned a normal inflow velocity (V_{in}) in the range of (1 mm/s to 1 m/s). The feed consists of various proportions of oxygen, nitrogen, and water vapor. The water vapor mass fraction in the feed is kept at 1%, and the mass fraction of oxygen (W_{21},W_{22}, W_{213}) is varied from 20% (corresponding to the air) to as low as 1%. Thus, the remaining part of the feed is nitrogen, an inert gas that carries heat and does not participate in the reaction. The outlet boundary condition has zero reference pressure. The flow is assigned as a no-slip boundary condition on the all-circular carbon fiber surface on the carbon fiber in the gas diffusion layer (GDL) on a micro-scale. At the wall, a no-slip boundary condition is applied based on the assumption of laminar flow in the PEMFC.

Similarly, the adjacent Pt interface on the membrane and bipolar interface are assigned no-slip boundary conditions for flow (implies temperature is the same at the interface in the two neighbouring domains). Temperature is assigned a continuity condition wherever the gas domain is in contact with other phases such as carbon fibre, Pt surface, and bipolar surface. On the Pt

surface, the water vapor formation reaction takes place by the electrochemical reaction and is assumed as an instantaneous reaction. This requires that oxygen concentration equals to zero at the Pt surface. Since zero assignment of mass fraction leads to non-convergence of the solution, it is assumed as a small value of 0.001 mass fraction.

All the remaining interfaces in the gas flow channel are assigned impervious to the nitrogen gas. The left boundary of the bipolar plate, top boundary, and bottom boundary are assigned thermal insulation to simulate a work case no-cooling system. Similarly, the Pt catalyst surface on the right side of Figure 3.2 is also assigned a heat flux boundary to represent that the entire heat generated from water formation is only passed into the cathode side.

The heat source is at the Pt surface of Figure 3.2 since water vapor formation by the electrochemical reaction is a surface phenomenon where the heat of reaction evolved is given as inward surface heat-flux at the Pt catalyst layer as in Figure 3.2. The expression for heat flux source at Pt surface is shown in Equation [3.9].

$$q_w = -2\varepsilon_s \Delta H_R \, j_{o_2} \qquad [3.9]$$

where, j_{o2} is the mass flux of oxygen flowing towards the Pt surface where it is instantaneously consumed by the protons coming from the other side and resulting in the formation of water vapor, ε_s is the fractional coverage of the Pt on the catalyst layer and ΔH_R is the heat of reaction in the formation of water vapor. In chapter 4, the fractional coverage of the Pt loading on the catalyst layer is varied.

3.4 Simulation strategy

The simulations are executed using COMSOL Multiphysics 4.4 software. Initially, geometry is created as per the schematic in Figure 3.2. It consists of three distinct domains by type of material. It consists of solid bipolar plates, a gas flow channel, and an array of micro-sized carbon cylindrical solids to represent the scaffold of carbon cloth used as a porous structured gas diffusion layer (GDL). There are five Multi-physics phenomena, namely: (1) laminar flow in the gas flow channel (compressible up to Mach number 0.2), (2) transport of concentrated species in the gas flow channel, (3) heat transfer by convection and conduction in the gas flow channel, (4) heat transfer by conduction in bipolar plate, (5) heat transfer by conduction in each of the solid cylinder in carbon fiber array representing the porous gas diffusion layer (GDL). The dimensions of the entire

cathodic portion are of a magnitude similar to the literature [132]. Although the gaps between carbon fiber are only a few micrometers, Knudsen diffusion is not imposed, but continuity is assumed and simulated successfully.

The initial velocity for laminar flow physics in the gas layer is assumed to be zero for all locations. The program was also found to converge on such an initial guess. The inlet velocity (V_{in}) of the gas layer is assigned four different values: 0.001 m/s, 0.01 m/s, 0.1 m/s, and 1 m/s. These are chosen to see the effect of low and high convection in the gas flow channel. The composition of inlet feed comprises oxygen, nitrogen, and water vapor (humidity). Since the concentrated species transport equation uses modified Fick's law restricts that none of the three components can be mathematically zero in numerical simulation, at the inlet for all the simulations, the water vapor mass fraction in the feed is kept as 0.01 (1% by Wt.). The oxygen mass fraction in the air is approximately 20%, and the rest is nitrogen. In the first part of the present study (presented in next chapter), the oxygen mass fraction varies below its value in ambient air and the chosen mass fractions of oxygen gas in the feed inlet are 0.2, 0.1, 0.05, and 0.01. The selection of this operating condition in the feed stoichiometry is a novel work as compared to the literature [18].

The modified Fick's law-based transport of concentrated gaseous species has an additional term in the form D_i^T .This accounts for the Soret effect, implying that there can be mass flux due to the temperature gradient. In the mathematical model, the density, thermal conductivity, and heat capacity of the gas phase are given as a function of temperature in Equation 3.10 (a-c).

$$\rho = \frac{\frac{p_1}{RT_1}}{\frac{w_{21}}{32}+\frac{w_{22}}{28}+\frac{w_{213}}{18}} \quad [3.10a]$$

$$k = w_{21} \times k_1 + w_{22} \times k_2 + w_{213} \times k_3 \quad [3.10b]$$

$$c_p = w_{21} \times c_{p1} + w_{22} \times c_{p2} + w_{213} \times c_{p3} \quad [3.10c]$$

Where, w_{21} represents oxygen mass fraction, w_{22} represents nitrogen mass fraction, w_{213} represents the water vapor mass fraction used in the simulation study.

The solid phases of the bipolar plate and gas diffusion layer fibre are assigned constant ρ, k, c_pvalues. They are represented in Table 3.1.

Table 3. 1 Properties of GDL carbon fiber structure (carbon cloth) and bipolar plate [133, 134].

Material	Property	Value
Carbon fiber	Thermal conductivity	180 W/ (m.K)
	Density	1780 kg/m^3
	Specific heat capacity	1520 J/ (kg. K)
Bipolar plate	Thermal conductivity	24 W/ (m.K)
	Density	2250 kg/m^3
	Specific heat capacity	690 J/ (kg. K)

Table 3. 2 Initial and boundary conditions of a steady-state and time-dependent study.

Parameters	Symbol	Value
Inlet velocity	V_{in}	0.001,0.01,0.1,1(m/s)
Inlet mass fraction	W_{21}	0.01,0.05,0.10,0.20
Inlet temperature	T_{in}	80 °C
Outlet pressure	P_O	1×10^5 Pa
Catalyst loading	ε_s	0.05,0.10,0.15,0.20
Amplitude	δ	0.01,0.02,0.03,0.04
Time Period	T_c	20 s

3.5 Solving methodology

A commercial finite element method (FEM) based software COMSOL Multiphysics (COMSOL Multiphysics 4.4a) was used to solve a three-dimensional coupled fluid flow, transient heat transfer, and mass transfer equations (Transport of Concentrated Species model). All the simulations were carried out on an HP workstation with two 3.10 GHz Xeon CPUs and 32 GB RAM running Windows 7 64-bit. The stages in the simulation are shown in Figure 3.3. Very fine mesh was created in the gas diffusion layer and the gas flow channel to ensure the accuracy of temperature distribution. Other components of the system were meshed using tetrahedral meshes of conventional size. The mesh size was determined based on the convergence research when the temperature differences between subsequent computations were less than 0.1%. This

investigation's beginning and maximum time steps were set to 0.01 and 0.01 seconds, respectively. It took around 72 hours to finish each simulation.

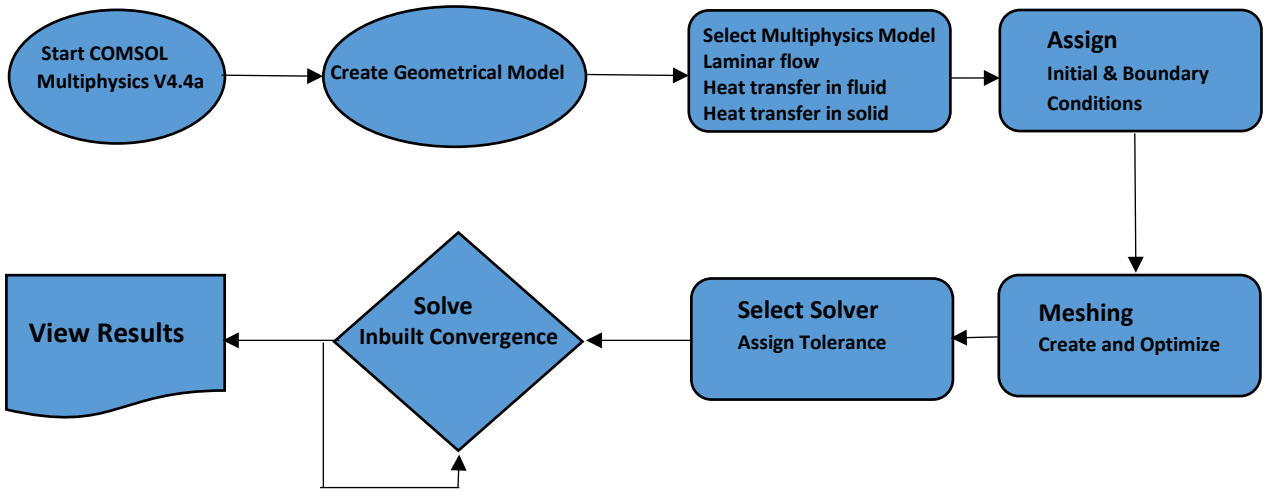

Figure 3. 3 Flow chart of COMSOL Multiphysics simulation processes.

The numerical calculations were done using tetrahedral, triangular, edge, and vertex elements, assuring independent mesh outputs. The MUMPS solver (Multifrontal Massively Parallel Sparse Direct) was used to solve the iterative matrix solution, enabling the solution of massive systems. One iterative Newton technique was devised with an initial damping factor of 1 and a minimum damping factor of 0.001. By default, all other numerical parameters were retained.

3.6 Meshing and Grid independent studies

The chosen meshing scheme is physics controlled, which means that COMSOL internally assigns small to large triangular meshes depending on location in the domain, whether close to Dirichlet, Neumann, or Robin boundary conditions. Out of the available options for mesh as coarse, normal, and fine, the normal mesh size is chosen because it is sufficient to resolve the temperature and concentration gradients even at the microscale in the carbon fiber (gas diffusion layer).

Since the phenomena in PEFC are very complex, a high quality of the computational cells is needed to receive a converged solution. Studies must be conducted to reach this convergent solution with low computational power and temporal grid independence. The balance between accurate results and computational time has to be carefully considered. Therefore, the primary analysis, such as grid-independent analysis, has to be done initially to ensure the quality of the

results [134]. These studies are carried out at an operating temperature of 60 °C, reactant relative humidity of 1%, and operating pressure of 1×10^5 Pa.

Table 3.3 shows a list of the three different meshes (coarse, normal, and fine mesh) used for grid independence study for various geometry considered in the present study. Figure 3.4 illustrates three different types of mesh: coarse, normal and fine. Figure 3.5 shows the grid-independent studies performed for cathode side PEM fuel cells. The total number of grid elements is varied by changing the distance between the adjacent nodes along the channel, plane, and in-plane in the fuel cell. There is a 0.078% change in the oxygen mass fraction at the outlet noticed with a change in mesh count by 40% (i.e., normal 65 lakhs to fine 1 crore). These simulations were performed using an HP-DL 380 G8P Server with 128 GB of RAM and a 16 Core Xeon E5-2650 processor. As a result, the normal mesh was taken into consideration for the rest of the simulations.

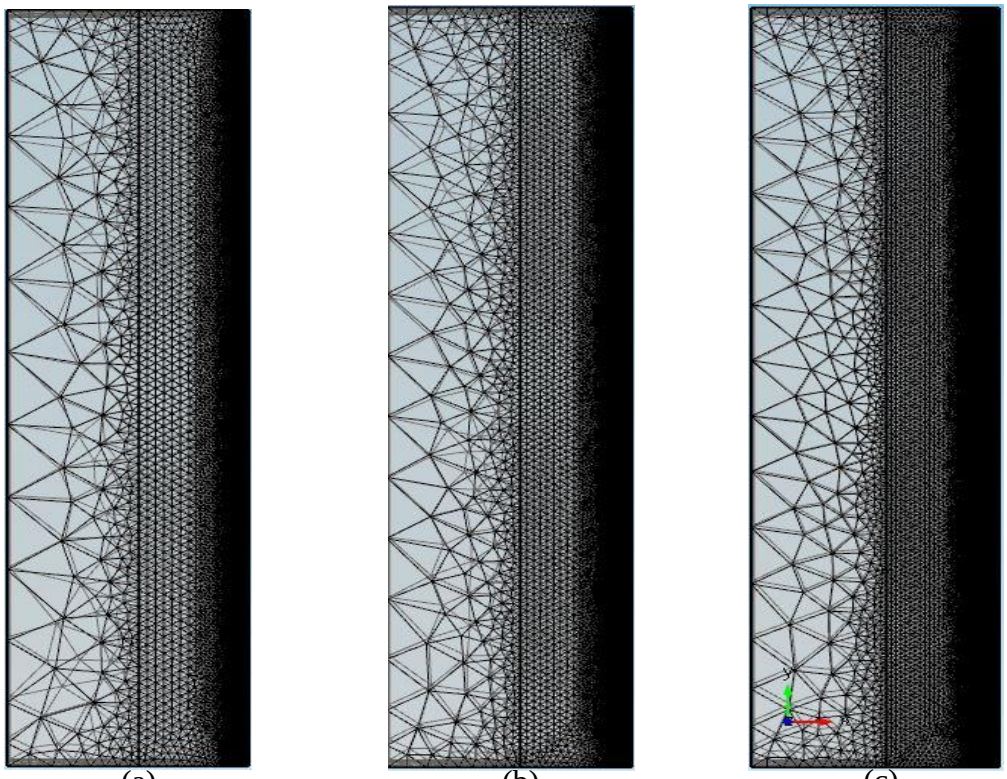

(a) (b) (c)

Figure 3.4 (a) Coarse (b) normal and (c) fine mesh of the cathode side of PEM fuel cell

Table 3.3 Complete mesh details

Mesh type	Coarse	Normal	Fine
Tetrahedral elements	1135437	6591450	16622812
Triangular elements	255264	888682	1520760
Edge elements	53702	102202	140294
Vertex elements	3016	3016	3016

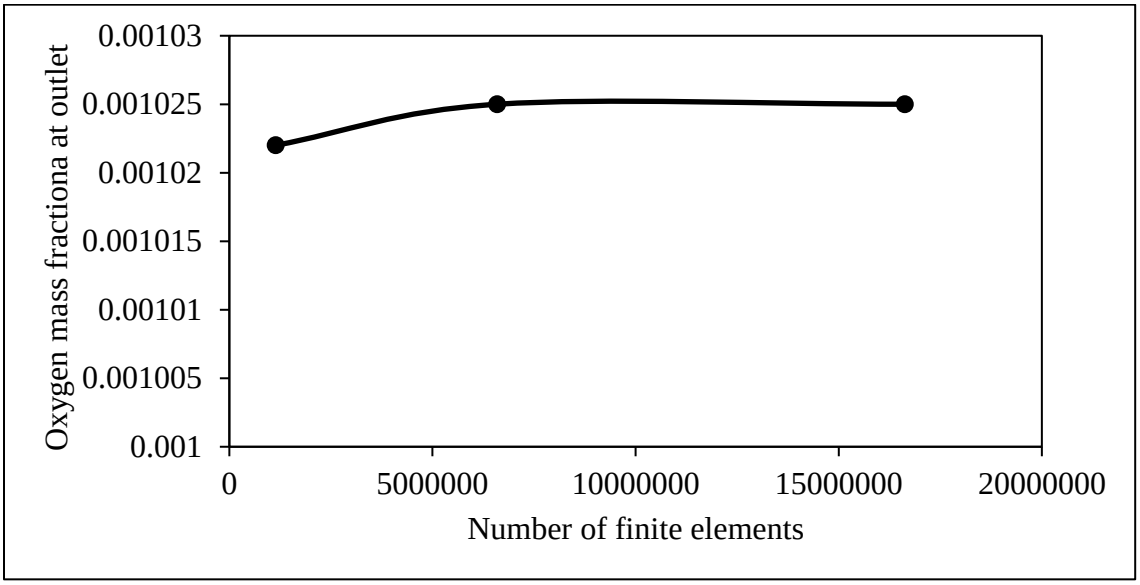

Figure 3.5 Grid independence study showing the variation of oxygen mass fraction at the outlet with different mesh sizes

3.7 Model validation

The validation of the modelling methodology was carried out by modelling a single cell with a straight channel design using COMSOL and comparing the results of the simulation against the experimental work reported by Alex [142.] The boundary conditions employed in the simulation are listed in Table 3.4 and Table 3.5 lists various operating conditions used for the validation of the modelling methodology. A very good agreement between the experimental results of Alex [142] and the COMSOL simulation can be seen from the comparison of the respective polarization curves as shown in Figure 3.6. The maximum deviation between the model results and the experimental results noticed is less than 3%. Therefore, the modelling methodology and simulation

strategy are considered as validated and the same has been used for the modelling of local hot spot formation and developing strategies for mitigation of the hot spots in PEM fuel cells.

Table 3.4 Boundary conditions

Domain	**Temp. T (K)**	**Molar Wt. (kg/mol)**	**Electric potential (V)**	**Gas composition at inlet**
Inlet-a (Anode)	333 K (60 ºC)	0.032 0.002 0.018		O_2 mass fraction 0 % H_2 mass fraction 0.743% H_2O mass fraction 0 %
Inlet-c (Cathode)	333 K (60 ºC)	0.032 0.002 0.018		O_2 mass fraction 0.228 % H_2 mass fraction 0 % H_2O mass fraction 0.023 %
Outlet-a	333 K			
Outlet-c	333 K			
Terminal-a	333 K		0	
Terminal-c	333 K		0.9 V	

Table 3.5 Operating parameters

Parameter	**Value**
GDL porosity	0.4
GDL permeability	1.18×10^{-11} (m^2)
GDL electric conductivity	222 (S/m)
Anode inlet flow velocity	0.4 (m/s)
Cathode inlet flow velocity	0.2 (m/s)
Anode viscosity	1.19×10^{-5} (Pa.s)
Cathode viscosity	2.46×10^{-5} (Pa.s)
H_2-H_2O binary diffusion coefficient	1.055×10^{-4} (m^2/s)
N_2-H_2O binary diffusion coefficient	2.95×10^{-5} (m^2/s)
O_2-N_2 binary diffusion coefficient	2.75×10^{-5} (m^2/s)
O_2-H_2O binary diffusion coefficient	3.23×10^{-5} (m^2/s)
Cell operating temperature	333.15 K (60 ºC)

Reference pressure	101×10^3 (Pa)
Cell voltage	0.9 (V)
Oxygen reference concentration	40.88 (mol/m^3)
Hydrogen reference concentration	40.88 (mol/m^3)
Membrane conductivity	9.82 (S/m)

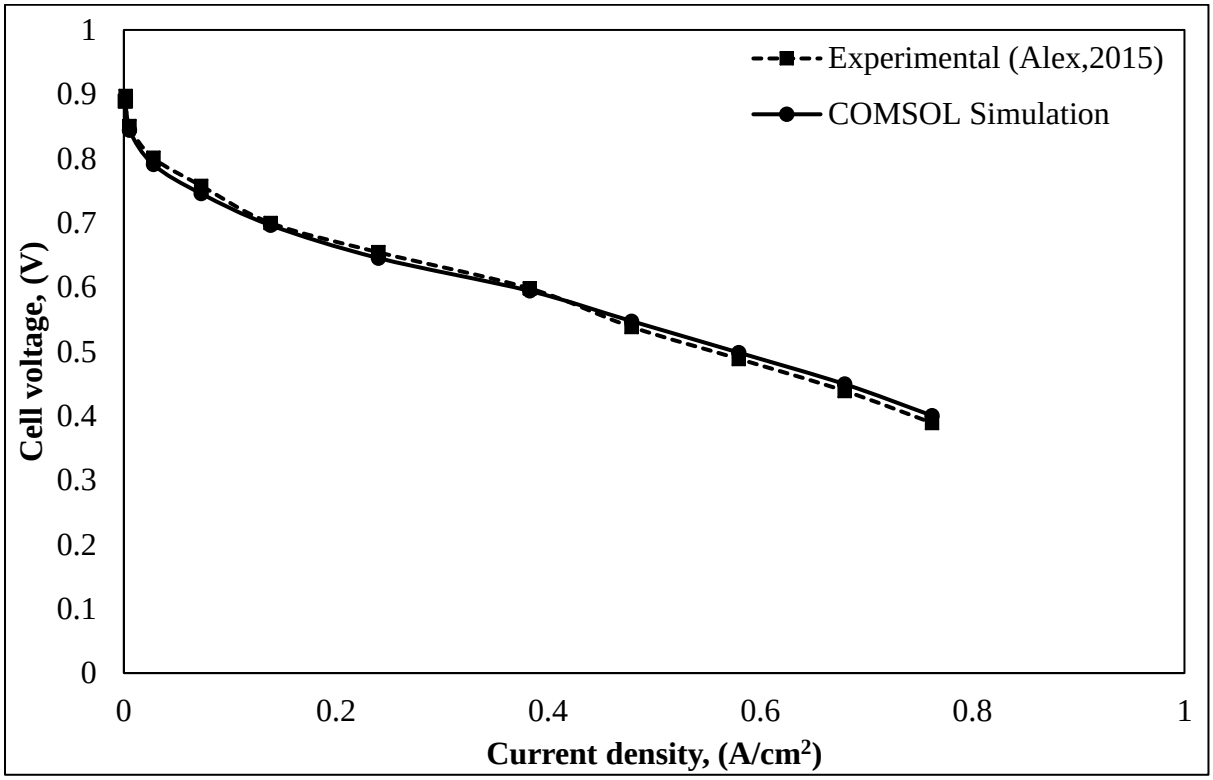

Figure 3.6 Validation of the modelling methodology by comparing the results of COMSOL model against the experimental results of Alex, 2015 [142].

Chapter – 4

Optimum supply and Utilization of Pure Oxygen

Chapter – 4

Optimum supply and Utilization of Pure Oxygen

This chapter addresses the first and second objectives of the current study using a 3D geometry of the cathode side of a proton exchange membrane fuel cell (PEMFC) since the cathode reaction is the limiting step. The oxygen and nitrogen mass fraction in the inlet feed on the cathode side is varied as well as the total feed flow rate consisting of traces of water vapor. The worst-case scenario of no-cooling with an insulated bipolar plate is assumed. This is to test the maximum thermal effect on the membrane layer. The flow, heat, and mass transfer multi-physics phenomena in the gas diffusion layer and scaffold layer are simulated using a simplified geometry in COMSOL Multiphysics 4.4 software. The electrochemical reaction of oxygen reacting with protons (H^+) and electrons (e^-) at the Pt catalyst surface is considered an instantaneous reaction at the catalyst surface. A performance factor comprising power density generated, the maximum temperature and oxygen utilization is defined. It is optimized to determine the optimum oxygen mass fraction in feed and net feed flow rate that gives long life thermally and low operating cost of a PEM fuel cell. Hot spot occurrence is noticed in the results. The results obtained from the simulation are discussed in detail in the following sections.

4.1 Description of the case and the geometry considered

This simulation work assumes that the inlet gases on the cathode side of the PEM fuel cell consist of oxygen and nitrogen supplied from independent storage cylinders. Hence, oxygen percentage could vary over a wide range. In particular, oxygen percentage below air (21%) was not explored, which is very relevant for submarine applications. In this work, the oxygen fraction in the cathode side inlet is modified, and only the cathode side of a PEM fuel cell is modeled and simulated for optimization. The assumptions are that the worst-case scenario of the thermally insulated bipolar plate and the entire heat generated due to water vapor formation being transferred into the cathode side gas diffusion layer is considered, as shown in Figure 4.1(a) below. The effect of water vapor condensation is not taken into consideration. The performance parameter is proposed to be measured in terms of oxygen conversion, maximum temperature, and power density. Below are descriptions of the findings, a model of the cathode side, and simulations.

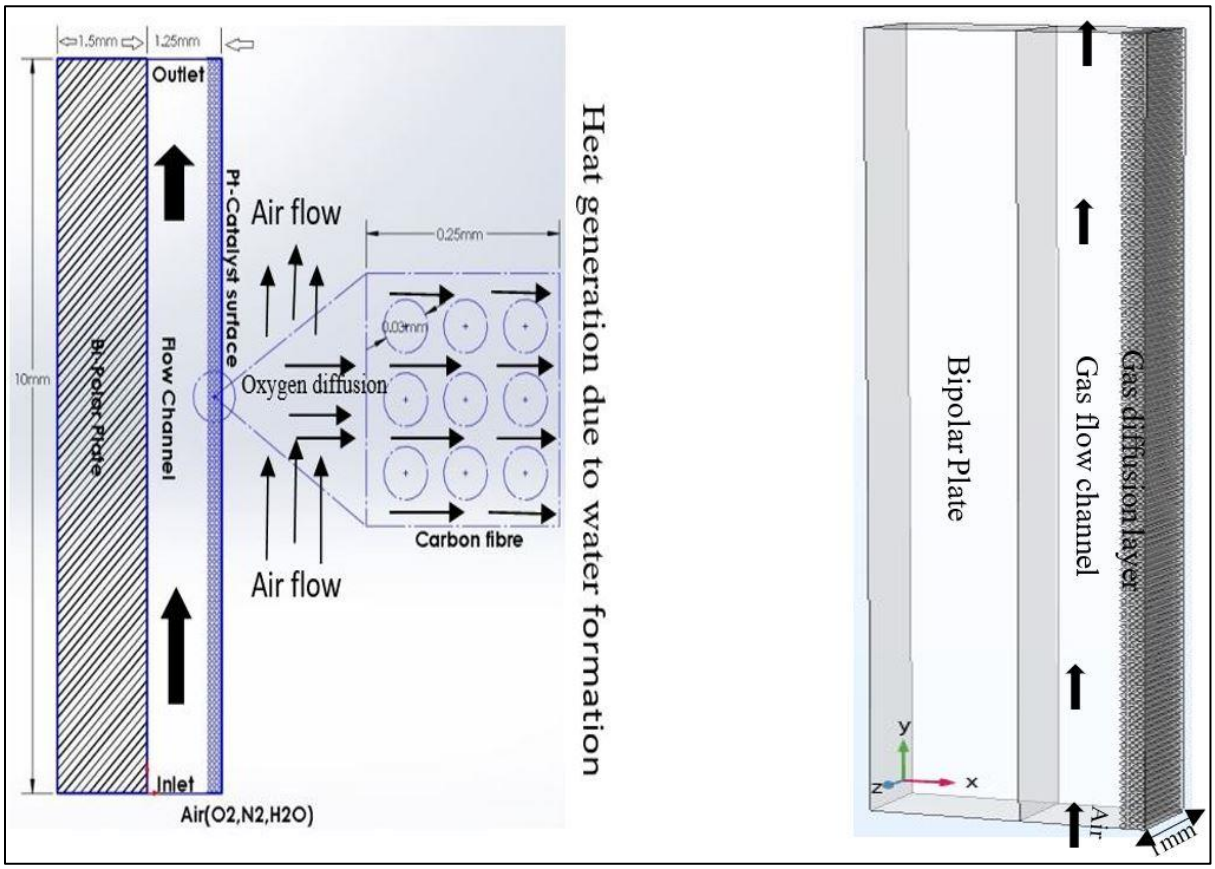

(a) (b)

Figure 4.1 (a) Cross-sectional view of the cathode side of a PEM fuel cell (b) used for simulation in this study.

PEM Fuel cell with the cathode side containing bipolar plate, gas flow channel, and gas diffusion layer represented as three layers of orderly arranged micron-sized solid cylinders, as shown in above Figure 4.1 (b) is considered as the computational domain. The dimensions of various parts of the domain are as follows: bipolar dimensions (1.5mm×10mm×1mm), an inlet gas flow channel (1mm×10mm×1mm), and a gas diffusion layer (0.25mm×10mm×1mm).

4.2 Operating conditions

The present studies are carried out by varying oxygen inlet velocity and mass fractions. Instead of pure oxygen gas, atmospheric air is considered on the cathode side in the present study. Material properties considered for the present simulations are listed in Table 3.1 (previous chapter). The following procedure found the best combination of reactive gas flow velocities and oxygen mass fractions in terms of the optimum performance factor. The inlet oxygen mass fraction is determined

for each simulation based on the total nitrogen and water vapor gases, and additional parameters are shown in Table 4.1. This study examines the performance factor of PEM fuel cells by changing the oxygen mass fraction from 20% to as low as 1%.

Table 4. 1 The operating parameters and boundary conditions used in this current study.

Parameters	**Symbol**	**Value**
Inlet velocity	V_{in}	0.001,0.01,0.1,1 (m/s)
Inlet temperature	T_{in}	80 °C
Outlet pressure	P_O	10^5 Pa
Catalyst loading	ε_s	0.20
Oxygen mass fraction at the inlet	w_{21}	0.01,0.05,0.10,0.20

Reactant availability at the catalyst surface has a significant impact on the performance of a fuel cell. Pure oxygen mixed with nitrogen must be supplied and used on the cathode side of PEMFCs in order to ensure thermal stability, velocity and oxygen mass fraction without waste. The reactant feed velocities and mass fractions are varied in the present work while running at constant operating temperature, pressure, and percentage of Pt-catalyst coverage.

4.3 Temperature distribution for different feed velocity and oxygen mass fraction

The temperature slice maps obtained from a steady-state simulation of the above cathode portion of the PEM fuel cell are shown in Figure 4.2.

It can be noticed from the above Figure 4.2 that the highest temperature or hot spot patch occurs close to the entrance near to catalyst layer. Nevertheless, as the feed velocity of the reactive gas is increased, this local hot spot gets spreads along the length of the gas flow channel close to the Pt-catalyst surface and carbon fiber layer (GDL). It is essential to record maximum surface temperature so that the operating condition can be suitably selected. The maximum temperature is below the safe operating temperature of the membrane layer, which is present immediately adjacent to the Pt surface, as in Figure 4.1(a). The obtained maximum surface temperature for various feed oxygen compositions and feed velocity at the inlet is plotted in Figure 4.3.

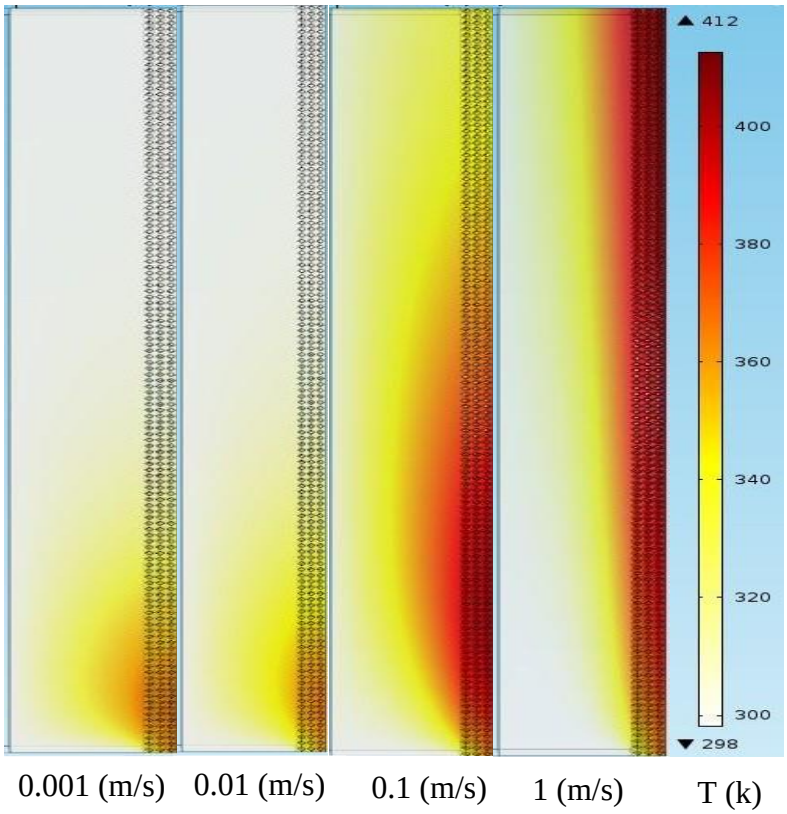

Figure 4.2 Temperature color maps in the gas diffusion layer for various inlet velocities and an oxygen inlet mass fraction of 0.2.

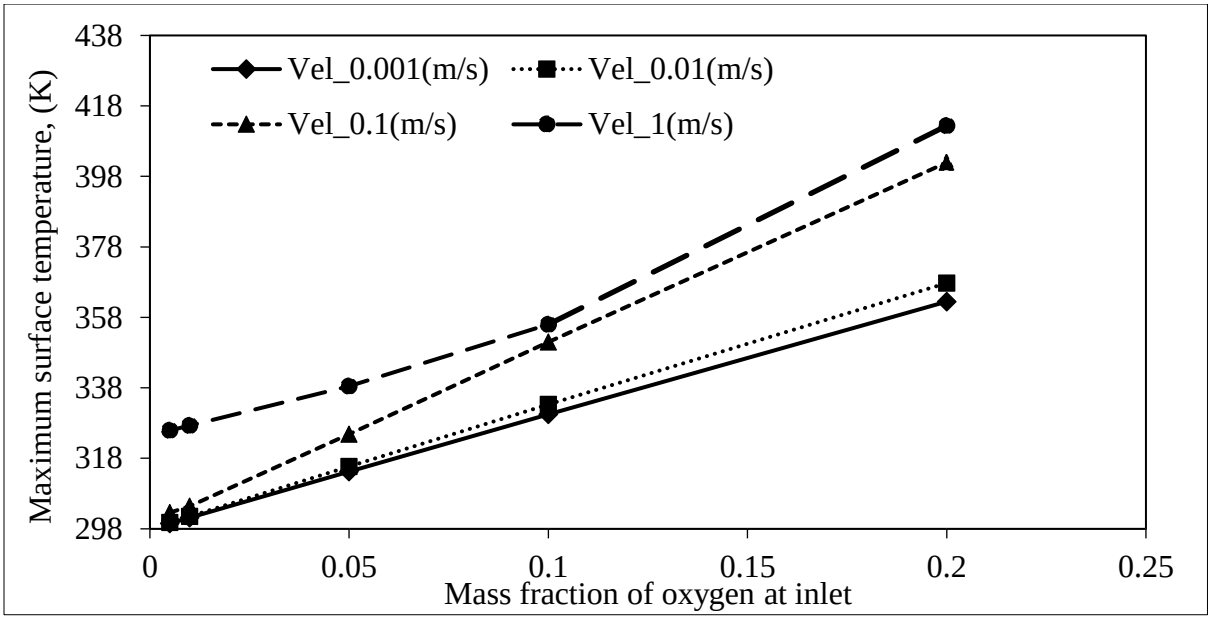

Figure 4.3 The maximum surface temperature in the gas flow channel for various oxygen mass fractions in the inlet.

The relationship between the oxygen mass fraction and the feed velocity at the inlet is shown in Figure 4.3. The maximum surface temperature obtained for the inlet feed velocity is 1 (m/s), and the oxygen mass fraction is 0.2. When a higher oxygen mass fraction is fed, the oxygen availability will increase, and hence, oxygen consumption also increases. The overall surface temperature rise was owing to electrochemical reactions at the catalyst-membrane layer interface, which consumes a greater amount of the available oxygen.

4.4 Oxygen conversion percentage

Color maps of oxygen concentration distribution at a steady-state in the flow channel for various feed flow rates and inlet oxygen concentrations of 0.2 mass fractions (corresponding close to the air) are presented in Figure 4.4. As expected intuitively, more oxygen is consumed for lower feed velocities. The conversion of oxygen is calculated as $1 - \frac{w_{o_2}(\text{outlet})}{w_{o_2}(\text{inlet})}$. This conversion in terms of percentage is plotted in Figure 4.5 for various inlet oxygen mass fractions and feed velocities.

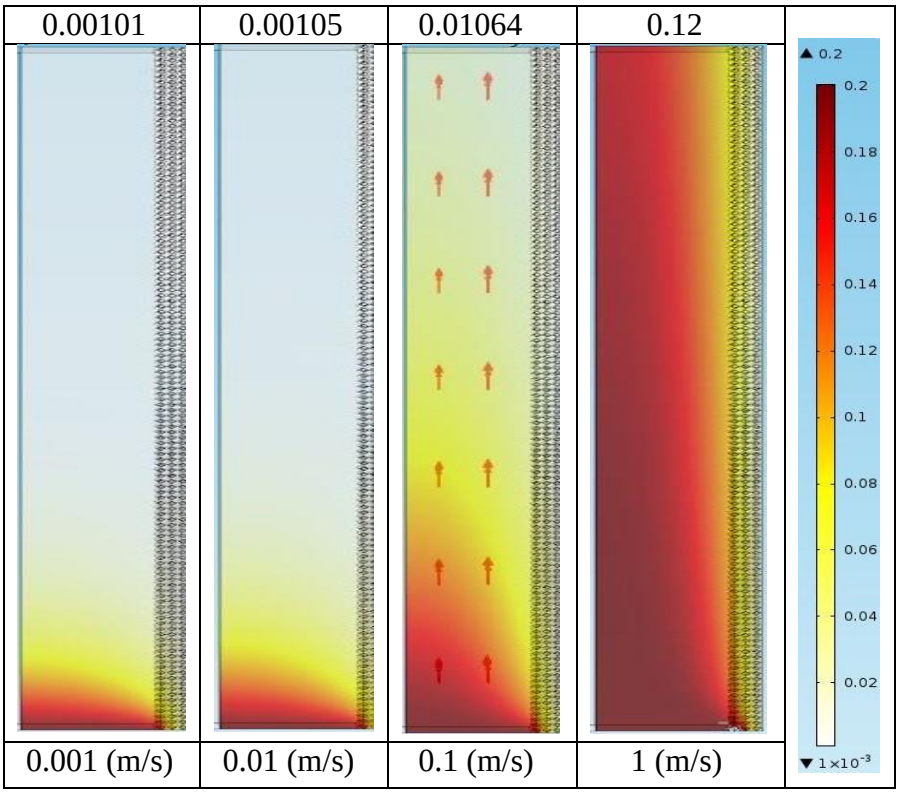

Figure 4.4 Color map of the oxygen mass fraction in the gas flow channel and gas diffusion layer for an inlet oxygen mass fraction of 0.2.

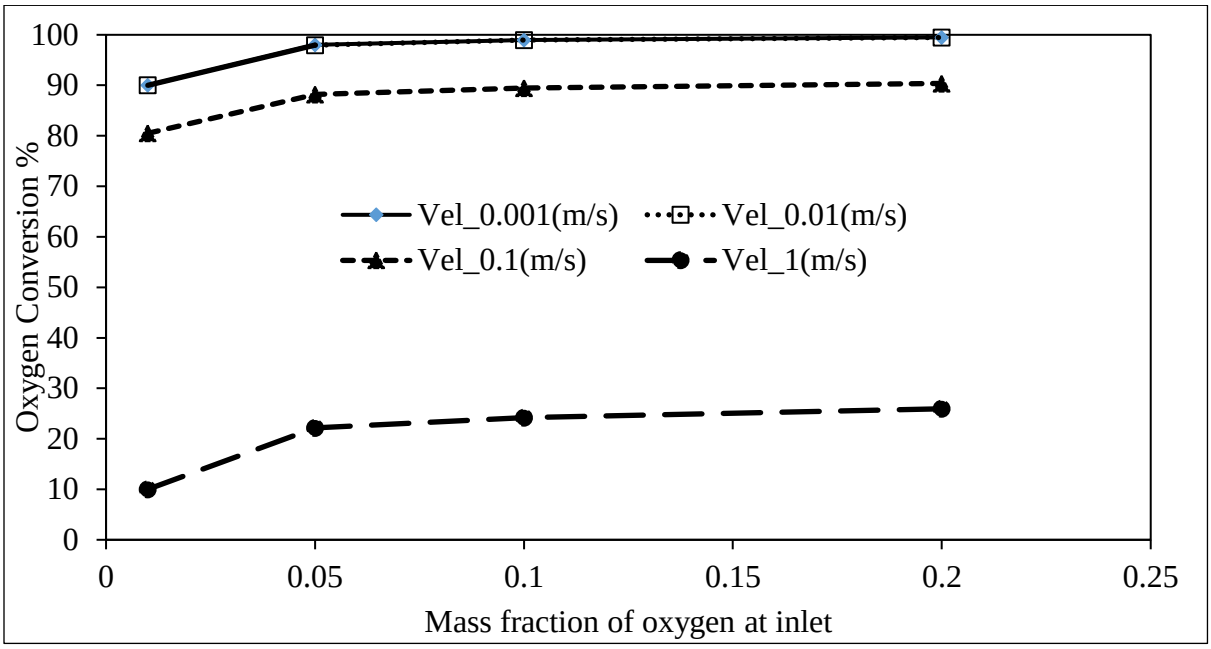

Figure 4.5 Oxygen conversion calculated at the outlet for various oxygen mass fractions in the inlet and various feed flow rates.

It can be noticed that the conversion percentage of oxygen is the highest for low inlet feed velocities, which can be explained by the fact that for low velocities, there is sufficient residence time for the oxygen to diffuse through the carbon fiber layer and be consumed at the Pt surface. Hence, the conversion is high for low feed velocities this result is also important towards characterizing the performance of PEMFC because less wastage of fuel increases the economic viability of this novel energy source. Another variable to be evaluated is the current produced by the fuel cell for various feed conditions. Since the oxygen consumption at the Pt surface is assumed to be an instantaneous electrochemical reaction, the mass fraction of oxygen at the Pt surface is assumed to be negligible but as a small mass fraction of 0.001. If it is assigned exactly zero, the simulation does not converge owing to the appearance of a mass fraction of oxygen (and all species) in the denominator of some of the expressions used to evaluate the thermodynamics and transport properties. Hence, the convergence of the COMSOL Multiphysics 4.4 code is achieved by the present approach. The flux of oxygen at the Pt surface is proportional to the current density. To examine the performance of the PEMFC in terms of current generated, oxygen flux at the Pt surface is plotted against the mass fraction of oxygen in the inlet for various feed velocities as in Figure 4.6.

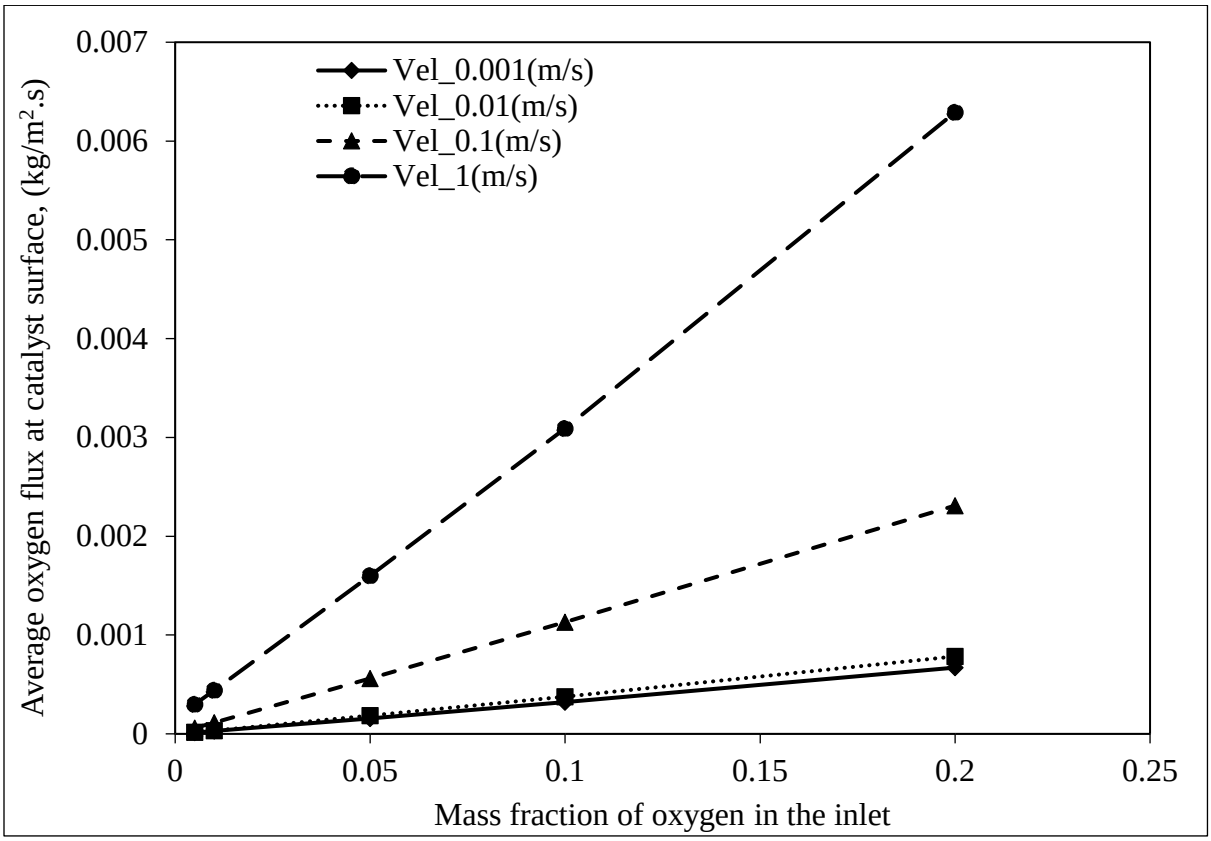

Figure 4.6 Average consumption rate or mass flux of oxygen at Pt-catalyst layer for various oxygen mass fractions in the inlet and various feed velocities

It can be noted from Figure 4.6 that current density increased monotonically with increasing the inlet oxygen mass fraction. These current density values can be transformed into power density produced using the literature correlation or the polarization characteristics of PEM fuel cell as in Figure 4.7 [129].

4.6 Contour plot of performance factor

It shows that there is a maximum performance factor possible, and it is in the regime of medium feed velocities and medium oxygen mass fraction in the feed. Thus, the modeling and simulation results of the present work have provided a greater insight into selecting the operating conditions on the feed of fuel on the cathode side for higher performance, optimization, and intensification of PEMFC. Thus, there are three performance variables namely maximum temperature, oxygen conversion, and electrical power density at Pt surface. Optimum temperature was assumed as 333

K, beyond which the membrane becomes deteriorates. Based on their direct or inverse proportionality, an overall fuel cell performance factor is defined as in Equation [4.1]

$$\text{Performance factor} = \frac{\text{Power density} \times \text{Oxygen conversion at the outlet}}{\text{ABS(Maximum Temperature} - \text{Optimum Temperature)}} \quad [4.1]$$

This performance factor is evaluated for various inlet feed gas velocities and oxygen mass fractions in feed and is plotted in Figure 4.8 as a contour map. Figure 4.8 shows the maximum performance factor possible of the PEM fuel cell is high, and it is in the regime of medium feed velocities of 0.01 m/s and medium oxygen mass fraction (0.1-0.14) in the feed.

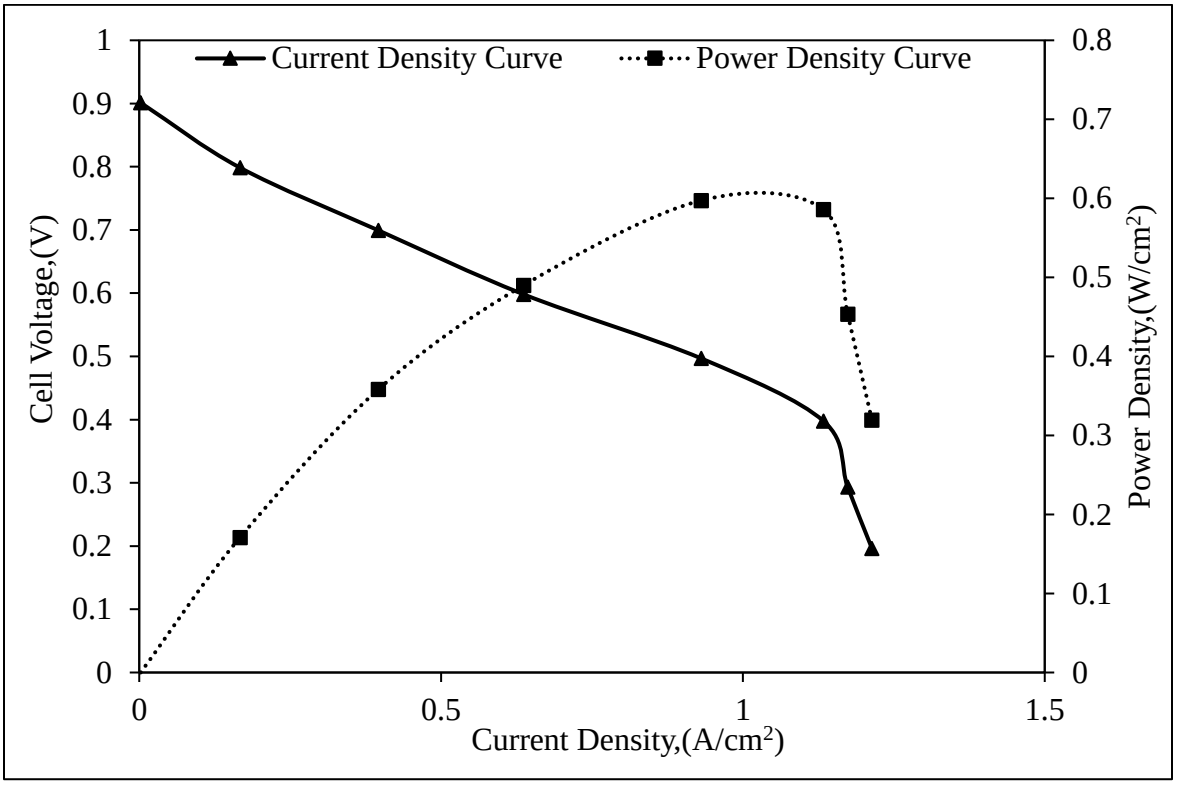

Figure 4.7 The polarization characteristics of a PEM fuel cell [129].

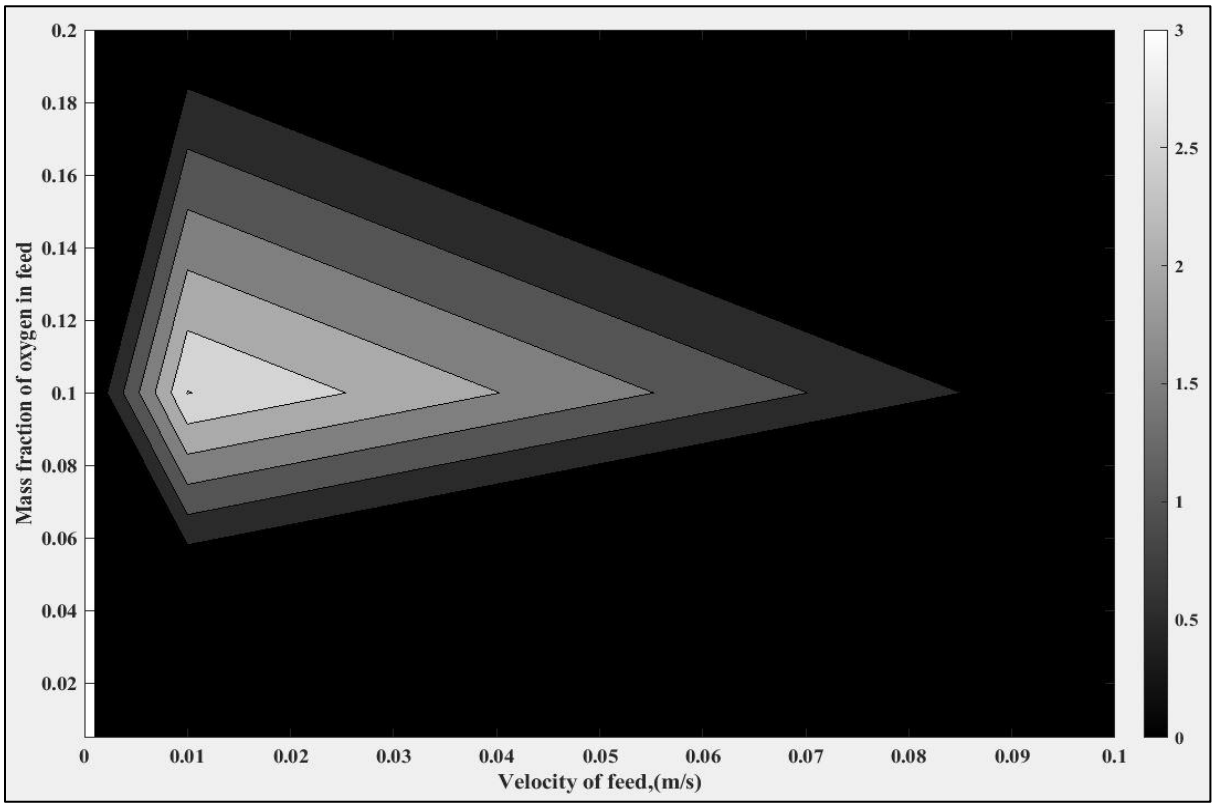

Figure 4.8 Contour map of the fuel cell performance factors for various oxygen mass fractions in the inlet and velocity of feed.

4.7 Comparison of the simulation with experimental data

The experimental findings of the literature reference [130] are found to be suitable for comparing the simulation results of the present work. The authors in the reference paper [130] have conducted experiments on the PEMFC by varying hydrogen flow rate, oxygen flow rate, current density, and temperature. By doing so, the voltage obtained from the PEMFC was tabulated [130]. These findings are reframed in terms of performance factor, defined as below in Equation [4.2].

$$\text{Performance Factor}_{\text{Expt.}} = \frac{\text{Power Density}}{\text{ABS(Temperature}-70°\text{C)}*\text{H}_2\text{ flow rate}*\text{O}_2\text{ flow rate}} \quad [4.2]$$

This performance factor from experiments [130] is represented against operating temperature for various hydrogen and oxygen flow rates at the current density of 1 (A/cm^2) in Figure 4.9.

In Figure 4.9, the performance is high for low flow rates of hydrogen and oxygen rather than for high flow rates. Another experimental investigation on the effect of oxygen flow rate on PEMFCs

performance is presented in Figure 4.10 [132]. It can be noticed from Figure 4.10 that a maximum power density is possible at a certain oxygen flow rate on the cathode side of the PEM fuel cell. Thus, the present modeling and simulation efforts of PEM fuel cells have opened up new areas for an investigation to optimize PEM fuel cells for longevity.

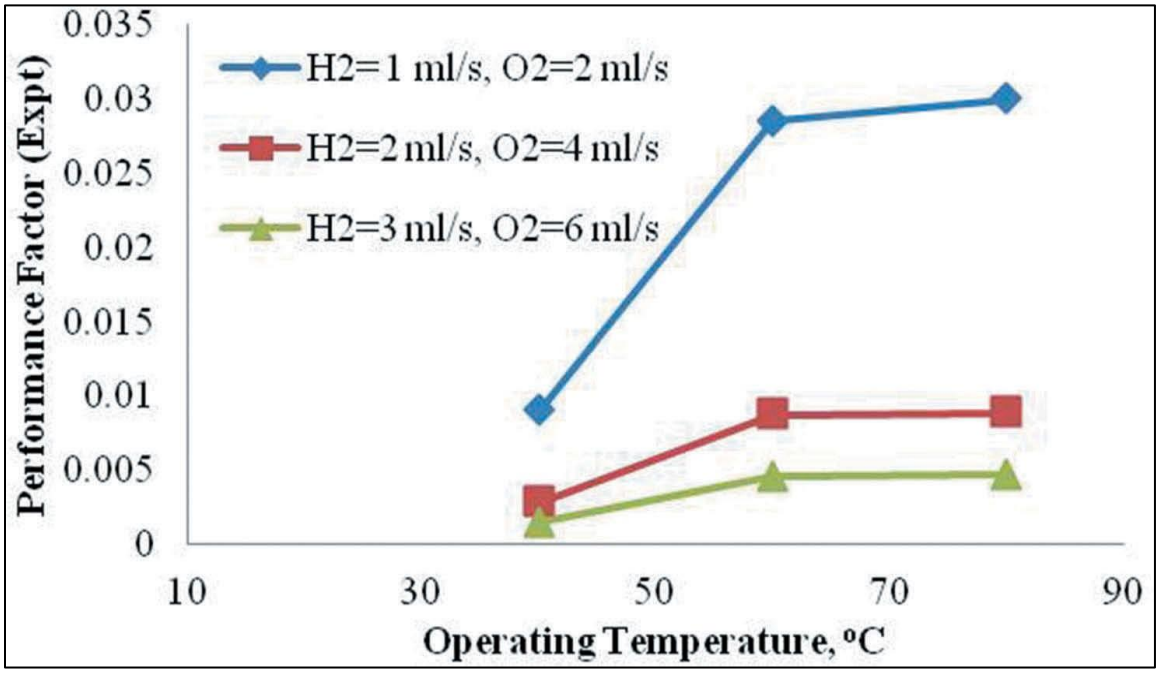

Figure 4.9 Performance factor as per Equation [4.2] from experimental data [130]

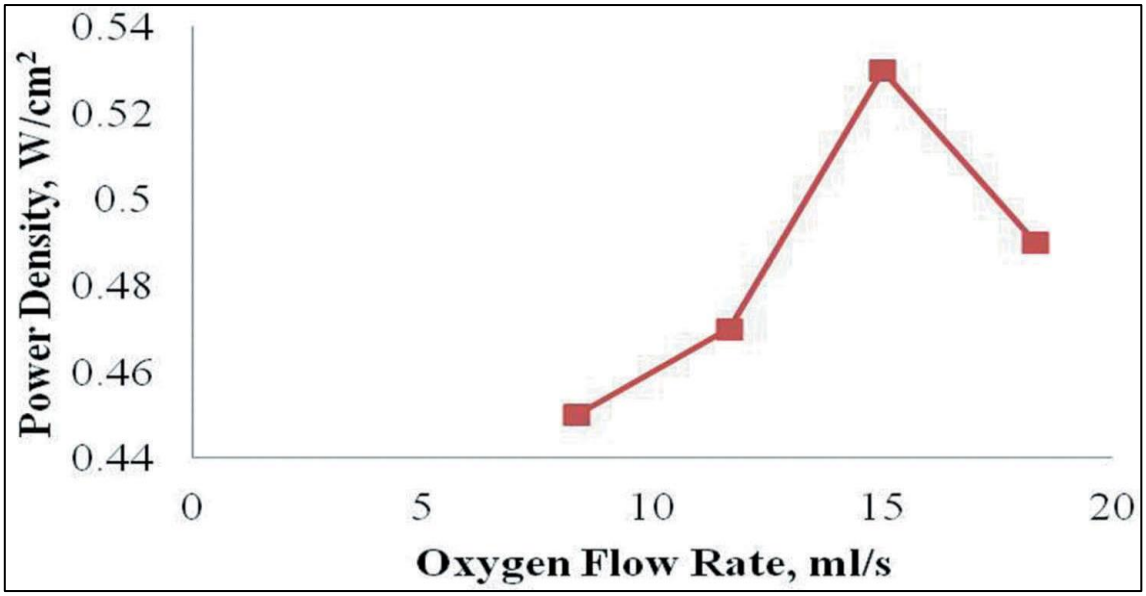

Figure 4.10 Representation of PEM fuel cell power density obtained at various oxygen flow rates on the cathode side with hydrogen flow rate as 5 ml/s, current density as 1 A/cm^{2,} and temperature as 60 °C [132].

According to Khazaee and Ghazikhani [132], a higher power density may be produced on the cathode side when the purity of the oxygen is higher; nevertheless, the temperature penalty on the membrane will be larger. Hence the present work discloses the possibility of high performance of a PEM fuel cell which can be verified by an experimental study with an oxygen percentage less than the air on the cathode side.

4.8 Summary

In this study, a single-cell straight channel cathode side of the PEMFCs was first simulated in the 3-D model using COMSOL Multiphysics, and the results were compared to those obtained from experimental data published in the literature. Based on this simulation analysis, the following conclusions can be summarized:

- A simplified geometry and boundary conditions were considered for simulating flow, heat transfer, concentrated species transport and instantaneous surface reactions on the cathode side of a PEM fuel cell.
- The temperature maps obtained from a steady-state simulation of the cathode portion of PEMFC show that the highest temperature or hot spot occurrence close to the entrance.
- As expected intuitively, oxygen is converted or utilized more effectively for lower feed velocities because of high residence time. By combining multiple factors of low-temperature requirement, high conversion of oxygen, and high-power density at a catalyst surface, the mass fraction of oxygen in feed should be less than that in the air for achieving better performance of the PEM fuel cell.
- According to the literature [132], higher power density may be produced on the cathode side when the purity of the oxygen is higher; nevertheless, the effect of hot spots on the membrane will be severe. Hence, the present work discloses the possibility of high performance of a PEM fuel cell, which can be verified by an experimental study with an oxygen percentage less than that of air on the cathode side.
- The study (as shown in Figure 4.8) reveals that an inlet velocity of 0.01 m/s for the reactant gas is ideal for avoiding excess use of pure oxygen and nitrogen mass fractions, while an oxygen mass fraction of 0.1- 0.12 is optimal for the PEM fuel cell to operate appropriately.
- In the entrance region, hot spot patches are detected in the gas diffusion layer (GDL), close to the membrane layer. The optimal oxygen and nitrogen mass fractions of 0.14, 0.85, and

- 0.01 for water vapor (relative humidity) are calculated to produce better performance of PEMFC.

According to the performance factor parameter, this study showed that the cathode-side of the PEM fuel cell operates at its best when using pure oxygen, with the optimal velocity of the inlet reactant gas being 0.01 m/s. The optimized mass fraction and inlet velocity values are obtained by comparing various inlet mass fractions and inlet velocity values. The local hot spot occurrence was also shown in this chapter using the developed non-isothermal model. The present 3-D model has been reduced to a 2-D model, and transient simulations have been conducted in the next chapter to identify the formation of the hot spot and propose different strategies for mitigating the hot spots.

Chapter -5

Hot spot identification and mitigation using 2D simulations

Chapter -5

Hot spot identification and mitigation using 2D simulations

It was shown in the previous chapter that a hot spot was formed close to the entrance of the PEM fuel cell cathode side near the membrane layer. The present study aims to identify local hot spot patch as well as propose mitigation strategies. COMSOL Multiphysics was used to conduct time-dependent simulations on a 2-D model of the cathode portion of the PEM fuel cell. The start-up dynamics show that hot spot build-up and its expansion are time taking processes. In the present chapter, two strategies are proposed to mitigate hot spots: first, introducing bumps in the reactive gas flow channel and, secondly, supplying a higher fraction of nitrogen relative to oxygen on the cathode side of the straight flow channels. Parametric studies on both techniques were conducted by varying the size of the bump, the amplitude of the cyclic nitrogen gas composition and the Pt-catalyst fractional coverage. Both strategies significantly decreased hot spot patch temperature, enhancing membrane layer endurance. Finally, an approach that combines the two proposed techniques is also analyzed.

This chapter addresses the third objective of hot spot mitigation using bumped channel design and the fourth objective of use of cyclic inlet on the hot spot removal.

Oxygen is consumed at the Pt catalyst surface, where it reacts with hydrogen ions to form water vapor along with the heat of the reaction at the cathode compartment [144]. A 2-D model containing the bipolar plate, gas diffusion layer (GDL), scaffolds of carbon cloth and the platinum catalyst fraction, the effect of operating variables such as the oxygen mass fraction in the inlet stream and the velocity of the gas mixture on the development of local hot spots (localized high-temperature regions) on the GDL were investigated (Chapter 4). In this investigation, an operational strategy is introduced and applied for the first time, potentially being used to offset the detrimental influence on the membrane.

5.1 Description of the case and the geometry considered

When PEM fuel cells operate for a long time, a local hot spot patch develops near the entrance of gas diffusion, catalyst, and membrane layers. This damages the membrane layer and causes it to

rupture. One of the leading causes of the breakdown of the PEM fuel cell is polymer electrolyte membrane deterioration.

One of the main problems is finding the local hot spot patch temperature by numerical simulation and how to mitigate it once detected. In the first part of this work, a two-dimensional cathode side PEM fuel cell geometry similar to the previous chapter shows how start-up thermal dynamics can be used to find the local hot spot patch. In the second part of this work, two approaches to mitigating the local hot spot temperature are proposed. The first approach involves using a straight gas flow channel with bumps in the flow path to reduce the hot spot temperature. In the second approach, using an oscillatory oxygen and nitrogen gas stream in the straight gas flow channel is proposed to reduce the hot spot temperature.

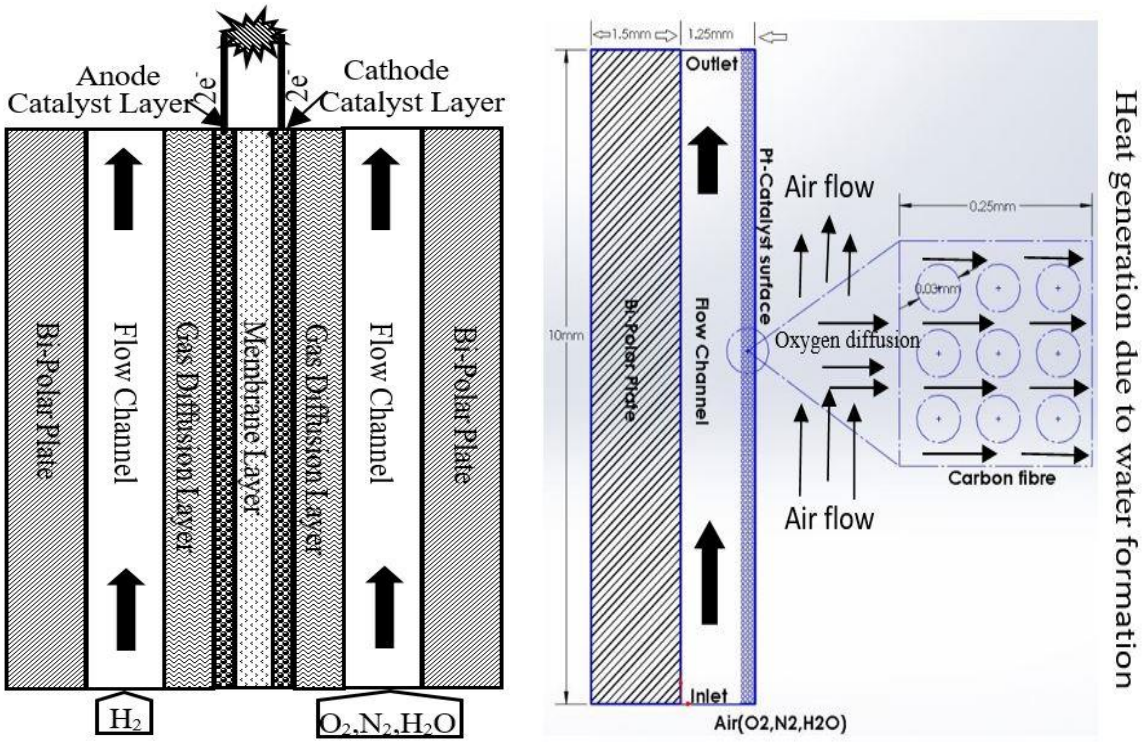

Figure 5.1 (a) Schematic of a PEM fuel cell (b) 2D computational model with dimensions of the cathode side of a PEM fuel cell.

The base value of the composition and velocity of the oxygen-nitrogen gas mixture is taken from the previous Chapter 4. The Pt catalyst coverage fraction at the interface varies. The heat source at the wall is due to the surface reaction between the oxygen, protons, and electrons to produce water vapor. There are two distinct parameters, namely, the amplitude (δ) of the oxygen and

nitrogen gas mixture oscillatory composition at the inlet and the catalyst coverage fraction (ε_s) at the catalyst interface are varied to study the local hot spot patch temperature. After obtaining the T_{max} or the hot spot temperature over a time period of, i.e., 20 sec, a performance factor is defined to find the optimum values of the amplitude (δ) and catalyst coverage fractions (ε_s). The numerical modeling methods, findings of the bumping channel design, oscillatory composition supply, and insights gained from the time-dependent model are detailed in the sections that follow.

5.2 Operating conditions

The present studies are carried out at boundary conditions as specified in section 3.3.7 of Chapter 3. The feed velocity in this chapter is 0.01 m/s, and the operating temperature of 333.15 K (60°C) was used as the reference temperature.

5.3 Constant composition and cyclic supply

At the inlet boundary (Figure 5.1 b), a gas mixture of specified composition (weight fraction) of oxygen (0.14), nitrogen (0.85), and a minute amount of water vapor (0.01) is fed at a velocity of 0.01 m/s. A lower oxygen composition than atmospheric air was chosen based on the study's conclusions reported in Chapter 4. This constant composition boundary condition is used to depict hot spot formation and the first hot spot mitigation strategy proposed in this study. In the second strategy, cyclic inlet gas mixture composition is introduced as a novelty. The inlet nitrogen and oxygen weight fractions are assigned as the cyclic composition as Equation 5.1 (a) -5.1 (b). This is to pass gas with higher nitrogen frequently enough to purge the hot spot in the GDL. When the higher composition of the nitrogen gas flow is supplied, it does not react, and the oxygen will be less available at the Pt surface and hence reduces the reaction rate, which in turn reduces j_{O2} the flux towards the Pt surface and finally reduces the wall heat flux (as mentioned in the previous chapter). The inlet mass fraction of the water vapor (relative humidity) at the catalyst is kept at a value of 0.01 for all the simulations.

$$N_2 = 0.9 + \delta + \delta * \sin(\frac{2\pi t}{T_C}) \quad [5.1a]$$

$$O_2 = 0.09 - \delta - \delta * \sin(\frac{2\pi t}{T_c}) \quad [5.1b]$$

$$H_2O = 0.01 \quad [5.1c]$$

The equations 5.1(a) -5.1(c) represent the sinusoidal or oscillatory inflow composition of the three gaseous components in the inlet of the cathode side. These are framed so that the sum of the three fractions of oxygen, nitrogen and water vapor equals 1 at any point in time. Here, δ is the amplitude of nitrogen and oxygen oscillatory compositions. In the inlet boundary conditions, the amplitude of the oscillatory composition (δ) ranges from 0.01 to 0.04. The time-period (T_c) has been taken as 20 seconds in the present simulation. Table 3.1 in Chapter 3 shows the material properties considered in the current model.

5.4 Grid Independent Study

In order to present results that are not grid-sensitive, the grid-independent study was conducted by considering three different sizes of the computational mesh, such as 150918, 157534, and 208066, as the number of elements. The oxygen mass fraction at the outlet is observed with all three different mesh sizes, and it can be observed from Figure 5.2 that the maximum % change in the oxygen mass fraction is less than 1%. Hence, a computational mesh of 157534 domain elements and 10250 boundary elements corresponding to the grid-sensitive solution has been used for further simulations in the present study.

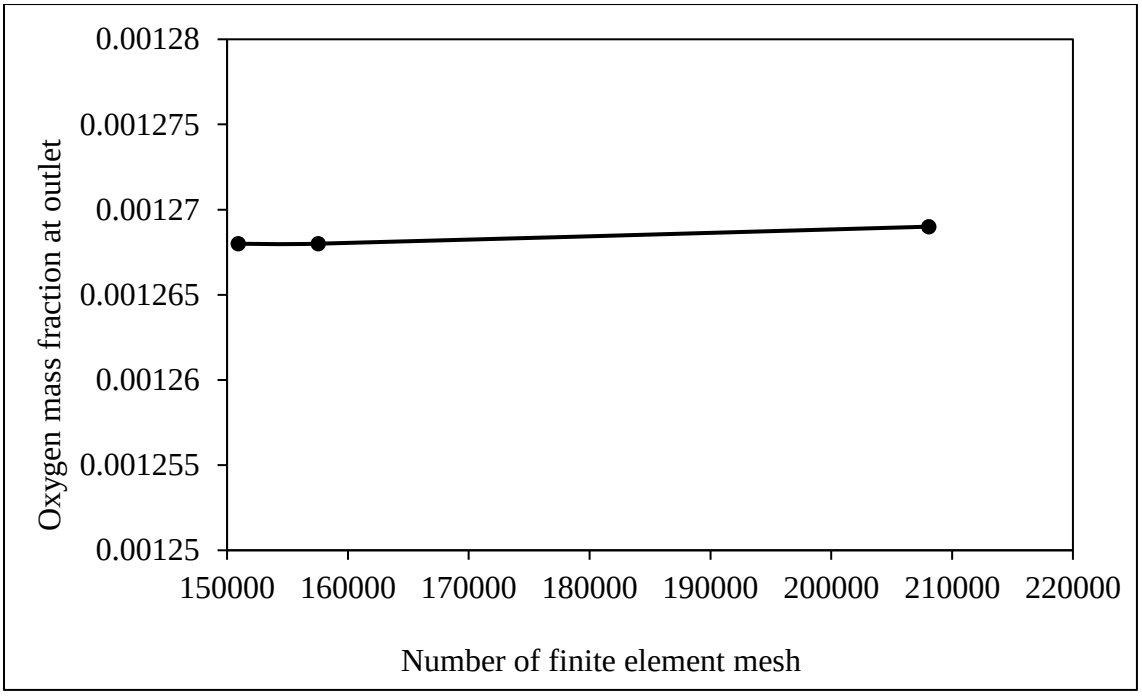

Figure 5.2 Grid independent study showing the variation of oxygen mass fractions at outlets with different mesh sizes

5.5 Hot spot formation in conventional straight channels

Initially, the temperature dynamics in the gas diffusion layer (GDL) during start-up were obtained from simulation. The entire gas diffusion layer of the 2D geometry is assigned the same composition of gases as that in the inlet. The inlet composition taken is in weight fractions such as oxygen: 0.14, nitrogen: 0.85, and water vapor: 0.01. The initial temperature of the entire gas diffusion layer is 298.15 K. The transient model for straight channel incorporating the equations mentioned in the modeling section is simulated using COMSOL Multiphysics 4.4 software. The results of temperature maps at 1 second, 10 seconds, and 100 seconds are shown in Figure 5.3 (a), along with a color indication for the straight channel.

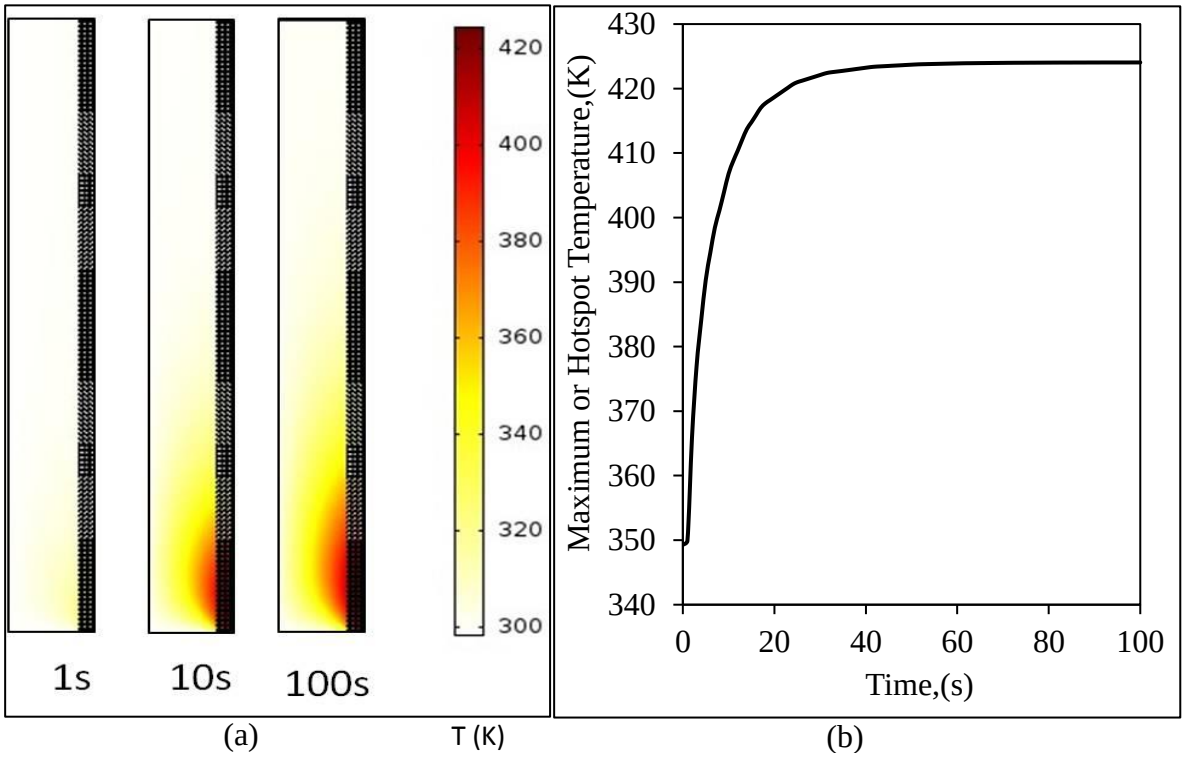

Figure 5.3 (a) Temperature distribution in cathode side GDL for constant inlet composition. (b) The start-up dynamics for maximum or hotspot temperature versus time.

Figure 5.3 (a) shows that the hot spot (in the red color) is formed near the entrance and on the catalyst surface on the cathode side of the gas diffusion layer. The hot spot is nothing but the thermal effect of the instantaneous electrochemical reaction on the catalyst layer, which does not entirely dissipate the heat into the surrounding area. Nonuniform reactants distribution within the fuel cell is the predominant cause of local hot spot generation throughout the operation. A

maximum temperature of 420 K is observed in 100 seconds. The heat generated at the catalyst-coated surface can be carried away by either convection along the channel or by conduction towards the bipolar plate, as also observed by Li et al. [145]. Because of this, a local hot spot patch appears around the catalyst surface and the inlet of the gas flow channel as a consequence of the heat produced. A similar trend in the requirement of a lower coolant temperature for the location close to the channel entrance was observed to maintain isothermal conditions on the cathode side of a PEM fuel cell by Chinannai et al. [146]. Nitrogen is the major carrier gas, which helps in convective cooling of the proton exchange membrane (on which the catalyst is coated), whereas oxygen is consumed in the electrochemical reaction. It is best when the entire oxygen content of the inlet gas is utilized in the reaction resulting in the electric current generation.

5.6 Approaches to mitigate hot spot temperatures

Two methods are presented in this work to avoid excessive local hot spot patch temperature in the catalyst and membrane layers.

5.6.1 Using bump channel design model

First, as illustrated in Figure 5.4, the gas flow channels are amended by inserting bumps in a pattern on the inner surface of the channel in the flow direction. Three different bump designs were created inside the gas channel using bumps of 0.25, 0.5, and 0.75 mm in radius. The edge-to-edge spacing of 0.5 mm between the bumps is maintained constant for all three cases. In this simulation analysis, the computational mesh after the grid sensitivity test consists of 156460 finite triangular elements and 10339 boundary elements.

For different bump sizes, the transient behavior of maximum temperature on the Pt surface for the same gas inlet velocity is shown in Figure 5.5. Unlike the flow in straight channels, the reactant gases (air) entering through the flow channel will have a constrained area in the case of bumped channel designs. Because of this, there is a considerable increase in the velocity in the bumped channels compared to the straight channel without bumps. This aids in the convective removal of the heat generated on the cathode side, which reduces the cell's hot spot temperature. As can be seen from the temperature contour plots in the flow channel without bumps (Figure 5.3 a) and with bumps (Figure 5.5), both the magnitude of the maximum surface or hot spot temperature and the

region of high-temperature decrease in the case of the bumped channel case. It can also be seen in the contour map; the temperature of the gas flow channel is also very low for all bumped channels.

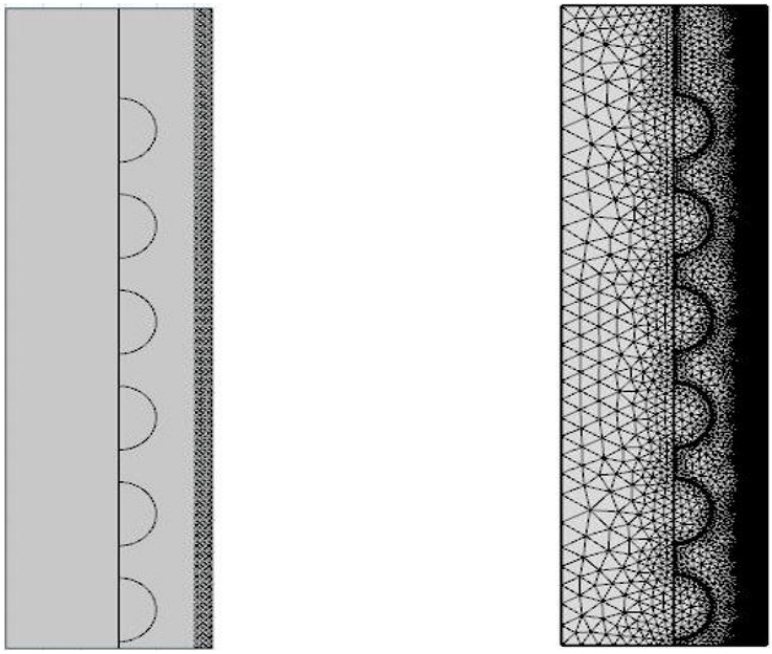

(a) (b)

Figure 5.4 (a) A 2D model created with a 0.5 mm radius bumps into the gas flow channel, and (b) finite element mesh is used in the simulation.

The maximum hot spot temperature observed with time near the entrance of the gas flow channel, the GDL, and the membrane interface for the conventional straight channel without bumps and with different size bumps are shown in Figure 5.6. This can be clearly noted from these start-up dynamics, where the highest hot spot patch temperature is observed in the bump-free channel, and the development of hot spot patch temperatures is reduced with bumped flow channel designs. Initially, all four cases had the same temperature, and with time, the hot spot temperature increased and stabilized at different temperatures. The maximum hot spot temperatures observed are 423 K, 416 K, 404 K, and 394 K for the straight channel without bumps, with bump radii of 0.25 mm, 0.5 mm, and 0.75 mm, respectively. Hence, it is clear that the bump channel design helps in lowering the hot spot patch temperature. Though increasing the bump size mitigates the hot spot patch formation, a large bump of 0.75 mm radius highly restricts the reactant flow in the channel and results in a high-pressure drop.

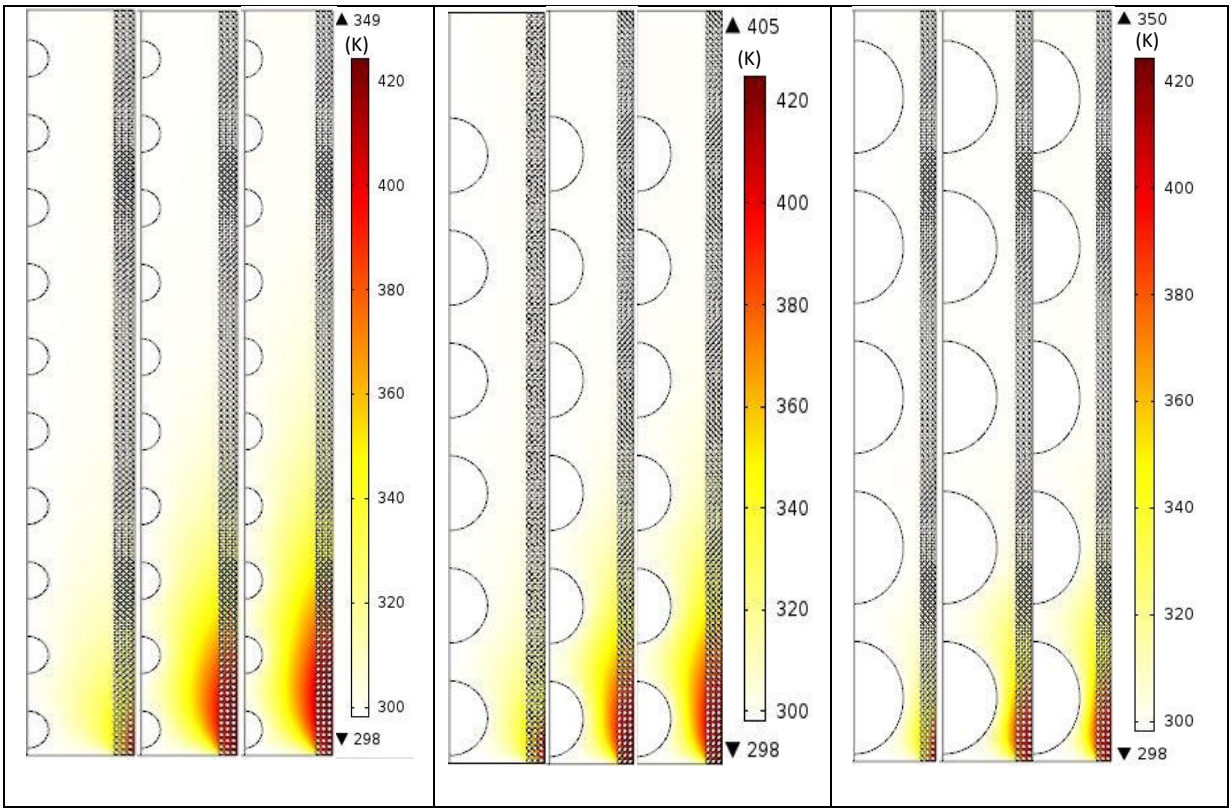

1 sec 10 sec 100 sec (c) 1 sec 10 sec 100 sec (c) 1 sec 10 sec 100 sec (c)

(a) 0.25 mm bumped (b) 0.5 mm bumped (c) 0.75 mm bumped

Figure 5.5 Transient temperature distribution in cathode side GDL in bumped channels with the constant inlet gas composition oxygen: 0.14, nitrogen: 0.85, and water vapor: 0.01 by weight fraction.

Figure 5.7 depicts the comparison of the pressure drop in the straight channels without bumps and with bumps. It can be seen that the pressure drop varies depending on the size of the bumps in the gas flow direction. The maximum pressure drop is observed in the case of a bump of 0.75 mm in radius, which is 20 times more than without bumps. The pressure drop in the case of channels with bumps of 0.5 mm radius and 0.25 mm radius is four times and two times the pressure drops in the case of channels without bumps, respectively. The pressure drop in the flow field is one of the important parameters in the design of fuel cells and stacks. The flow field channels that do not result in high-pressure drops are desirable to increase the life span of the delicate membrane, MEA of the cell and decrease the auxiliary power losses.

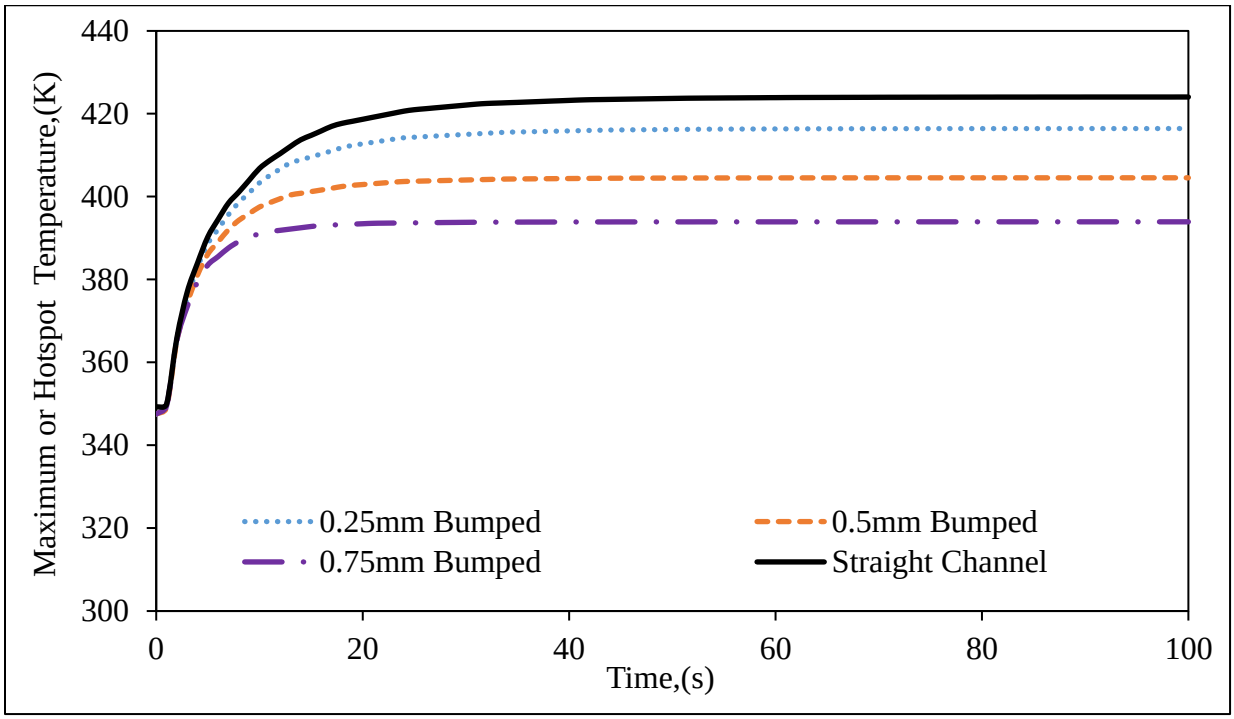

Figure 5.6 Start-up dynamics for local hot spot patch temperatures for different bump sizes.

Based on Figures 5.6 and 5.7, the bump channel design with a bump size of 0.5 mm can be taken as optimum as it offers a comparatively lower pressure drop while reducing the hot spot temperature considerably from that of a straight channel without bumps. Corrosion of bipolar plates is another essential factor to be considered while selecting a suitable channel design in the bipolar plate for PEM fuel cells besides pressure drop. Although the proposed bump channel design mitigates hot spot formation, the introduction of bumps may act as corrosion points and affect the life of the bipolar plates. As the corrosion rate is usually high at the sharp corners of the bumps in the channel adjacent to the bipolar plate, chamfering the sharp edges of the flow geometry and the corners are required. Hence, it is suggested to have bumped channel designs with chamfering of the sharp edges when preparing the bipolar plates for real applications.

5.6.2 Using a cyclic supply of the gas in the inlet of the straight gas flow channel

In an effort to reduce the local hot spot temperature, a cyclic supply of the gas at the inlet of the straight gas flow channel without bumps is proposed as a second mitigating strategy. The CFD simulation is carried out for a cyclic inlet, with the amplitude of the inlet composition being varied

as δ = [0.01, 0.02, 0.03 & 0.04] in Equation 5.1(a-c) and the fractional coverage of the Pt catalyst as ε_s =[0.05, 0.10, 0.15 & 0.02]. Figure 5.8 shows the maximum surface temperature obtained on the surface of the membrane-catalyst layer interface for different amplitude (δ) values of the cyclic supply and different fractional coverage of the Pt catalyst (ε_s).

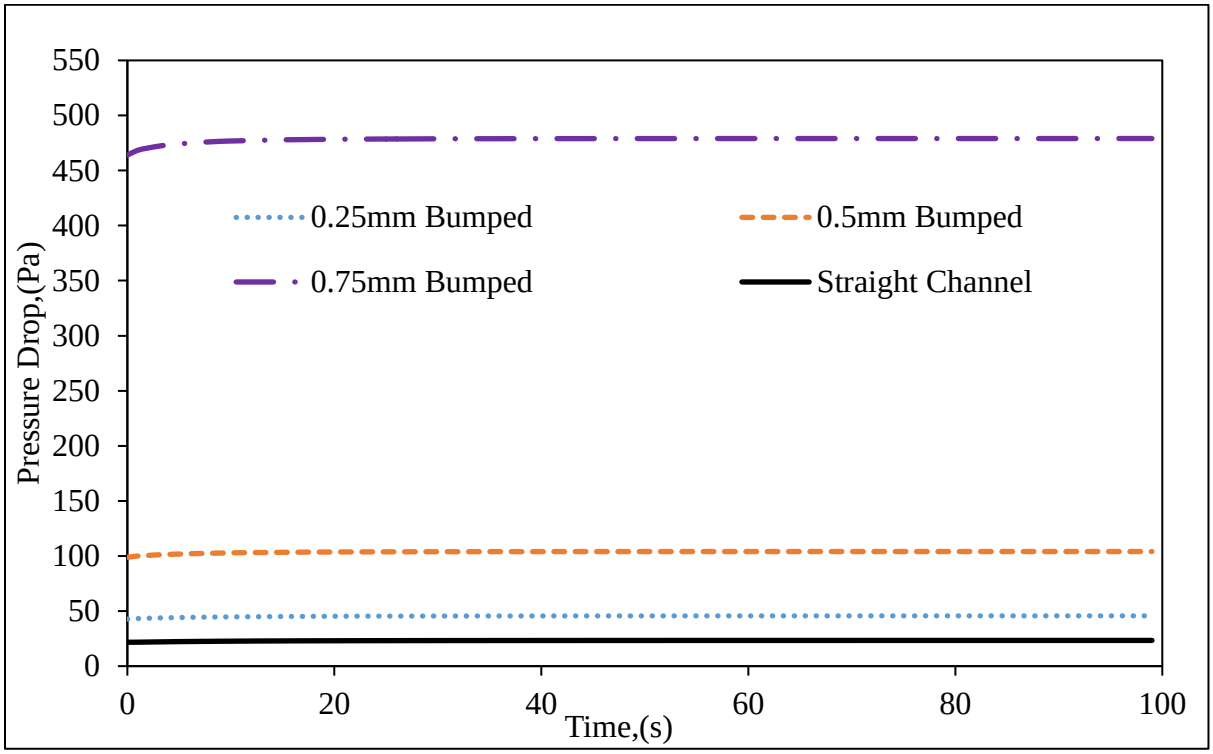

Figure 5.7 Pressure drops as a function of the size of the bumps in the gas flow channel.

It can be noticed from Figure 5.8(a) that for catalyst coverage of ε_s= 0.2, initially, the maximum membrane layer temperature is 298.15 K and gradually increases to as much as 375 K by 17 seconds, and then decreases to 365 K by 27 seconds. From this point of time onwards, a cyclic temperature variation is observed. Due to an increase in the mass fraction of nitrogen in the inlet composition cyclically, the temperature of the membrane layer drops. This strategy ensures the durability of the membrane layer. Similar trends can be seen for different Pt-catalyst fractional coverages, and with an increase in ε_s, the hot spot temperature also increases as more reaction happens to the availability of the catalyst. Similar results for maximum membrane surface temperature versus time are obtained and plotted in Figures 5.8 (b) to (d), corresponding to amplitudes of 0.02, 0.03, and 0.04 for different catalyst fractional coverage fractions.

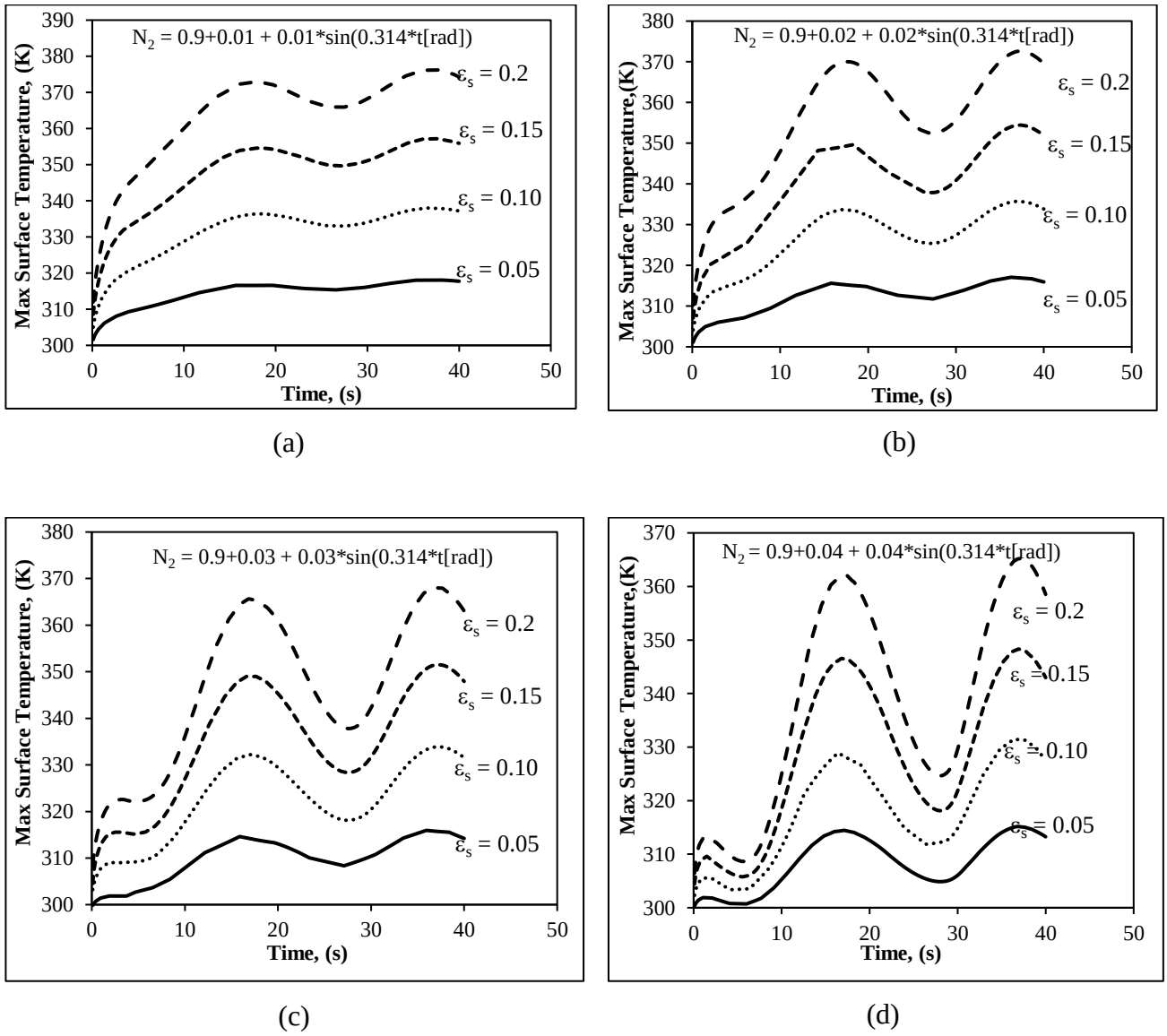

Figure 5.8 Maximum surface temperature in the straight channel on the membrane-catalyst layer interface for various Pt catalyst fractional coverage (ε_s) with nitrogen oscillatory amplitude as (a) $\delta = 0.01$, (b) $\delta = 0.02$, (c) $\delta = 0.03$, (d) $\delta = 0.04$.

In Figures 5.8 (b) to (d), the temperature response is also visible, which is cyclic for all inlet cyclic compositions. There does not seem to be any instability leading to a runaway situation like the temperature shooting up.

Similar to the temperature of the local hot spot, the current density generated or power density of the PEM fuel cell can also be inferred as proportional to the oxygen flux reaching the Pt catalyst. The average mass flux of oxygen for the nitrogen cycle with an amplitude of $\delta = 0.01$ and for

various catalyst coating fractions is shown in Figure 5.9 (a). It can be noted that the oxygen flux does not vary much with variation in catalyst coating in the range of values of ε_s=0.05 to 0.20.

Similarly, another factor to be considered is the conversion of the oxygen gas supplied. In Figure 5.9 (b), the average oxygen mass fraction at the exit of the gas diffusion layer/channel is plotted against the time for the nitrogen gas inlet amplitude of $\delta = 0.01$ and the catalyst coverage fraction of ε_s =0.05 to 0.2. The 0 to 5 seconds data points are not presented because of the steep descent from the initial value.

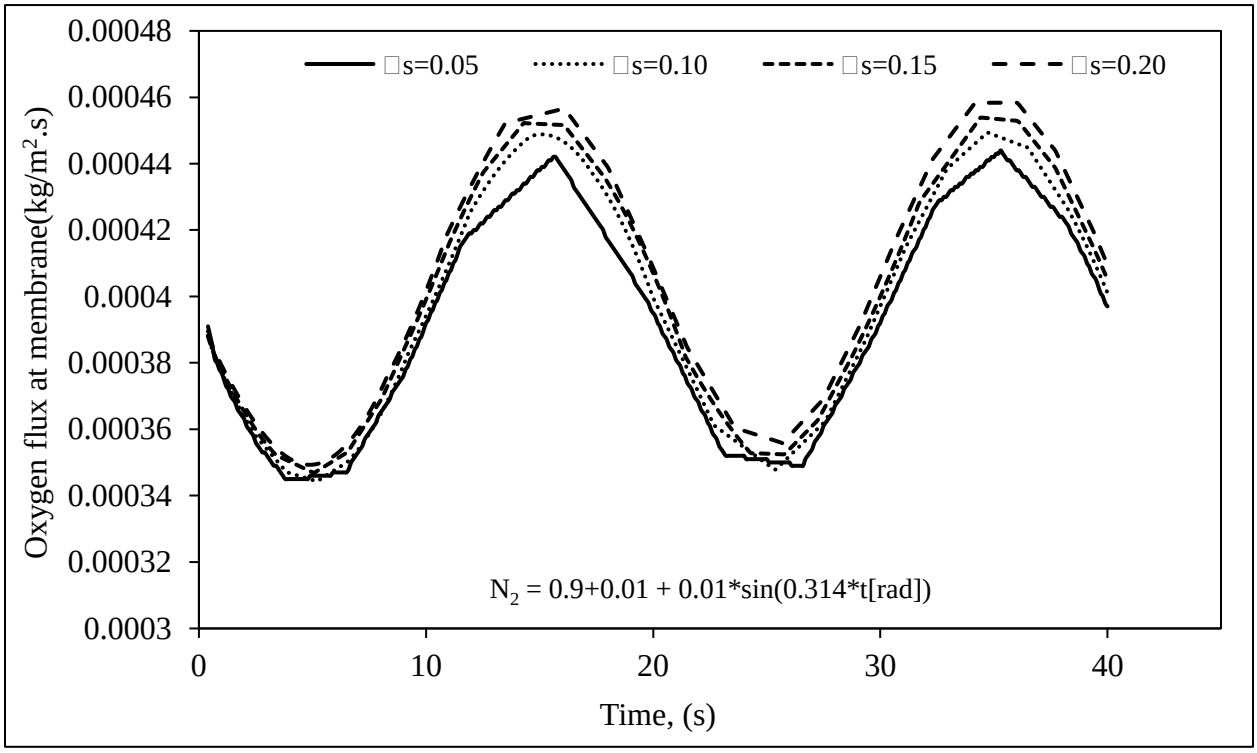

(a)

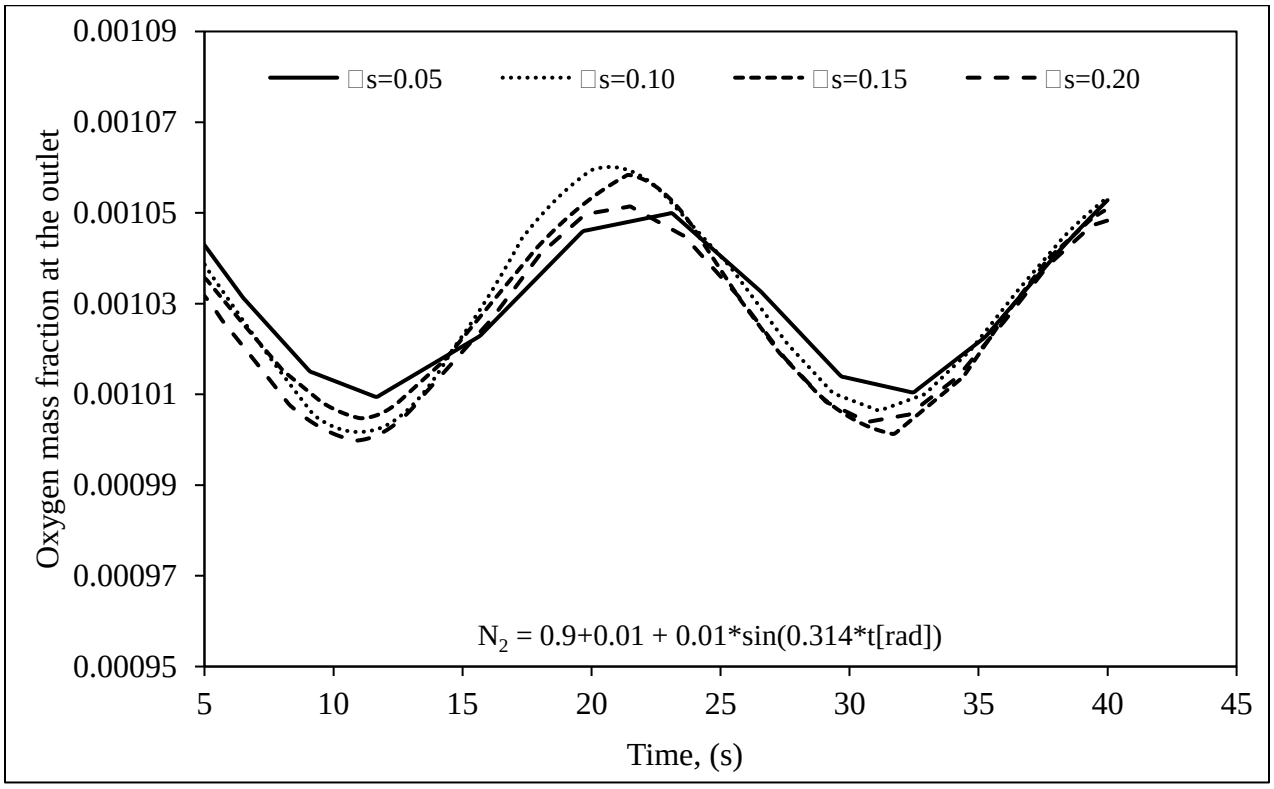

(b)

Figure 5.9 Time variation of (a) mass flux of oxygen at the Pt catalyst layer (b) oxygen mass fractions at the outlet for the cyclic nitrogen supply and for various catalyst coverage fractions in the straight channel.

In addition, the temperature of the hot spot during the second cycle of the oscillatory supply, i.e., from the time 20 seconds to 40 seconds, is tabulated in Table 5.2 for various values of the amplitude (δ) of the inlet composition and catalyst coverage (ε_s). Similarly, the time-averaged values of the oxygen weight fraction at the outlet are presented in Table 5.3, and the time-averaged oxygen flux at the catalyst layer is shown in Table 5.4. It can be noted that the oxygen weight fraction at the outlet is the same and negligible for the varied parameters of δ and ε_s. A performance factor is defined as the ratio of oxygen mass flux to $|T_{hotspot} - 333.15|$. As the performance factor is proportional to the oxygen flux at the catalyst, it can be treated as an indicator of the current generated in the cell. The operating temperature of 333.15 K (60 °C) is considered the reference temperature, where the hot spot patch is minimum. As shown in Table 5.5, the predicted performance factor is high at this temperature. There is a penalty for a high or low hot spot temperature in the performance factor.

Table 5.1 The maximum temperatures (K) are recorded during the second cycle of the oscillatory nitrogen supply for various amplitudes (δ) of inlet composition and catalyst coverage (ε_s).

	ε_s=0.05	ε_s=0.10	ε_s=0.15	ε_s=0.20
δ=0.01	318.06	338.01	357.18	376.20
δ=0.02	317.07	335.78	354.45	372.61
δ=0.03	315.93	333.88	351.51	368.09
δ=0.04	315.17	331.48	348.30	365.19

Table 5.2 The average oxygen weight fraction at the outlet during the second cycle of oscillatory nitrogen supply for various amplitudes (δ) of the inlet composition and catalyst coverage (ε_s).

	ε_s=0.05	ε_s=0.10	ε_s=0.15	ε_s=0.20
δ=0.01	1.0313E-3	1.0316E-3	1.0287E-3	1.0275E-3
δ=0.02	1.0291E-3	1.0255E-3	1.0257E-3	1.0261E-3
δ=0.03	1.0278E-3	1.0217E-3	1.0221E-3	1.0181E-3
δ=0.04	1.0173E-3	1.0196E-3	1.0101E-3	1.0168E-3

Table 5.3 The average oxygen flux (kg/m^2.s) at the catalyst-membrane interface during the second cycle of oscillatory nitrogen supply for various amplitudes (δ) of the inlet composition and catalyst coverage (ε_s).

	ε_s=0.05	ε_s=0.10	ε_s=0.15	ε_s=0.20
δ=0.01	3.94E-4	3.99E-4	4.03E-4	4.08E-4
δ=0.02	3.43E-4	3.46E-4	3.52E-4	3.54E-4

δ=0.03	2.90E-4	2.96E-4	2.98E-4	3.00E-4
δ=0.04	2.44E-4	2.46E-4	2.46E-4	2.49E-4

Table 5.4 The performance factor of the PEM fuel cell was calculated as Oxygen mass flux/ABS (Tmax-333.15) during the second cycle of oscillatory nitrogen supply for various amplitudes (δ) of the inlet composition and catalyst coverage (ε_s).

	ε_s=0.05	ε_s=0.10	ε_s=0.15	ε_s=0.20
δ=0.01	2.46E-5	7.96E-5	1.67E-5	9.44E-6
δ=0.02	2.15E-5	1.24E-4	1.64E-5	8.94E-6
δ=0.03	1.70E-5	3.36E-4	1.61E-5	8.55E-6
δ=0.04	1.37E-5	1.62E-4	1.61E-5	7.74E-6

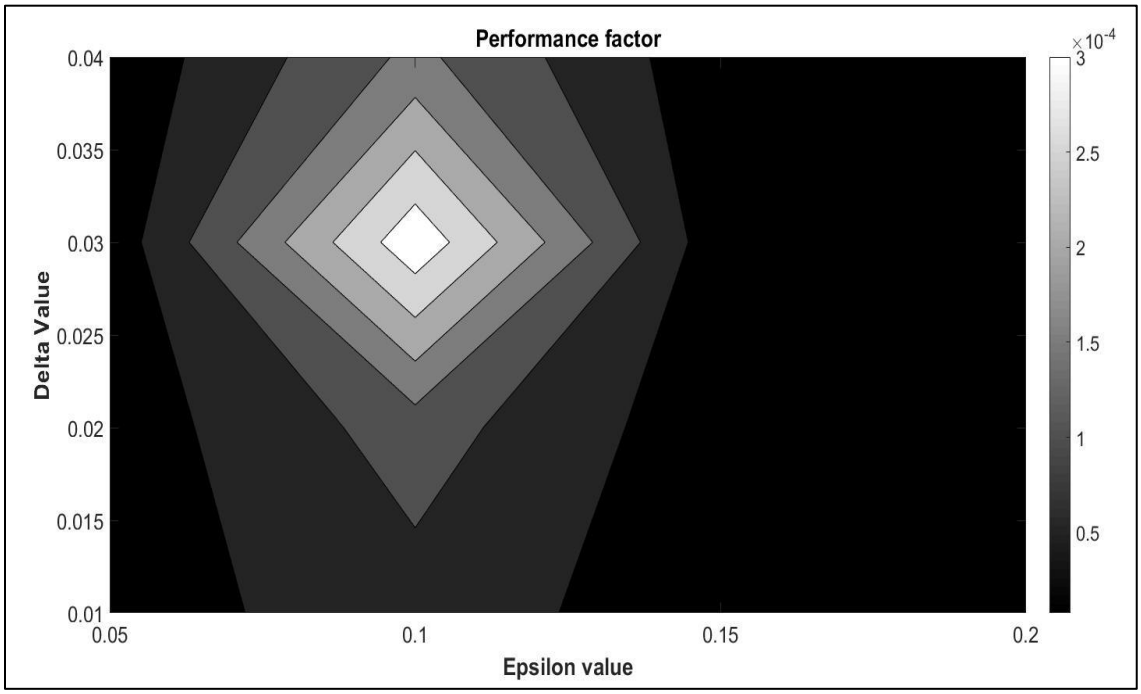

Figure 5.10 Contour plot of performance factor for indicating the optimum values of various amplitudes (δ) of the inlet composition and catalyst coverage (ε_s).

Figure 5.10 shows that the performance factor of the PEM fuel cell is high for an intermediate value of the δ $(0.02 - 0.03)$ and ε_s $(0.1 - 0.15)$, where δ is the amplitude of the nitrogen gas and oxygen gas stream composition of the inlet stream, and (ε_s) is the fractional coverage of the Pt catalyst surface on the membrane layer.

Finally, a strategy combining cyclic gas inlet with the bumped flow gas channel is being studied to mitigate the hot spot. Based on the above analysis of cyclic gas inlet through the straight gas flow channel, $\delta = 0.03$ and $\varepsilon_s = 0.15$ is considered for studying the effect of cyclic input on the bumped channel design. Figure 5.11 shows the simulation analysis of the maximum hot spot temperature for the different bump sizes compared to the straight gas flow channel for the cyclic supply. The cyclic supply of nitrogen gas can reduce the hot spot temperature in all cases, but the reduction in temperature was higher in the case of the bumped channel design compared to the straight channel. This is advantageous for ensuring the membrane and MEA durability. Though the lowest surface temperature of the membrane is achieved for the bump size of 0.75 mm, the pressure drop associated with the design would be high and may limit its application in the actual case. However, as seen in section 5.4.1 and as observed in Figure 5.11, a bump size of 0.5 mm may be a better option for cyclic supply for an early and more significant reduction of local hot spot temperature in fuel cells, which aids in the improved stability and durability of membranes.

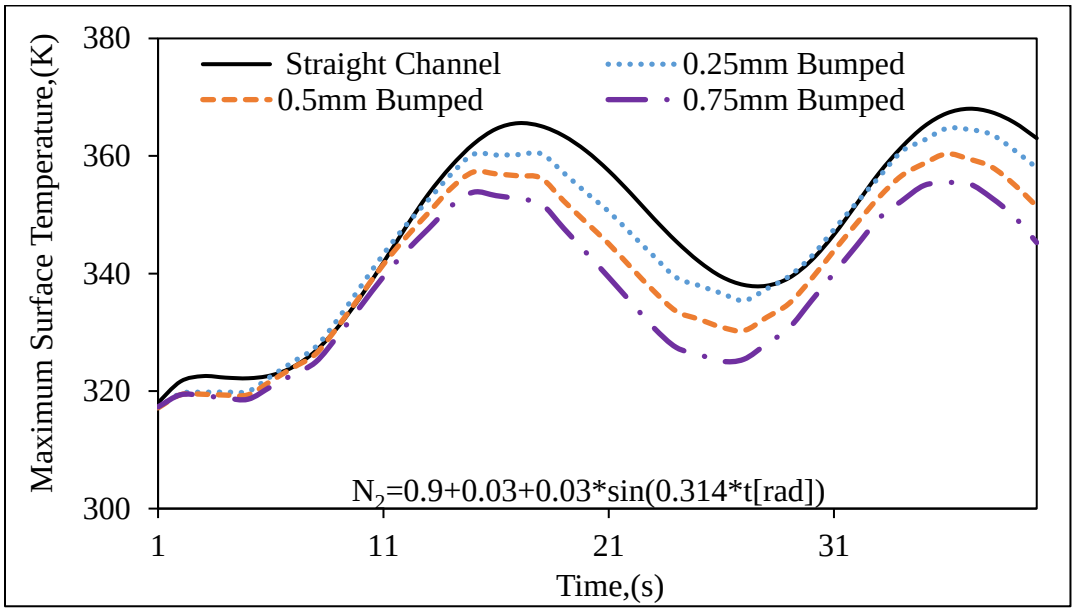

Figure 5.11 Comparison of maximum surface temperature on the membrane-catalyst interface for ε_s=0.10 and cyclic input with amplitude of δ = 0.03 for straight and bumped channel designs

5.7 Summary

This study presents a transient, two-dimensional simulation on the cathode side of a PEM fuel cell to identify hot spots in the catalyst-membrane interface. Two different techniques – using bumps in the gas flow channels and giving cyclic input of the gas at the inlet of the channel, are proposed for reducing hot spots in this study. The key findings of this work are summarized as follows:

- The gas stream with a constant inlet composition of oxygen and nitrogen results in local hot spot formation on the cathode side close to the entrance and near the membrane layer in a PEM fuel cell.
- Gas flow channels with bumps are shown to have much lower hot spot temperatures compared to straight channels.
- Though an increase in bump size increases the reduction in the hot spot temperature, the corresponding increase in pressure drop is found to be much higher. Hence, a bump size of 0.5 mm can be recommended from a hot spot temperature and pressure drop perspective.
- The second strategy of the cyclic supply of nitrogen gas and oxygen gas was also found to reduce the local hot spots considerably. This can be attributed to convective cooling.
- The simulation analysis of the combination of the two techniques, i.e., cyclic input to the bumped gas flow channel, has shown a further reduction in the hot spot temperature.
- The transient state simulation based on the assumption of the thermally insulated bipolar plate, 2D geometry, and the net heat liberated into the cathode side as a worst-case scenario has shown scope for optimizing PEM fuel cell operating conditions and prolonging the durability of the membrane layer.
- The service life of the membrane is expected to be improved if the oxygen and nitrogen in the inlet on the cathode side are supplied with a cyclic amplitude.

The gas diffusion layers (GDLs) are primarily made of carbon fibers and are available in various forms, such as woven carbon fibers and carbon papers. However, the majority of the commercially available GDLs are carbon paper, such as Sigracets by SGL Carbon [147] and Toray carbon paper. The 2-D model considered in this chapter do not consider the random structure of the carbon fibres in carbon paper. This limits the prediction of hot spot temperature. As a result, it would be interesting to apply the notion of carbon paper in the gas diffusion layer model to the identification and mitigation of local hot spot patches. The 3-D random structure of the gas diffusion layer as

part of the computational domain is considered as the 5th objective which is covered in the next chapter.

Chapter 6

Hot spot identification using transient 3-D simulation of the cathode with random porous GDL structure

Chapter 6

Hot spot identification using transient 3-D simulation of the cathode with random porous GDL structure

Identification of hot spot and its purging strategies were proposed and shown in the previous chapter using a 2-D simulation of the cathode side of a PEM fuel cell. The model considered GDL as a structured array of cylinders placed in a regular arrangement. However, the actual carbon paper, typical GDL used in the PEMFCs, consists of a highly random porous structure. This study investigates the oxygen transport and hot spot formation in a procedurally generated three-dimensional gas diffusion layer model. In this multi-scale simulation, a 3D reconstruction model of the gas diffusion layer that closely mimics the SEM image of carbon paper is used to explore gas transport mechanisms and the development of hot spot patches. Hence, this chapter addresses the fifth objective of the current study. The results obtained from this transient study on the local hot spot identification in the conventional straight channel using a 3D carbon paper with constant feed composition at the inlet are discussed in the following sections.

6.1 Numerical model description

The 3D numerical model used in this study is based on the 2D numerical model presented in previous chapter 5. Patnaikuni and Jayanti [153] established a method for recreating the microstructure of the carbon paper GDLs and simulated the fluid flow through it. They verified the application of Darcy's law and the Bruggemann correction to determine the permeability and effective diffusivity of the GDL. The fluid, heat, and mass transport through this complicated porous structure is critical in accurately anticipating local hot spots, localized flooding areas, and reactant starvation zones. Most of the 3D simulation studies reported in the literature considered GDL as a simple, porous zone and do not account for heat transfer, hot spot generation, and identification in the reconstructed GDL structure. Many numerical modeling investigations into the 3D gas diffusion layer, whether carbon fabric or paper, have solely used the isothermal condition. The investigation of the local hot spot patch detection that was provided in the previous

chapter considers GDL as three layers of circles in the two-dimensional computational domain of the cathode side of a PEM fuel cell.

The current study is an extension of the previous work by considering the 3D computational domain of the cathode side with a more realistic randomized porous structure for the GDL. This simulation study explores the local hot spot patch identification using fluid, heat, species, and energy transport in a new 3D reconstructed carbon paper GDL used in a single-phase, time-dependent, non-isothermal model simulation using a conventional straight gas flow channel.

6.2 Computational geometry and mesh

The schematic representation of the PEM fuel cell consisting of various zones on the anode and cathode sides of the cell is shown in Figure 6.1(a). The computational domain considered for the present study is only the cell's cathode side, consisting of a bipolar plate, gas flow channel, and gas diffusion layer. While the 3D geometry of the cathode side is shown in Figure 6.1(b), the 3D geometry of the reconstructed GDL structure is displayed in Figure 6.1(c). The computational geometry considered in this study is different from the previous chapter 5 in two ways:

(i) the three-dimensional geometry and
(ii) the reconstructed three-dimensional randomized structure of GDL.

The construction of the reconstructed randomized 3D structure of carbon paper is inspired by the actual microstructure of a typical carbon paper as observed from SEM images of its front and cross-sectional views, as shown in Figure 6.2. GDL made of carbon paper is composed of randomly superimposed fibrous layers. The porous architecture of the carbon paper GDL was recreated using COMSOL Multiphysics, a commercial tool for multiphysics, i.e., heat, mass, and transport species simulations. As it is not possible to exactly match the randomized porous structure of a real carbon paper (as seen in the SEM pictures), the methodology presented by Patnaikuni and Jayanti [153] has been adopted with the following assumptions for generating the porous fibrous structure of GDL –

(i) carbon paper in the GDL is cylindrical with a defined diameter,
(ii) these cylindrical fibres are straight and very long,
(iii) no fibres are aligned in the direction of the GDL thickness (to minimize the difficulty of grid generation and to obtain the solution), and

(iv) carbon particles present in the GDL are not considered.

The base layer is formed by uniformly inserting several 60-micrometre diameter cylinders. It is made by slanting a new layer on top of an old one and leaving a 20-micrometre gap between any two layers.

This novel 3D gas diffusion layer (carbon paper) arrangement is designed for modeling purposes. It is used in conjunction with the cathode side PEM fuel cell model to demonstrate the local hot spot in the catalyst-membrane layer. To avoid simulation problems, the COMSOL model included a surface reaction boundary condition to the gas diffusion layer rather than accounting for the catalyst and membrane layer thickness. As stated in the model specification, a comprehensive physics link was between the mass transfer at the cathode, the momentum transfer in the gas flow channel, and the gas diffusion through the reconstructed gas diffusion layer.

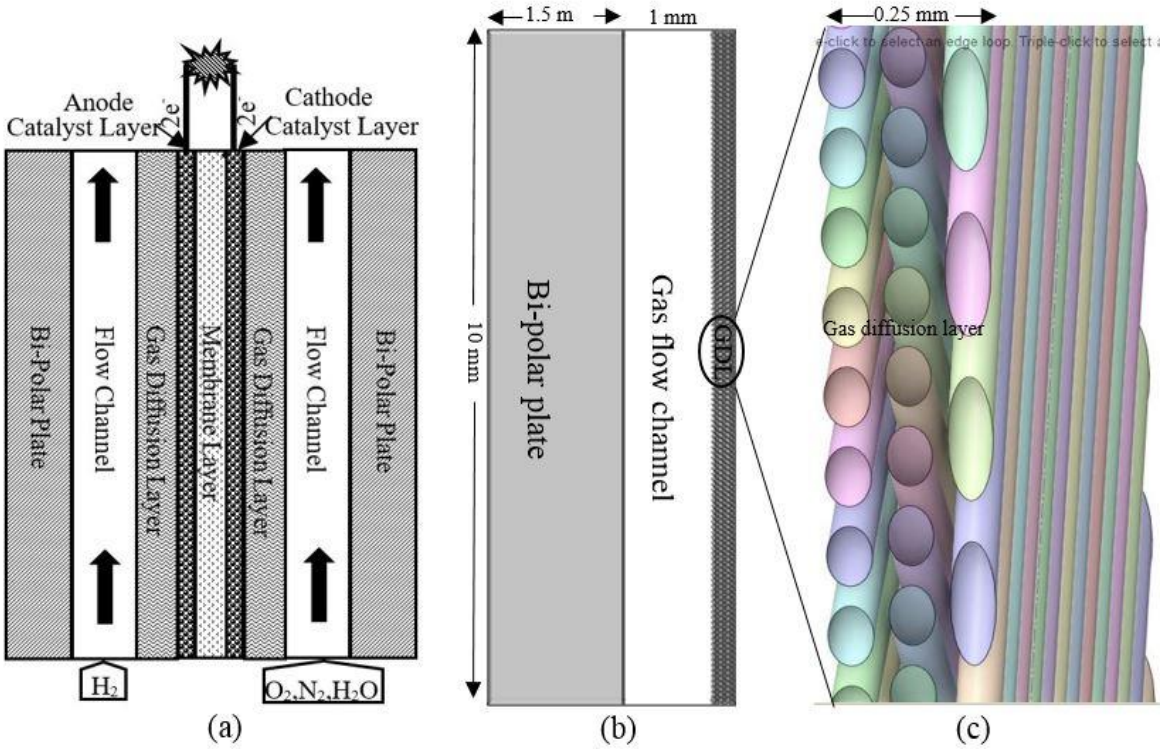

Figure 6.1 (a) A PEM fuel cell schematic is shown (b) computational model with a 3D gas diffusion layer arrangement (carbon paper) (c) A zoomed-in view of the GDL.

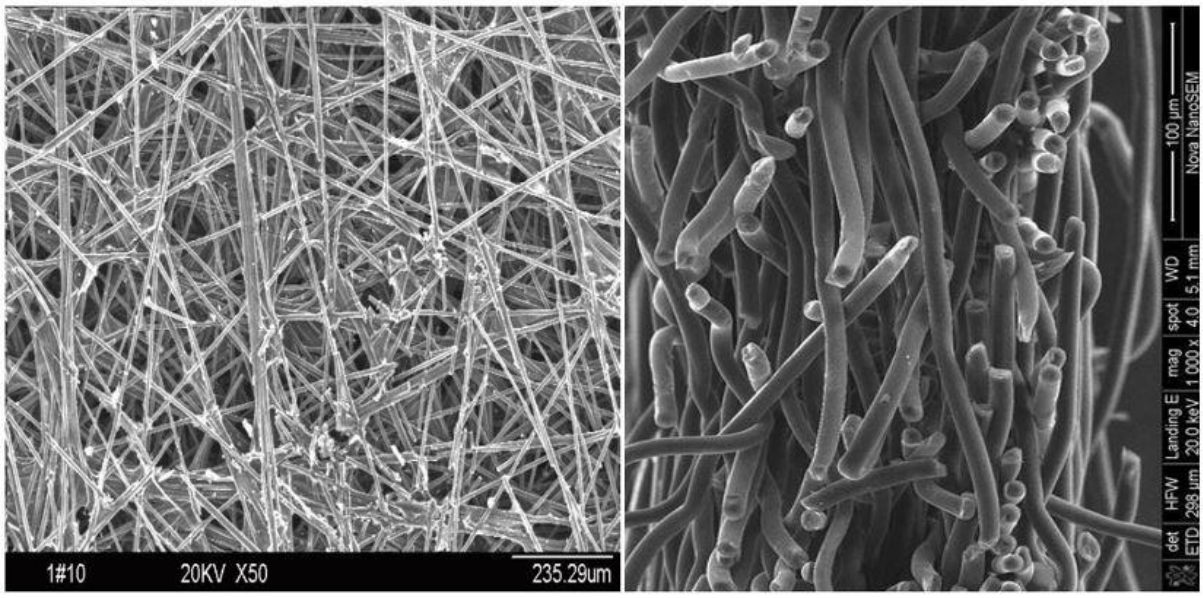

(a) (b)

Figure 6.2 (a) Microstructure of carbon paper GDL [154], (b) Cross-sectional view of carbon paper [155].

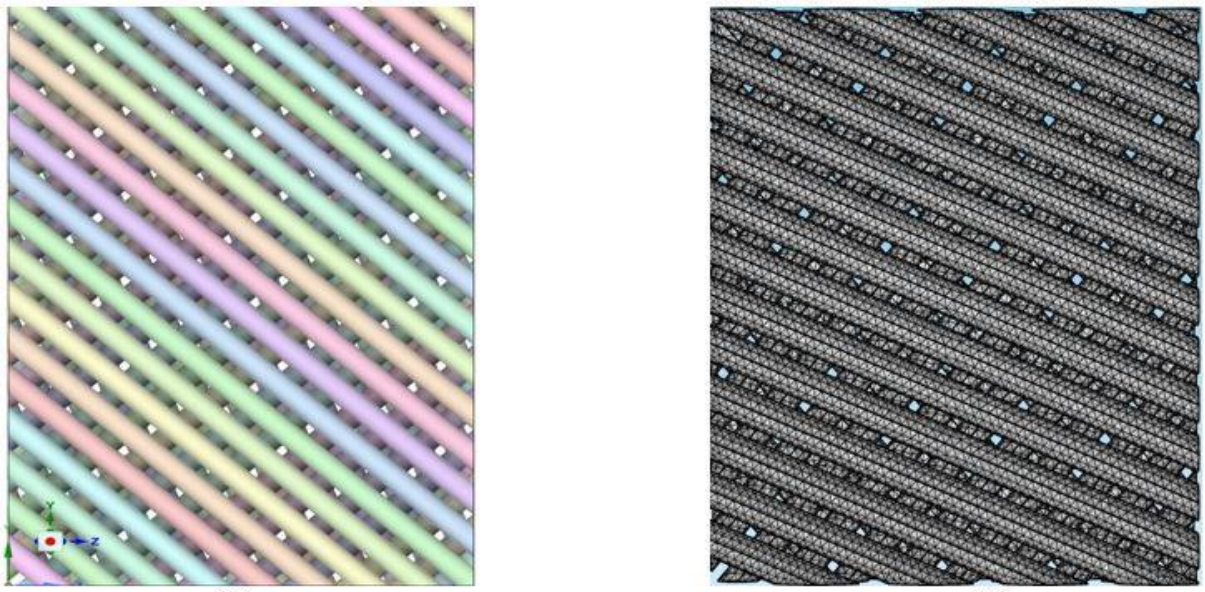

(a) (b)

Figure 6.3 (a) A novel GDL reconstruction arrangement, (b) mesh generation of the GDL

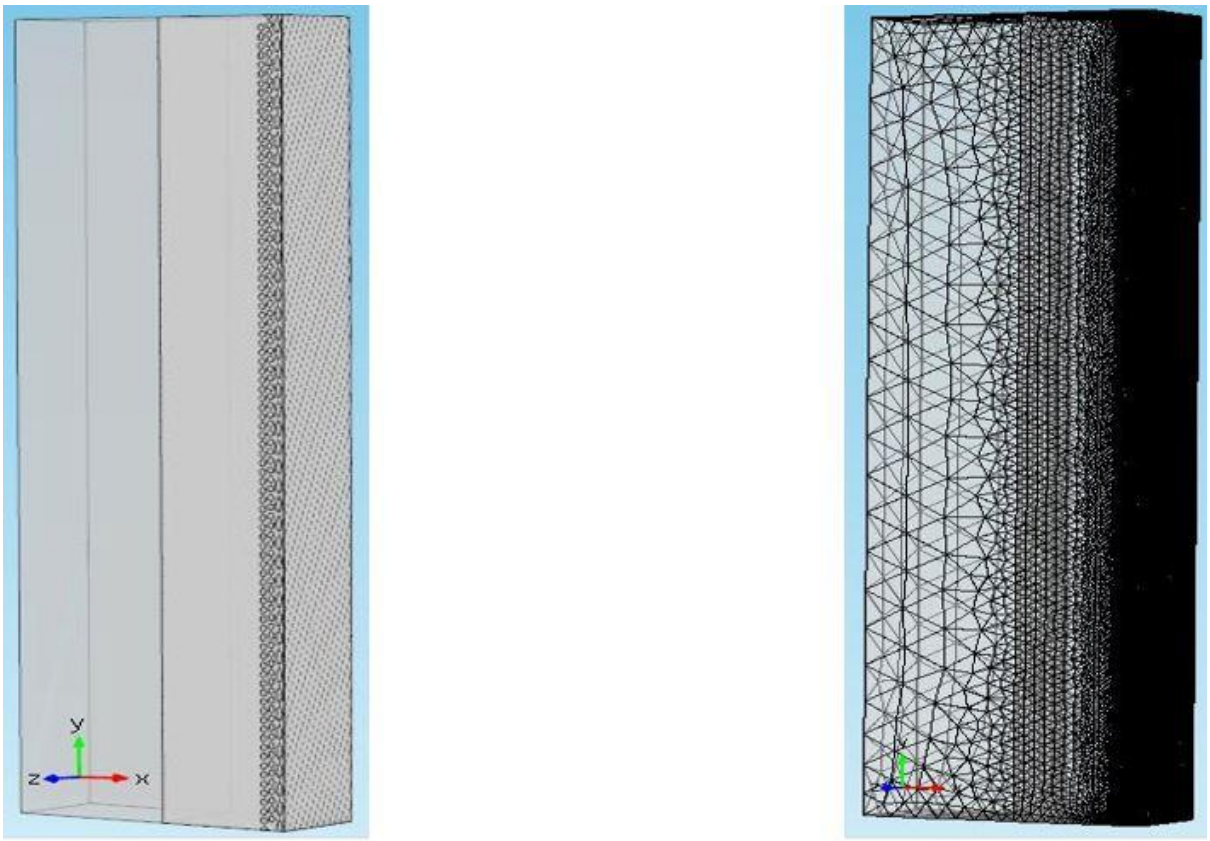

Figure 6.4 (a) 3-D model of cathode side PEM fuel cell with GDL (b) computational domain model.

6.3 Meshing and Grid independent studies

The CFD models were solved using a time-dependent solver with the direct MUMPS method using a relative tolerance of 1×10^{-3}. It is essential that a fine computational mesh is selected in order to achieve a satisfactory balance between the accuracy of the simulation results and the computational runtime required. The simulations employed tetrahedral, triangular, edge and vortex elements with 1338444 elements in total and a mesh volume of 27.5 mm^3. Even though the grid skewness and other conditions met the requirements, the number of grids at this location was increased to represent changes in the local hot spot temperatures in the membrane and gas diffusion layer and verify how the grids are interdependent.

Table 6. 1 Complete mesh details of the mesh independent study

Mesh type	Coarse	Normal	Fine
Tetrahedral	523851	1338444	7553276
Triangular elements	116208	234647	834940
Edge elements	37429	50070	99471
Vertex elements	1992	1992	1992

There are 1338444 grids that are suitable for simulation. Therefore, when the number of grids was 7553276, a maximum surface temperature of 396.703 at 100 seconds was calculated, which was 0.0000025 below the estimated maximum surface temperature of the previous grid numbers model change range, which was not more than 1% lower. Figure 6.6 illustrates the essential changes made to the grids to reduce computing load.

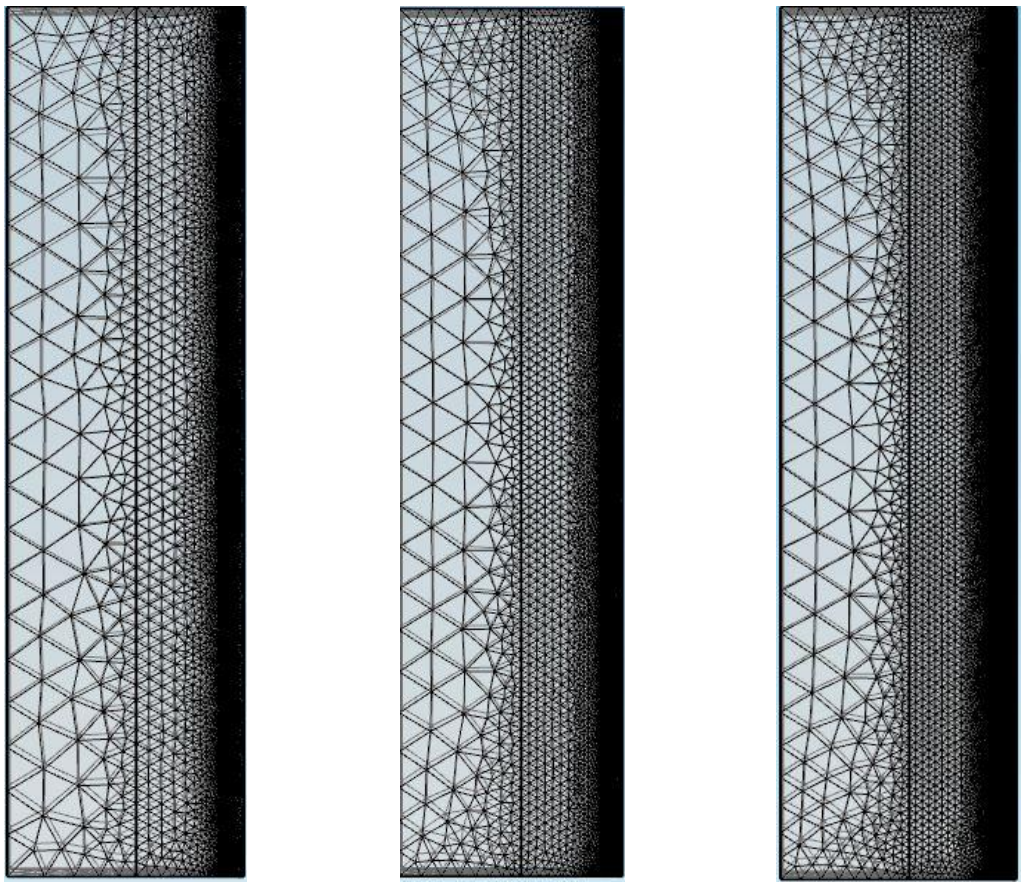

(a) (b) (c)

Figure 6.5 (a) Coarse (b) normal and (c) fine mesh of the cathode side of PEM fuel cell

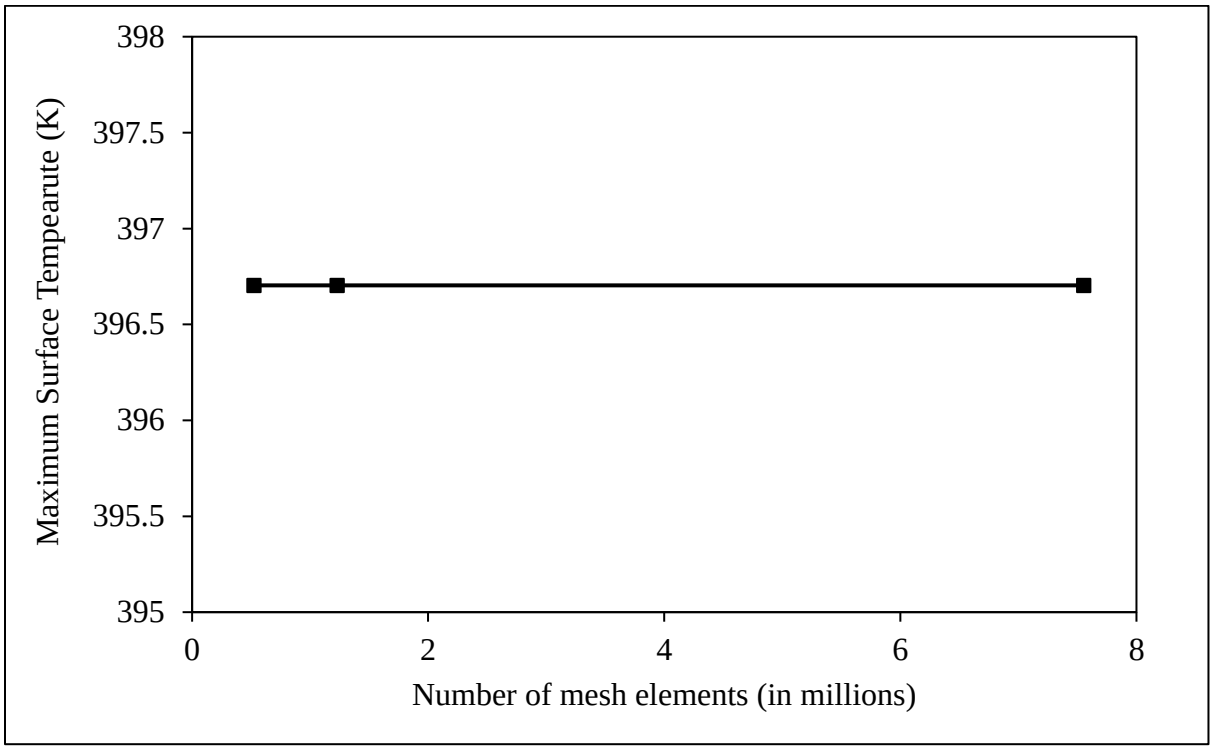

Figure 6.6 Grid independence study showing the variation of maximum surface temperature with different mesh

6.4 Boundary conditions and Material properties

The boundary conditions of the current study are also based on our previous chapter. The gas channel walls are subjected to a no-flux and no-slip condition. Temperature and heat flux continuity is used at the interfaces between the bipolar plate, flow channel and the GDL. The same boundary condition is used at the interface between the gas mixture and the fiber surface of the GDL. The inlet reactant velocity on the cathode side is 0.01 m/s. The inlet reactant gas mixture consists of 0.14 weight fraction of oxygen, 0.85 weight fraction of nitrogen, and 0.01 weight fraction of water vapor. This composition has been considered based on the previous chapter. The bipolar plate is insulated from the surroundings. The temperature of the cell is considered to be 333.15 K (60 °C), and the reference pressure is 101325 Pa. The wall heat flux is calculated based on equation [3.9] in Chapter-3 has been applied at the face of the GDL facing the catalyst layer [156]. The reactive gas density and viscosity are estimated as a function of pressure and

temperature. The properties of the materials used as GDL (carbon paper) and bipolar plate are presented in Table 3.1 of Chapter-3.

6.5 Results and discussion

Different simulations were carried out to observe the hot spot formation in the 3D cathode side PEM fuel cell, having reconstructed porous GDL structure with straight, bumped, and wavy gas flow channels. The results were analyzed to see how effectively the bumped and wavy type channel designs mitigate the hot spot formation.

6.5.1 Hot spot formation in the PEM fuel cell cathode having 3D reconstructed GDL and conventional straight flow channel

In the first simulation study, the temperature distribution in the cathode side regions of the straight bipolar plate, gas flow channel, and the reconstructed GDL is obtained. Figure 6.7 shows the color map of the temperature on the cathode side at different times and also the time variation of the maximum temperature observed. It can be observed that the maximum temperature regions (hot spot patches) are located at the GDL surface near the entrance of the gas flow channel, and the maximum temperature keeps on increasing up to 397 K (124 °C) beyond 40 sec (Figure 6.7) in case of conventional straight gas flow channel for the constant supply of species (O_2 and N_2) composition.

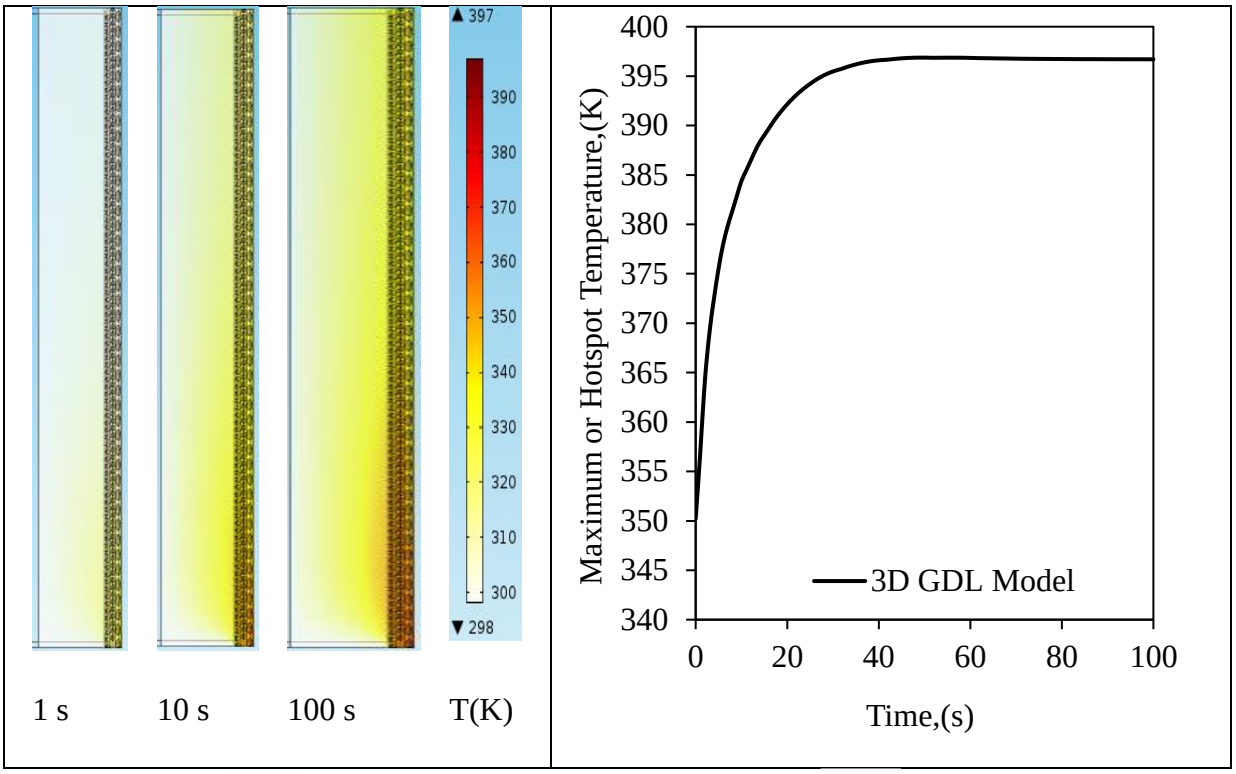

(a) (b)

Figure 6.7 (a) Temperature distribution on the cathode side of a 3D GDL with constant inlet composition, (b) Start-up dynamics for maximum or hotspot temperature versus time.

Large amounts of heat are liberated because of the instantaneous electrochemical reaction near the inlet, where the oxygen mass fraction is high. This may lead to increased local hot spot temperatures. This slowly drops along the channel length as the oxygen concentration decreases from the inlet to the outlet. It is consistent with the results reported in the previous chapter 2D simulation study on the cathode side with the conventional straight channel and regular GDL structure. However, the maximum temperature obtained in the 3D model study with reconstructed randomized GDL structure is less by 23 K in 100 sec compared to that observed in the 2D study with regular GDL structure. This could be because of the conductive heat transfer resistance offered by the carbon cylindrical fibres considered in the randomized 3D GDL structure, which would slow down the transfer of heat produced at the catalyst layers towards the channel. Figure 6.8 shows the streamlines of oxygen diffusive flux in the through-plane direction in the reconstructed GDL as well as the temperature variation among the layers of fibres in the GDL. Variation in the temperature of the fibres in the layers from the catalyst-coated end to the one

facing the channel can be evidently seen; for instance, the temperature of the first layer of GDL close to the catalyst and membrane layer is higher.

The electrochemical reaction between the catalyst and the gas diffusion layer generates heat and produces water. The total heat, including the reaction heat, ohmic heat, and phase transition heat of the water, will be carried away by either the diffused gas through the GDL or by convection along the channel by the flow of inlet gas or by conduction towards the bipolar plate. This can be observed from the temperature distribution along with the thermal diffusive flux vectors shown in Figure 6.9. The heat flux vectors show the direction of heat flow by the diffused gas from the GDL towards the channel. Bigger size arrows indicating higher thermal diffusive flux can be observed near the gas feed entrance, where the local hot spot patch development begins. The reaction heat that is not adequately evacuated will accumulate and result in a local hot spot close to the catalyst surface and the channel entrance. These hot spots may result in drying up of the membrane, which further causes puncture in the membrane and crossover of the gases. Hence, it is clear from the start-up dynamics that the PEM fuel cell's durability will be compromised if the hot spot formation is not mitigated.

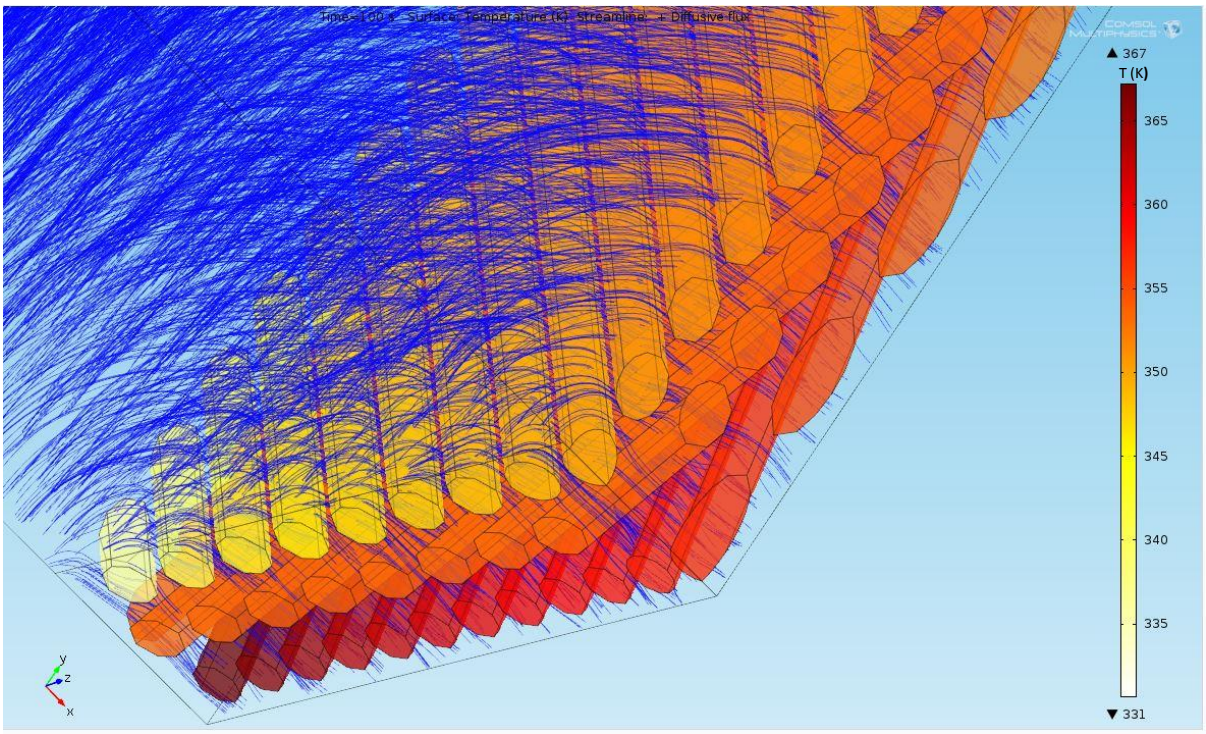

Figure 6.8 Streamlines of oxygen diffusive flux through the 3D reconstructed GDL and the temperature variation of its fibre layers.

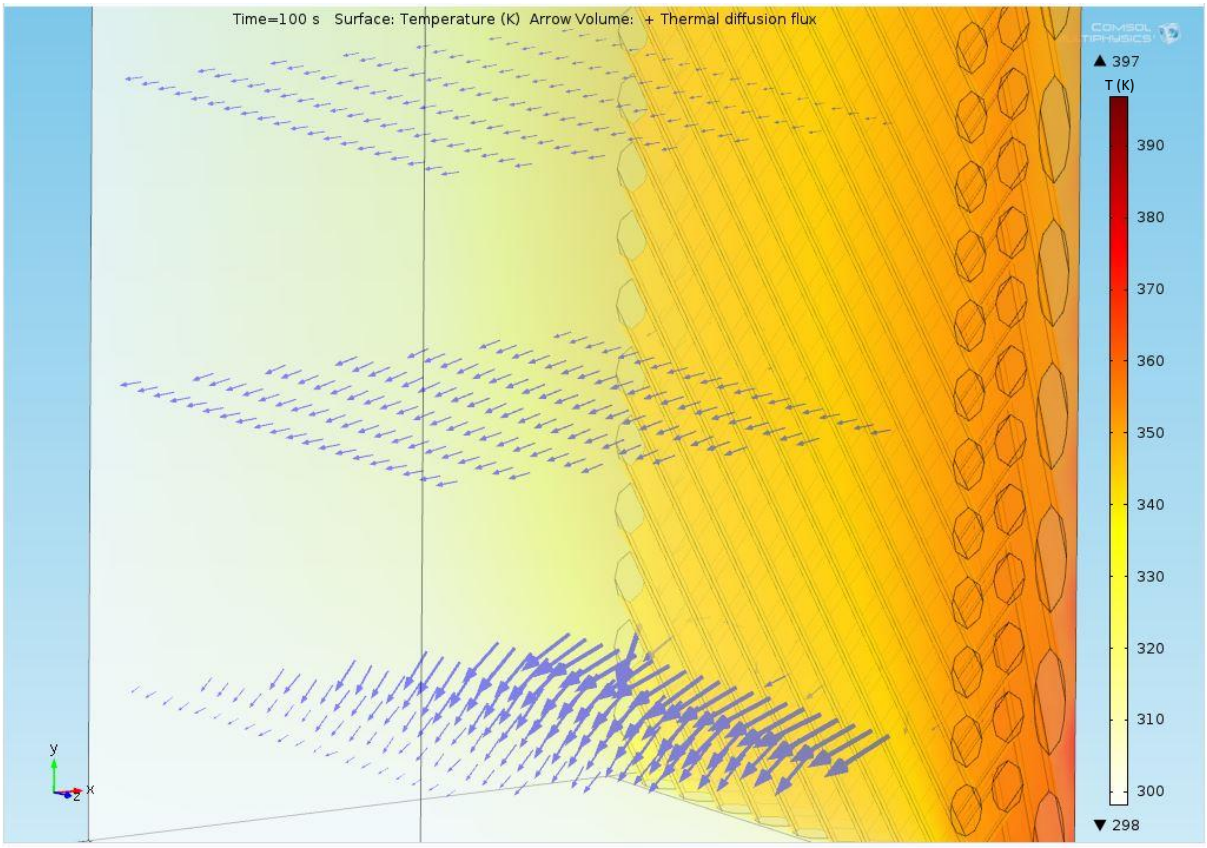

Figure 6.9 Temperature distribution in the three-dimensional GDL and channel regions. Arrows indicate the thermal diffusive flux.

In the previous chapter, 2D simulation analysis presented two strategies for mitigating the hot spot, such as using bumps in the channel flow path and oscillating supply of nitrogen and oxygen. The current 3D simulation study with the reconstructed porous structure is extended further by proposing variant designs for local hot spot mitigation in the next chapter. The following section presents the results obtained from the 3-D simulation study with the conventional straight channel designs for an oscillatory nitrogen supply.

6.5.2 Using an oscillatory supply of the nitrogen gas in the inlet of the proposed channels

The previous chapter described the efficacy of using an oscillatory supply of nitrogen gas for the conventional 2D straight flow gas channel in mitigating the local hot spot formation. The sinusoidal or oscillatory inflow composition of the three gaseous components in the cathode side inlet is represented by equations 5.1 [a-c] in chapter 5. These are set up such that at any moment in time, the total of the three fractions of oxygen, nitrogen, and water vapor equals one. Here, δ is

the amplitude of nitrogen and oxygen oscillatory compositions. Based on the analysis of the cyclic gas inlet through the 2D straight gas flow channel presented in the previous chapter, the optimum value for the amplitude of the cyclic gas supply and the fractional coverage of the Pt catalyst is considered as $\delta = 0.03$ and $\varepsilon_s = 0.10$ respectively, for studying the effect of cyclic input on the 3D straight channel geometric shapes of the channel designs. Figure 6.10 displays the simulation analysis of the maximum surface or local hot spot temperature for the constant inlet compared with that obtained with the cyclic input to a conventional straight gas flow channel. It can be clearly noted from Figure 6.10 that the cyclic supply greatly reduced the hot spot temperature realized with the constant inlet to the typical straight channel. This is advantageous for ensuring the membrane and MEA durability, which aids in the improved stability and durability of membranes.

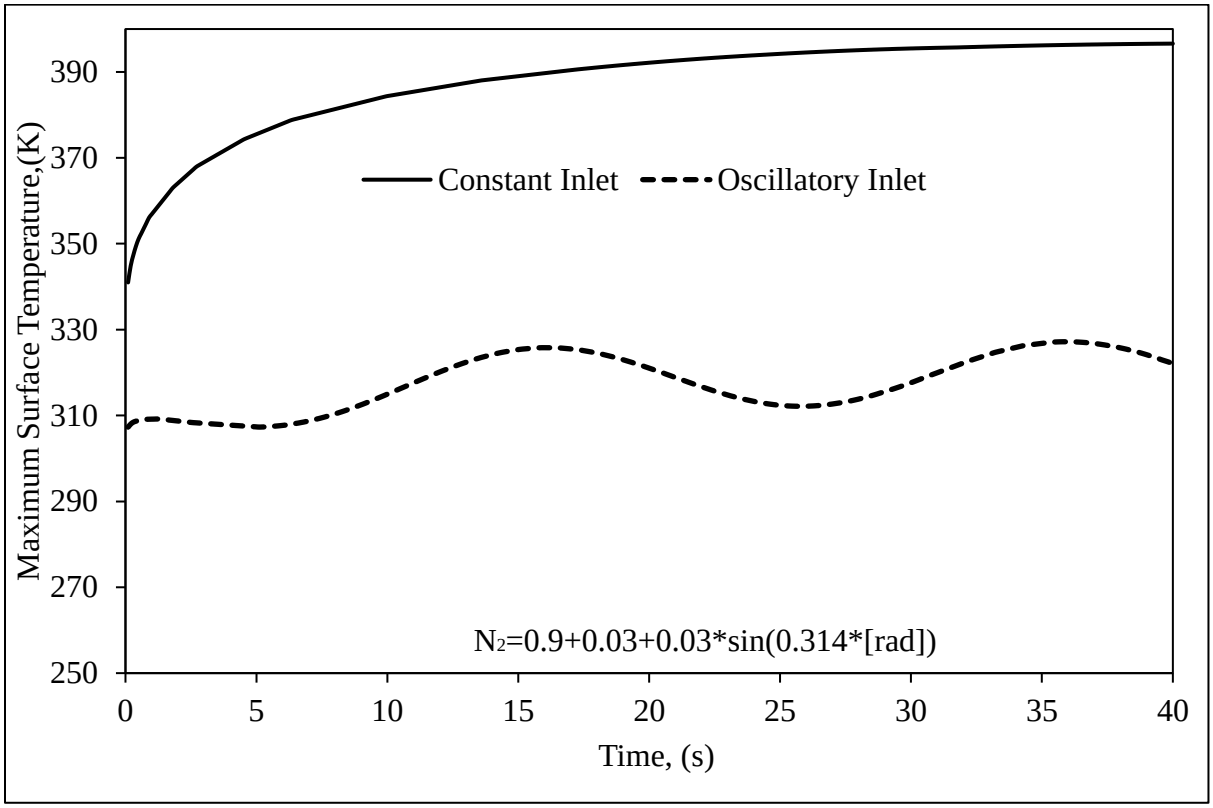

Figure 6. 10 Comparison of maximum surface temperature on the membrane-catalyst interface for ε_s=0.10 and cyclic inlet with amplitude of δ = 0.03 for straight channel designs

6.6 Summary

This study provides a transient, three-dimensional simulation performed on the cathode side of a PEM fuel cell using a reconstructed porous GDL structure to locate hot spots adjacent to the

catalyst-membrane interface. The efficacy of oscillating nitrogen gas feed at the channel's inlet to mitigate the local hot spot patch is also presented in this study. Here are the main conclusions that can be drawn from the study:

- Local hot spot formation was simulated by incorporating the reconstructed 3D porous GDL structure on the cathode side computational domain of the PEM fuel cell.
- The maximum surface or local hot spot temperature obtained in the straight channel during the 100 seconds of operation is 397 K (123.85 °C). This temperature is observed to be less by 23K compared to that noticed in the 2-D simulation of the cathode without considering the random GDL structure.
- It has also been demonstrated that when the oscillatory nitrogen is supplied, with an amplitude of 0.03 along with catalyst loading 0.1, the maximum temperature achieved is 325 K (54.85 °C) at 35 sec. Moreover, it can also be observed that there is a continuous variation in the maximum temperature over time. This helps in maintaining a lower operating temperature of the cell.

The study of hot spot identification and mitigation with the 3-D random GDL porous structure has been extended to different shapes of the channels in the next chapter. The effect of shape of the channels on the mitigation of the hot spots are studied in detail with the developed 3-D model of the cathode. Different shapes of the channel geometries also serve as another strategy for hot spot mitigation apart from the use of the oscillatory nitrogen gas supply.

Chapter 7

Further studies on hot spot mitigation using different channel configurations

Chapter 7

Further studies on hot spot mitigation using different channel configurations

Chapter -6 discussed the extension of the thermal model of the cathode side for identification of the hot spots using the computational domain with 3-D random porous structure of the GDL. The consideration of more realistic porous carbon paper as part of the computational domain resulted in conservative values of the hot spot temperatures, which are less by 23 K compared to the predictions from 2-D simulations in case of conventional straight flow channel. This chapter aims to propose different geometric shapes of the channel configuration as a strategy with the 3-D model for hot spot mitigation apart from the bumped channel design, which was discussed in Chapter-5. The effect of shape of the channel on hot spot mitigation is studied by considering six different variants, which include bumped, wavy, variable wavy A & wavy B, diverging and converging designs. The results obtained from the simulation of these cases in terms of hot spot temperature and pressure drop are discussed in detail in the following sections. Towards the end, the effect of oscillatory input on these variants is also presented. This chapter covers the last objective of the current computational study on the hot spot identification and mitigation.

7.1 Description of cases and geometries considered

This study is an extension of the work presented in the previous chapter on considering the 3D computational domain of the cathode side with a more realistic randomized porous structure for the GDL. This simulation study explores the local hot spot patch identification using fluid, heat, species, and energy transport in a new 3D reconstructed carbon paper GDL used in a single-phase, time-dependent, non-isothermal model simulation using different shapes of the flow channels. Following channel shapes are considered in this regard.

1. Bumped flow channel
2. Wavy flow channel
3. Variable wavy channel A
4. Variable wavy channel B
5. Diverging flow channel
6. Converging flow channel

It attempts to study how the channels of different geometric shapes would affect gas transport and hot spot formation. No studies on the non-isothermal studies with hot spot identification using 3D reconstructed GDL structure and the above channel configurations in the literature are available. This chapter aims to fill this gap by exploring how reactive gases diffuse over a new 3D reconfigurable carbon paper (GDL) in a single-phase three-dimensional transient model simulation based on the methodology described in the previous chapter. The study also explores how the geometric shape of the channel effects the hot spot temperature in the PEM fuel cell and thereby helps in improving the durability of the membrane.

Figure 7.1 shows the different geometric shapes of the channel designs that were studied in order to mitigate the development of hot spots. The design parameters for each of the channel shapes can be found in Figure 7.1. In the Chapter-5, the bumped gas flow channel was studied in detail with regard to the effect of bump size on the hot spot mitigation and pressure drop using a 2D cathode domain with a regular GDL structure. However, for the comparative study, the bumped channel design with a size of 0.5 mm radius and the spacing between the bumps as 0.5 mm (the optimized dimensions as discussed in Chapter-5) was simulated again on the 3D computational domain with reconstructed randomized GDL porous structure. The wavy flow channel was constructed with six peaks and five troughs of height as 0.5 mm and by maintaining uniform distance between two adjacent troughs and peaks as 1.8 mm. The variable wave channel A was constructed with the peaks and troughs close to the outlet of the channel. At the same time, they corresponded to the inlet position for the variable wave channel B [157]. In these variable wavy types, A and B, the spacing between the adjacent peaks or troughs was not maintained uniform but they were spaced with 10% increment in the spacing between the troughs/peaks from the outlet (type A) or inlet (type B) as shown in Figure 7.1 (c) & (d). The divergent flow channel has an inlet depth of 0.5 mm and an outlet depth of 1 mm. In convergent flow channels, the inlet depth is 1 mm, and the outlet depth is 0.5 mm.

The computational domains with the above six types of channel configurations were meshed using unstructured mesh. The domains were divided into the tetrahedral mesh elements using the multi-region method. The details of the mesh count are presented in Table 7.1.

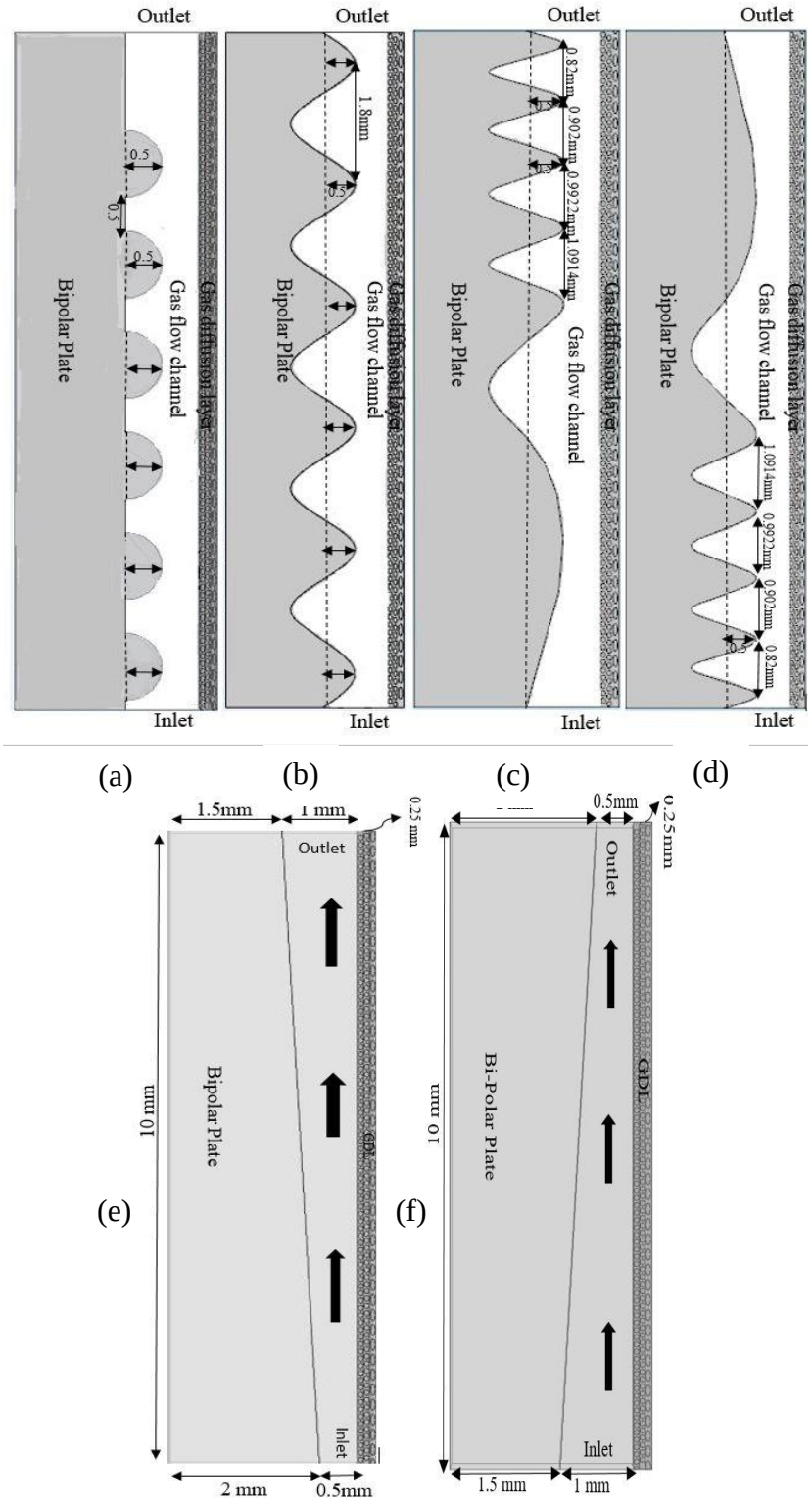

Figure 7.1 Different geometric shapes of the channels were studied for mitigation of hot spots: (a) bumped, (b) wavy, (c) variable wavy-type A, and (d) variable wavy-type B, (e) diverging and (f) converging

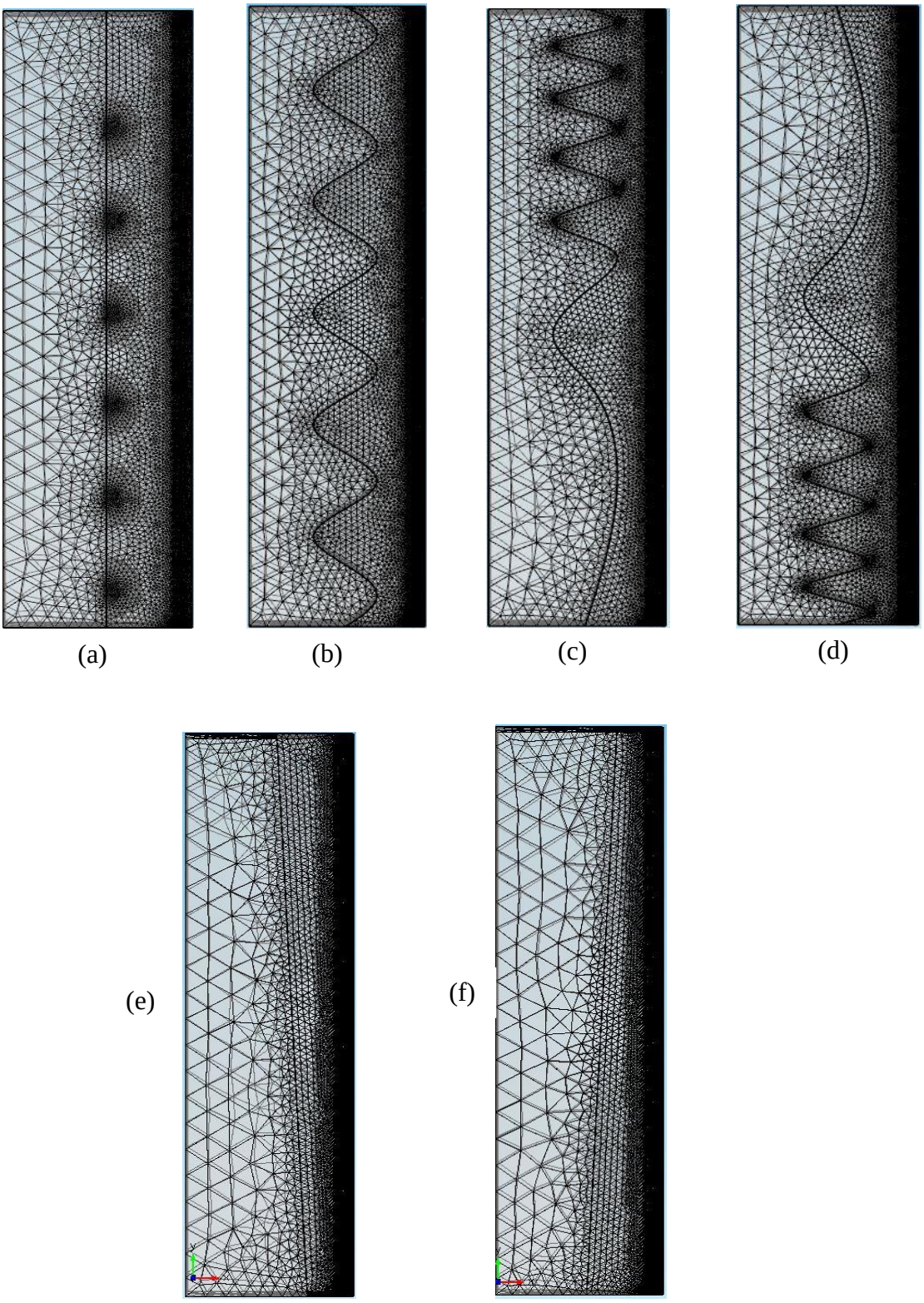

Figure 7.2 Computational mesh used for channels of (a) bumped (b) wavy (c) variable wavy-A (d) variable wavy- B, (e) diverging and (f) converging

Table 7.1 Mesh details of the computational domains with six types of channel shapes

Mesh type	Bumped	Wavy	Variable A	Variable B	Diverging	Converging
Tetrahedral	1418461	1358632	1442837	1441878	1309815	1309802
Triangular	246809	239353	244701	244609	233445	232609
Edge	5077	50469	50709	50709	50062	50055
Vertex	2022	2034	2034	2034	1992	1992

7.2 Numerical model description

The equations solved and the methodology adopted were discussed in detail in the previous chapter-3 and this served as the foundation for the numerical 3D model used in this study. The inlet boundary of the cathode was defined using the inlet velocity and humidity. The composition of the inlet gas mixture was defined as (weight fraction) consisting of oxygen (0.14), nitrogen (0.85), and a minute quantity of water vapor (0.01) and was fed at a velocity of 0.01 m/s. This oxygen composition, which is less than that present in the ambient air was used as per the optimum composition obtained in Chapter-4. Table 7.2 lists different operating conditions used in the present study. The density and dynamic viscosity of the mixture of gases were given as operating temperature and pressure-dependent properties. All exterior walls were defined as thermally insulated domains. The cathode channel outlet was designated as a pressure (1 bar) outlet to prevent backflow. On the surface of the Pt catalyst on the extreme layer of the GDL, it was assumed that the wall convective heat flux was transported into the gas diffusion layer; Chapter-3 may be referred for more information on the methodology and solution strategy.

Table 7.2 Operating conditions used in the present study.

Variable	Units	Value
Operating Temperature	°C	80
Operating Pressure	Pa	100,000
Cathode Gas Inlet	m/s	0.01
Oxygen	Mass fraction	0.14
Nitrogen	Mass fraction	0.85
Water vapor	Mass fraction	0.01

7.3 Result and discussion

Different simulations were carried out to observe the hot spot formation in the 3D cathode side PEM fuel cell, having reconstructed porous GDL structure with straight, bumped, different wavy types, converging and diverging gas flow channels. The results were analysed to see how effectively these different geometric shapes of the gas flow channel mitigate the hot spot formation.

7.3.1 Hot spot formation in flow channels with different geometric shapes

The contours of the temperature distribution in the four-channel designs at different times are shown in Figure 7.3. In all the cases, the maximum hot spot temperature was observed near the entrance of the gas flow channel, the GDL, and the membrane interface. Unlike the straight flow channel, the reactant gas has constricted area in its flow path, and this causes the fluid velocity to be high. As opposed to the straight flow channel, the reactant gas has a constricted area in its flow path in the case of these four-channel designs, and as a result, the fluid velocity is high. This assists in removing heat generated on the cathode side by convection, thereby minimizing the hot spot temperature in the cell. As can be seen from a comparison of Figures 6.7 and 7.3, both the magnitude of the maximum hot spot temperature and the area of the hot spot patches decrease in the channels having bumped and three waveform shapes compared to that of a straight gas flow channel. Among the four-channel variants - bumped, wavy, variable wave A and variable wave B, it can be observed that the wavy and variable wavy B channel offers more reduction in the maximum surface or local hot spot temperature.

Figures 7.4 (a) and 7.5 (a) illustrate the highest surface (hot spot) temperature for diverging and converging channels, respectively. Since the inlet size is smaller, the velocity in the diverging flow channel is greater near the inlet boundary, as illustrated in Figure 7.4 (b). The total flux (convective and diffusive) of oxygen mass fraction through the gas diffusion layer reduces due to the higher velocity at the inlet boundary and diffusing less towards the catalyst layer surface, which is an essential variable for electrochemical reaction. Figure 7.4 (a) above shows that the oxygen mass fraction consumes completely at the inlet boundary close to the gas diffusion layer, where minimal velocity can be noticed. Moreover, the heat production is decreased owing to the electrochemical reaction at the catalyst layer due to low total diffusion toward the catalyst layer.

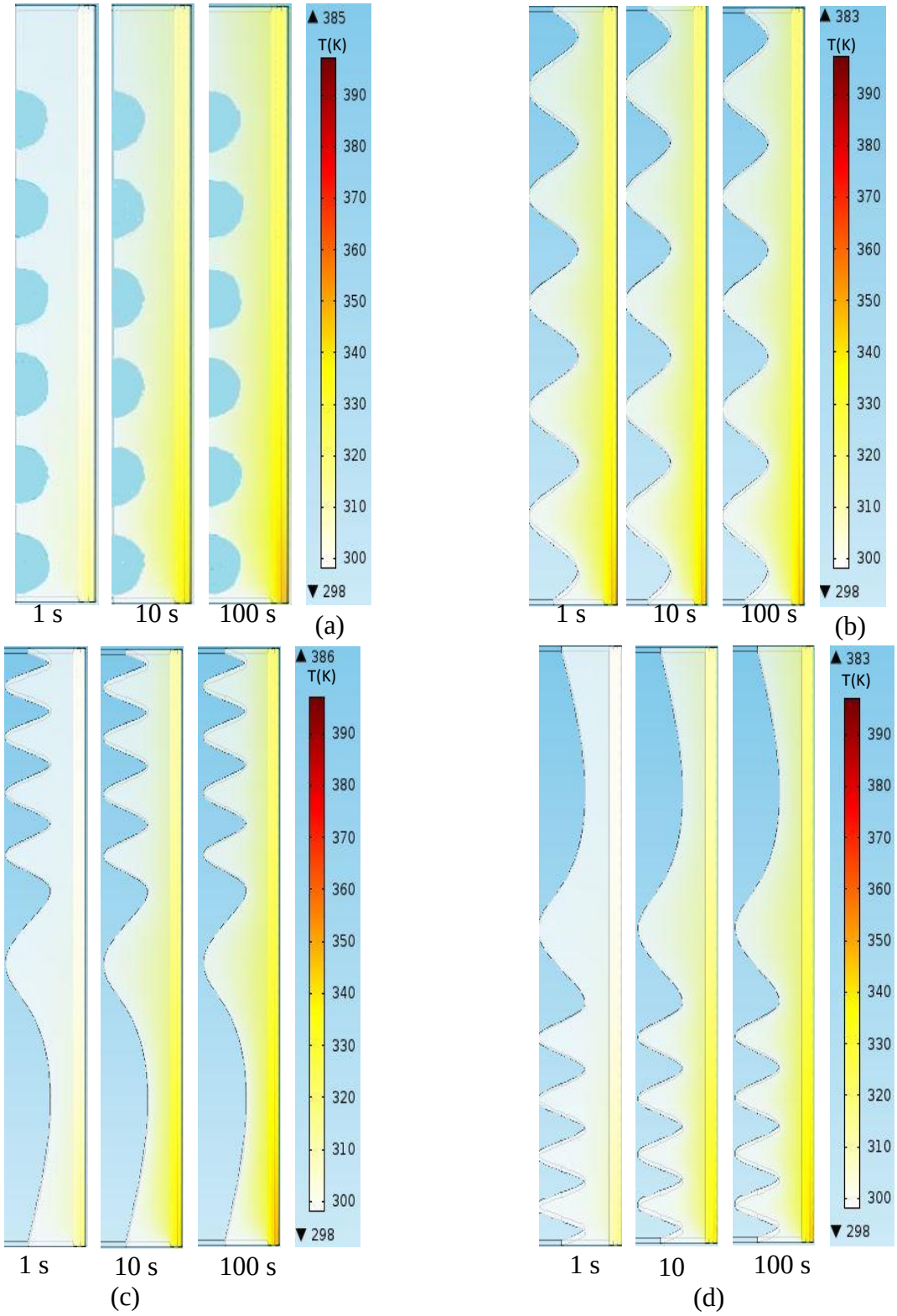

Figure 7.3 Temperature distribution in the cathode side of the PEM fuel cell at different times with (a) bumped (b) wavy, (c) variable wavy type A, and (d) variable wavy type B

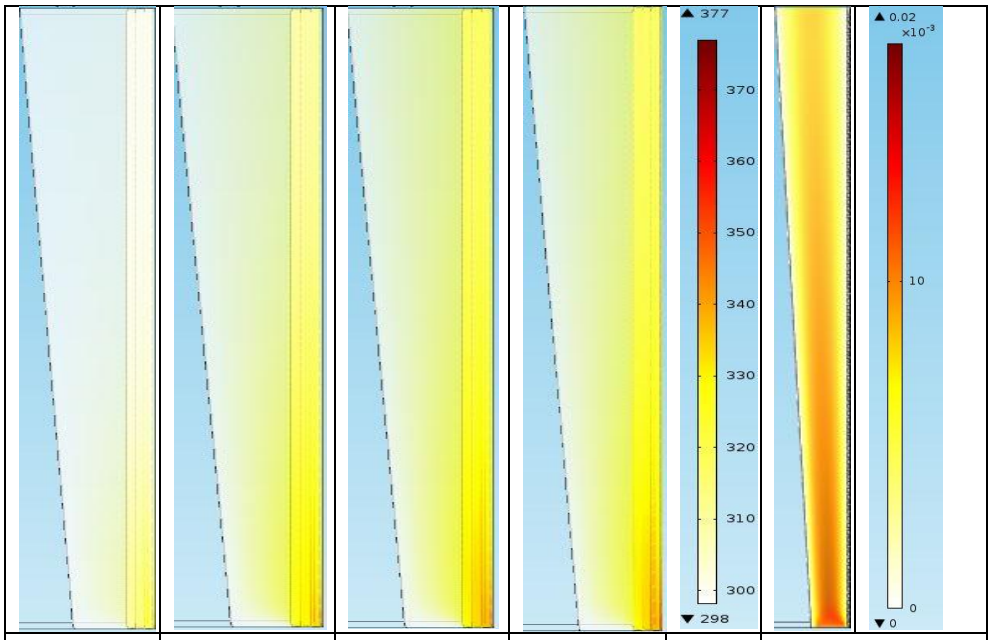

Figure 7.4 (a) Maximum surface or local hot spot temperature (K) map, (b) velocity in the diverging gas flow channel (at 100 s of operation).

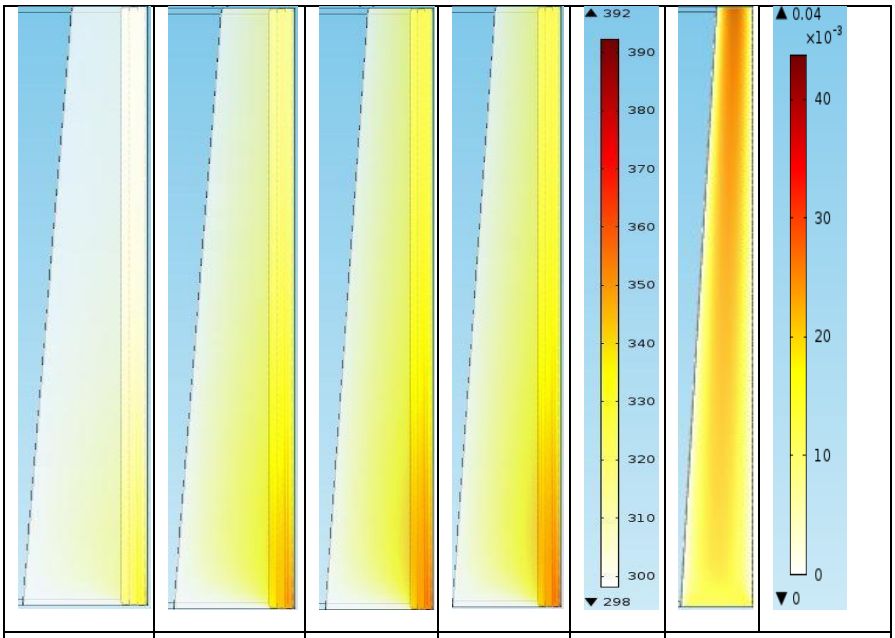

Figure 7.5 (a) Maximum surface or local hot spot temperature (K) map (b) velocity in the converging gas flow channel (at 100 s of operation).

The spatial location of the local hot spot patch in the divergence and convergence flow channel, which is closed to the inlet boundary of the reactive gas flow channel, is also illustrated in Figures 7.4 (a) and 7.5 (a). As the operating duration progressively grows, the intensity of the local hot spot patch near the inlet boundary grows more intense in the catalyst and membrane layer, as illustrated in Figures 7.4 (a) and 7.5 (a). Consequently, the maximum surface temperature is limited to 377 K (103.85 °C).

As shown in figure 7.5 (b), the inlet feed velocity of the air in a converging flow channel is less than that of a diverging flow channel due to the increased area at the entrance boundary; nevertheless, when reactant gas approaches the outlet boundary, the feed velocity accelerates. In addition, there is a higher mass fraction of oxygen in the inlet region of the converging flow channel than in the inlet region of the diverging flow channel. Moreover, the reactants have more residence time at the entrance region; consequently, oxygen starts to be consumed faster at the inlet boundary region. An electrochemical reaction occurs more due to more oxygen diffusion in the catalyst layer because the reactive gases have a longer residence time than in the divergence flow channel case at the inlet area in figure 7.5 (a). Contrary to diverging designs, it has been shown that the converging channel helps to enhance the total diffusion of reactants. Consequently, the maximum surface temperature is restricted to 392 K (118 °C) in the converging gas flow channel. However, increasing gas velocity is due to a decreased area at the outlet boundary.

It can be clearly noted from the start-up dynamics shown in Figure 7.6 that the highest hot spot temperature is observed in the straight gas flow channel compared to that observed with different channel geometric shapes. The initial temperature corresponding to t=0 sec was the same for all seven cases, and the hot spot temperature increased with time and stabilized at different temperatures. The maximum hot spot temperature can be observed at 397 K for a straight flow channel, whereas the lowest hot spot temperature within 100 seconds can be observed at 378 K (104 °C) for a diverging flow channel. The stabilized hot spot temperatures noticed were 385 K, 383 K, 386 K, 383 K, 377 K and 392 K, respectively, for the bumped, wavy, variable wave A, variable wave B, diverging and converging channels, which were lower than that observed (397 K) in the straight flow channel. Among all the different channel shapes, the diverging, bumped and wavy flow channels are found to attain the maximum temperature quickly. It can also be observed that the diverging channel design helps in lowering the hot spot temperature (377 K) to

a larger extent than other designs. Next best channel shapes showing good reduction in the hot spot temperature are the wavy and the variable wave type – B channels by around 383 K compared to the straight flow channel. Though these shapes mitigate the hot spot formation, these designs restrict the reactant flow in the channel and result in a high-pressure drop. Therefore, due care has to be exercised in choosing the proper shape of the channel.

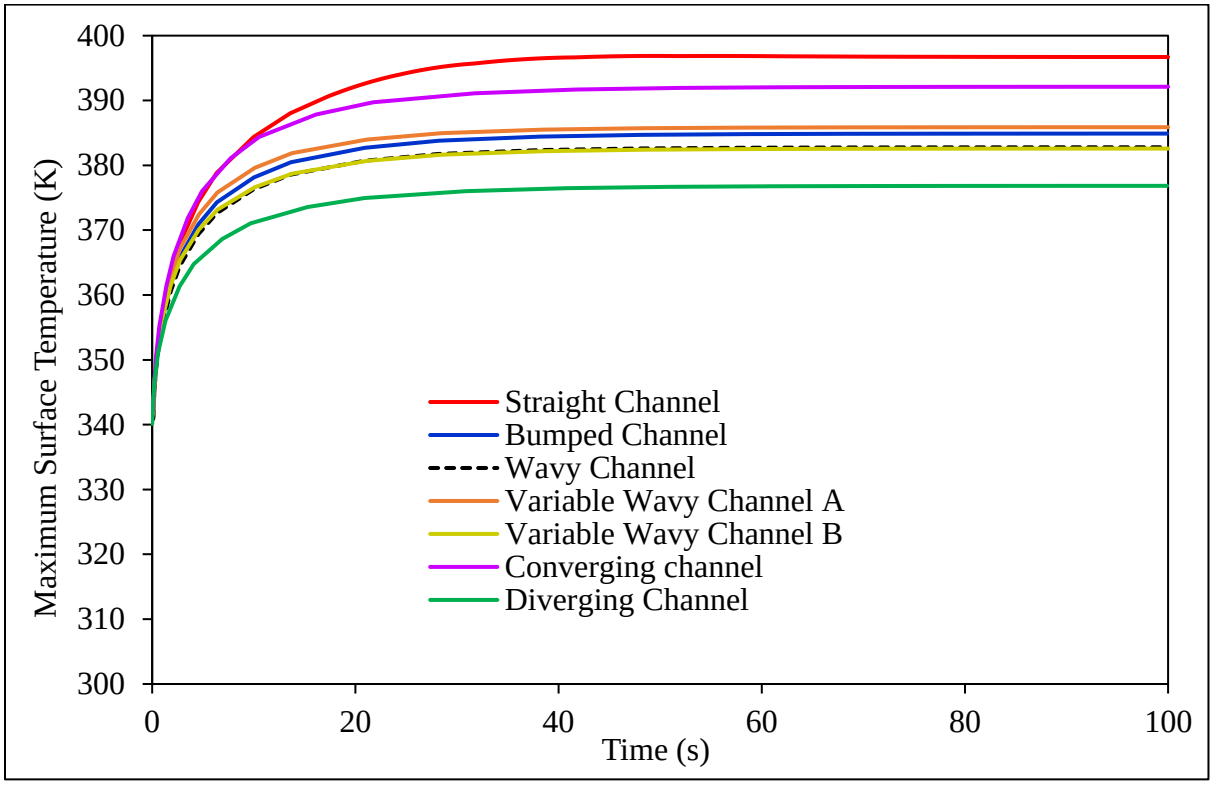

Figure 7.6 Influence of channel shapes on the maximum hot spot temperature over time.

7.3.2 Pressure drop for all flow channel shapes

Figure 7.7 displays the pressure drop comparison among the different geometric shapes of the channels considered. It is evident that the conventional straight flow channel which has no constrictions in the flow path offers the lowest pressure drop compared to the bumped, wavy, wavy A, wavy B, and converging channels. The maximum pressure drop noticed is 400 Pa with the wavy channel B, which is eight times more than that in the conventional straight flow channel. The pressure drops in the case of wavy, variable wave A, bumped, and converging channels are 2.6, 2.2, 2.2, and 2 times the pressure drop in the case of the straight channel (54 Pa) respectively, while the pressure drop in case of diverging channel is found to be 49 Pa, slightly lower than the conventional straight flow channel. It is desirable for the flow field channels not to result in high-

pressure drops in order to extend the life of the delicate membrane, the MEA of the cell, and to reduce the auxiliary power losses. Hence, flow field pressure drop is an important consideration in the design of fuel cells and stacks. Considering the channel structure and the pressure drop offered into account, the use of diverging shape would be a favorable design to mitigate the local hot spot formation in the cell. It provides no increase or comparatively very less increase in pressure drop while reducing the hot spot temperature considerably from that of a straight channel, bumped channel, converging channel and other wavy channel designs. Although the bumped and other wavy channel designs reduce hot spot temperature compared to that of straight flow channel, there are chances for corrosion in these designs because of the presence of sharp corners and edges. A diverging channel shape is advantageous in extending the life of bipolar plates by avoiding corrosion, as corrosion is another essential characteristic of bipolar plates that must be considered when selecting a suitable channel design for bipolar plates. The difficulty of manufacturing will also be less for diverging design compared to the bumped and other variable waveforms.

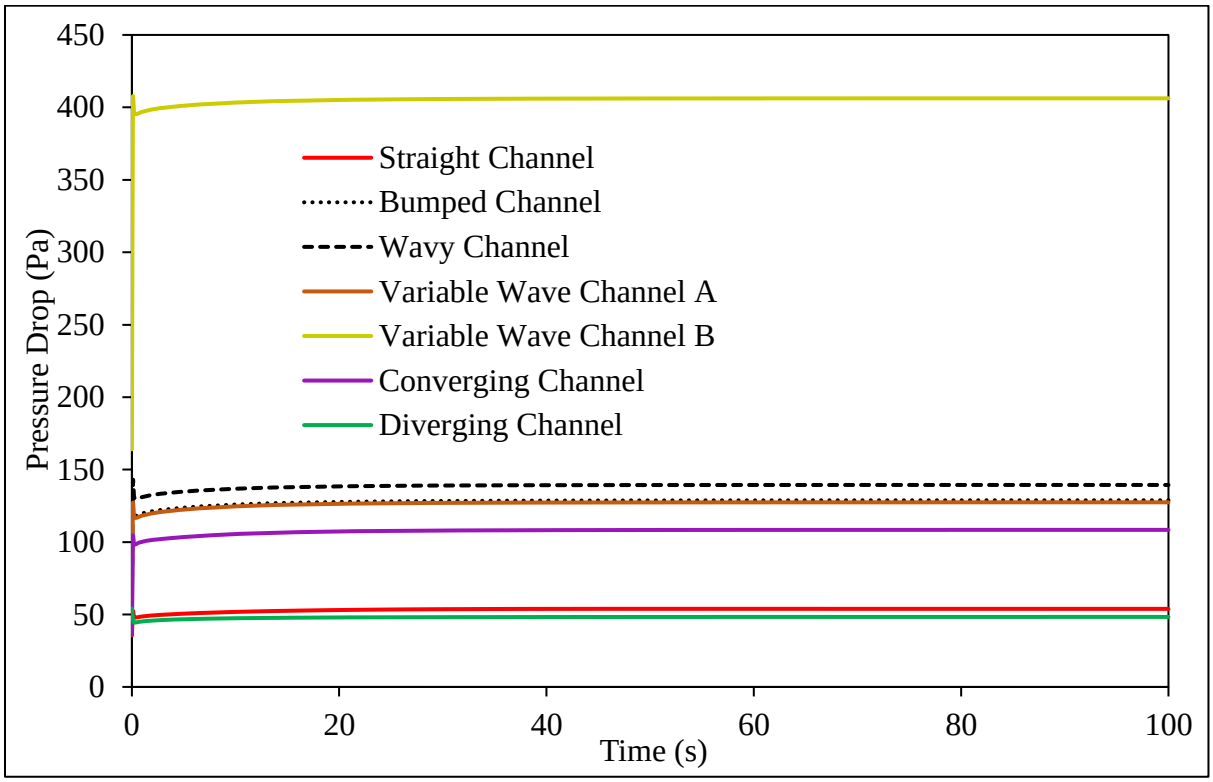

Figure 7.7 Pressure drop across the channel for different shapes of the gas channel designs

7.3.3 Using an oscillatory supply of the nitrogen gas in the inlet of the proposed channels

The effectiveness of using an oscillatory supply of nitrogen gas for the typical 3D straight flow gas channel in minimizing the formation of hot spot temperature was discussed in depth in the previous chapter. This has been used in this case for the channels that have bumps, three distinct waveforms, divergent and convergent flow patterns, and the outcomes of these have been contrasted with those of the conventional straight channel. The sinusoidal or oscillatory supply composition of the three gaseous components in the cathode side inlet is represented in the previous chapter. These are set up such that at any moment in time, the total of the three fractions of oxygen, nitrogen, and water vapor equals one. Here, δ is the amplitude of nitrogen and oxygen oscillatory compositions. According to the findings of the prior chapter's investigation of the cyclic gas supply through the straight gas flow channel, the amplitude of the cyclic gas supply and the fractional coverage of the Pt catalyst was effectively chosen as $\delta = 0.03$ and $\varepsilon_s = 0.10$ respectively for the purpose of exploring the impact of the oscillatory supply on the various geometric shapes of the channel design.

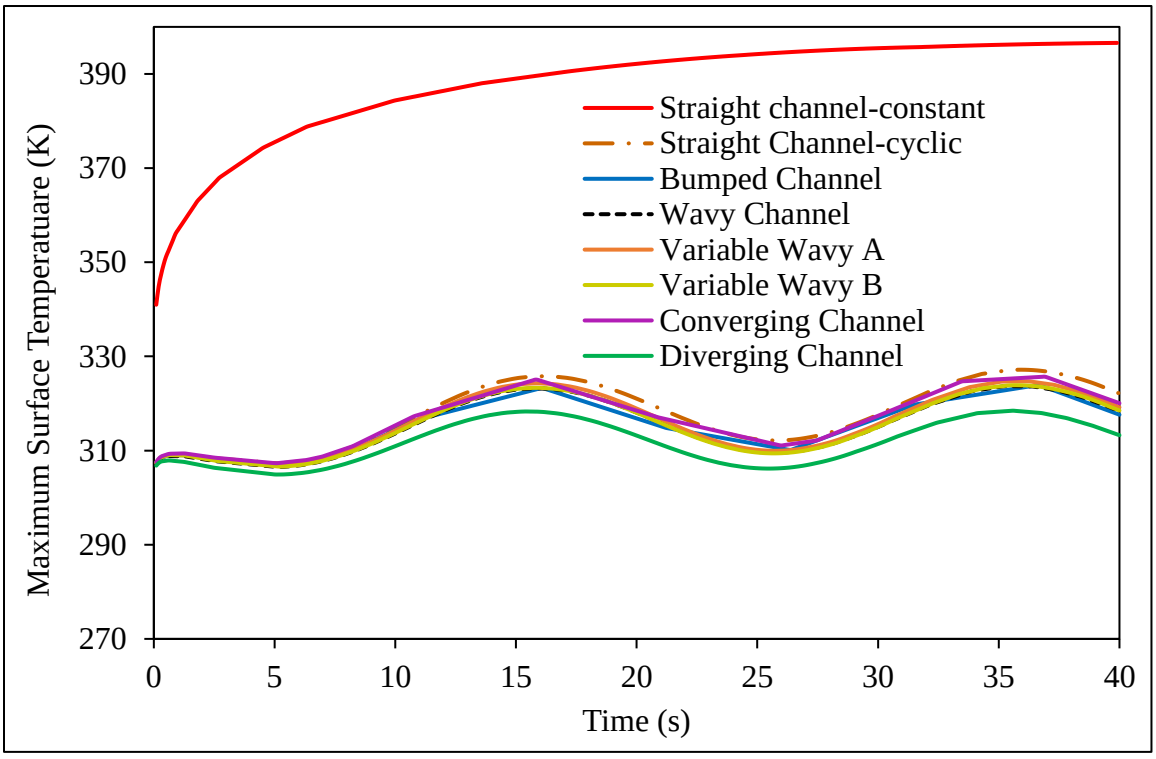

Figure 7.8 Comparison of maximum surface temperature on membrane-catalyst interface for ε_s=0.10 and oscillatory supply with amplitude, δ = 0.03 for different channel designs.

Figure 7.8 shows the maximum temperature obtained for the oscillatory input for the six different geometric shapes of the channels. For comparison purposes, maximum temperature obtained in conventional straight flow channel with constant gas composition and oscillatory gas composition at the inlet are also shown in Figure 7.8. It can be seen that the cyclic supply of nitrogen gas along with oxygen at the inlet reduced the maximum hot spot temperature almost by the same extent i.e., 72 to 80 K (72 K in case of straight channel and 80 K in case of diverging channel) for all the shapes of the channels when compared to hot spot temperature in straight flow channel with constant gas composition at the inlet (i.e., 397 K). On the other hand, pressure drop across in these shapes of the channels, except for diverging channel was higher compared to that of the straight channel as illustrated in Figure 7.7. Hence, it can be inferred from this result that when the oscillatory gas composition at the inlet is used as strategy for hot spot mitigation, applying it on either straight flow channel or on diverging channel is effective rather than applying it on any other geometric shape of the channel. In that case, the maximum temperature attained can be maintained as low as 317 K (diverging with cyclic) or 325 K (straight with cyclic) for the oxygen and nitrogen mass fractions considered in this study. This would ensure safe thermal operation of the fuel cell as far as membrane durability is considered. It can also be concluded that the cyclic input at the cathode inlet is an effective strategy to reduce the local hot spot temperature early and more significantly, which ultimately contributes to the improved membrane stability and durability of the PEM fuel cell.

7.4 Summary

The effect of geometric shape of the gas flow channel on the hot spot mitigation was studied by considering bumped, wavy, variable wavy A, variable wavy B, converging, and diverging flow channels in this work. The key conclusions from the study are summarized as follows:

- All the different shapes of the channels lowered the maximum surface temperature at the cost of increased pressure drop, while the diverging channel helped in reducing the maximum hot spot temperature to a greater extent (20 K) with low pressure drop compared to that of the conventional straight flow channel.

- The cyclic (sinusoidal) input of oxygen and nitrogen with amplitude of 0.03 and time period of 20s at the cathode inlet resulted in lowering of the maximum hot spot temperature

to 317 to 325 K for different shapes of the channels including straight channel compared to that realized in straight channel with constant input of gases.

- When the oscillatory gas composition at the inlet was used as strategy for hot spot mitigation, applying it on either straight flow channel or on diverging channel was effective rather than applying it on any other geometric shape of the channel.

Chapter- 8

Overall Conclusions and Scope for Future Work

Chapter- 8

Overall Conclusions and Scope for Future Work

This chapter presents the conclusions drawn from the entire study discussed in the previous chapters and the potential scope for further investigation.

8.1 Overall Conclusions

The aim of this study was to come up with a simulation analysis of the cathode side of single-cell PEM fuel cell for the identification and mitigation of the local hot spots. The CFD simulations carried out in COMSOL Multiphysics 4.4 were able to effectively simulate the local hot spot patches near the channel inlet regions. Two different strategies were proposed through simulations to mitigate the hot spot formation – (i) using different shapes of the gas flow channels and (ii) using cyclic input of nitrogen and oxygen at the cathode inlet. Following are the major conclusions drawn from the entire study.

- The temperature maps obtained from the steady-state simulation of the cathode portion of PEMFC showed that the highest temperature or hot spot occurrence was close to the entrance.
- When the purity of the oxygen is higher, a higher power density may be generated on the cathode side; nevertheless, the hot spots will be formed and effect the life of the membrane.
- The study revealed that an inlet velocity of 0.01 m/s for the reactant gas was ideal for avoiding excess use of pure oxygen and nitrogen mass fractions, while an optimal oxygen oxygen and nitrogen mass fractions of 0.14, 0.85, and 0.01 for water vapor (relative humidity) were shown to produce better performance of PEMFC.
- 2-D transient simulation study on the cathode side of the PEM fuel cell revealed that gas flow channels with bumps were resulting in lower hot spot temperatures compared to straight channels. A bump size of 0.5 mm was recommended from the hot spot temperature and pressure drop perspective.
- The strategy of the cyclic supply of nitrogen gas and oxygen gas was found to be effective in the mitigation of the local hot spots significantly.
- The simulation analysis of the combination of the two techniques, i.e., cyclic input to the bumped gas flow channel, has shown a further reduction in the hot spot temperature.

- Local hot spot formation was simulated by incorporating the reconstructed 3D porous GDL structure on the cathode side computational domain of the PEM fuel cell.
- The maximum surface or local hot spot temperature obtained in the straight channel during the 100 seconds of operation is 397 K (123.85 °C). This temperature is observed to be less by 23K compared to that noticed in the 2-D simulation of the cathode without considering the random GDL structure.
- Different shapes of the channels (such as bumped, wavy, variable wavy A, variable wavy B, converging and diverging) lowered the maximum surface temperature at the cost of increased pressure drop, while the diverging channel helped in reducing the maximum hot spot temperature to a greater extent (20 K) with low pressure drop compared to that of the conventional straight flow channel.
- The oscillatory nitrogen gas supply strategy significantly reduces the local hot spot temperature in different flow channel designs, including straight, bumping, wavy, variable A, variable wavy B, converging, and diverging channel designs.
- The cyclic (sinusoidal) input of oxygen and nitrogen with amplitude of 0.03 and time period of 20s at the cathode inlet resulted in lowering of the maximum hot spot temperature to 317 to 325 K for different shapes of the channels including straight channel compared to that realized in straight channel with constant input of gases.
- When the oscillatory gas composition at the inlet was used as strategy for hot spot mitigation, applying it on either straight flow channel or on diverging channel was effective rather than applying it on any other geometric shape of the channel.

8.2 Scope for Future work

Through the computational fluid dynamic studies, the present work simulated the possibility of formation of local hot spots at the membrane-catalyst layer interfaces near the entrance of the channels under worst case scenario of no cooling conditions in PEM fuel cells. The study also proposed different strategies for the mitigation of the local hot spots such as changing geometric shape of the channels and employing cyclic supply of oxygen and nitrogen at the cathode inlet. It is envisaged that the present work can be further continued as there is a good scope for future work in the following areas:

- Experimental studies using the proposed channel designs on the cathode side of the PEM fuel cell can be conducted to realize the findings of the present work.
- Full-scale 3D simulation of the single-cell model with both anode and cathode sides to examine the formation of hot spots.
- Cooling strategies using water and other heat transfer fluids can be explored for mitigation of the hot spot formation.
- The present study conducted on low temperature PEM fuel cells can also be extended to medium to high temperature PEM fuel cells operating at 100 to 180 ^{o}C.

List of Publications based on the Thesis

Journal Papers:

1. **Ramakant Gadhewal,** Sunil Kumar Thamida, Venu Vinod Ananthula, Venkata Suresh Patnaikuni, Hot spot Identification in PEM Fuel cell and its Purging Strategies, **Chemical Papers**, 76, 1199-1211, 2022. https://doi.org/10.1007/s11696-021-01932-0. (SCI)
2. **Ramakant Gadhewal,** Sunil Kumar Thamida & Venu Vinod Ananthula**,** Optimum supply and utilization of pure oxygen along with nitrogen on the cathode side for thermal stability of a proton exchange membrane fuel cell, **International Journal of Modelling and Simulation**, 41(1), 67-79, 2021. https://doi.org/10.1080/02286203.2019.1674766 (Scopus)
3. **Ramakant Gadhewal,** Venu Vinod Ananthula, Venkata Suresh Patnaikuni, CFD Simulation of hot spot in PEM fuel cell with diverging and converging flow channels, **Materials Today: Proceedings**, 2022 **(Under review: Revised version submitted)** (Scopus)
4. **Ramakant Gadhewal,** Venu Vinod Ananthula, Venkata Suresh Patnaikuni, Effect of geometric shape of the flow channel on hot spot mitigation in PEM fuel cell, **International Journal of Energy Research,** 2022 **(Under review)**

National and International Conference Papers:

1. **Ramakant Gadhewal**, Venu Vinod A, Sunil Kumar Thamida. Simulation of Multiphysics in a PEM Fuel Cell. 2nd International Conference on New Frontiers in Chemical, Energy and Environmental Engineering (INCEEE-2019) 15 – 16 February 2019 at National Institute of Technology, Warangal.
2. **Ramakant Gadhewal**, Venu Vinod A, Sunil Kumar Thamida. Determination of hot spots adjacent to the membrane of a proton exchange membrane fuel cell (PEMFC): Simulation. 22-23 March, 2019 at CBIT, Hyderabad. National.
3. **Ramakant Gadhewal**, Venu Vinod A, Sunil Kumar Thamida. CFD Simulation of PEM Fuel Cell for identification of hot spots.14-16 February, 2020. International conference on Energy and Environmental Technologies for Sustainable Development. MNNIT Allahabad.

4. **Ramakant Gadhewal**, Venu Vinod A, Venkata Suresh Patnaikuni. 3-Dimensional CFD modelling of PEM fuel cell cathode for Hot spot identification.2-4 April, 2021. A National e-conference on Recent Trends in Fluid Dynamics Research (RTFDR-21).NIT Rourkela.
5. **Ramakant Gadhewal**, Venu Vinod A, Venkata Suresh Patnaikuni. CFD simulation of hot spot in PEM fuel cell with diverging and converging flow channels.18-19 February, 2022. International conference on novel materials and technologies for energy and environment applications. BITS Hyderabad campus.

References

[1] UN DESA. World Population Prospects 2021: Highlights | Multimedia Library- United Nations Department of Economic and Social Affairs. United Nations 2021.

[2] Outlook BPE. BP Energy Outlook-2021 Insight from the Evolving Transition scenario - India's share of total global primary energy demand is set to BP Energy Outlook-2021 Insight from the Evolving Transition scenario - India 2021.

[3] IEA, Global CO2 emissions in 2021, International Energy Agency (IEA), Paris, https://www.iea.org/articles/global-co2-emissionsin-2021 (accessed: Jan 2022).

[4] Peijian Lin, Hongyu Wang, Guodong Wang, Jirui Li, and Juncai Sun. 2021. Numerical study of optimized three-dimension novel Key-shaped flow field design for proton exchange membrane fuel cell. https://doi.org/10.1016/j.ijhydene.2021.11.170

[5] Barbir F., PEM Fuel Cells Theory and Practice 2nd Edition. 2012

[6] Bilal A., Introduction to transfer phenomena in PEM fuel cells. 2018.

[7] Ryan O'Hayre, Suk-Won Cha, Whitney G. Colella, Fritz B. Prinz, Fuel Cell Fundamentals. John Wiley & Sons Inc. 2016.

[8] San Ping Jiang, Qingfeng Li. Introduction to Fuel Cells: Electrochemistry and Materials.2021.

[9] Liu H, Li P, Juarez-Robles D, Wang K, Hernandez - Guerrero A. Experimental study and comparison of various designs of gas flow fields to PEM fuel cells and cell stack performance. Front Energy Res 2014; 2: 1-8. https://doi.org/10.3389/fenrd.2014.00002.

[10] Polarization Curves n.d. https://www.fuelcellstore.com/blog-section/polarization-curves (accessed April 04, 2022).

[11] Viktor Hacker, Shigenori Mitsushima, Fuel Cells and Hydrogen-From Fundamentals to Applied Research, First ed., Elsevier Inc., United States, 2018.

[12] M. Dou, M. Hou, D. Liang, et al., Behaviors of proton exchange membrane fuel cells under oxidant starvation, Journal of Power Sources, 196: (5); (2011) 2759–2762, https://doi.org/10.1016/j.jpowsour.2010.11.005.

[13] M. Cai, M.S. Ruthkosky, B. Merzougui, et al., Investigation of thermal and electrochemical degradation of fuel cell catalysts, Journal of Power Sources, 160:(2); (2006) 977–986, https://doi.org/10.1016/j.jpowsour.2006.03.033.

[14] M. Zhao, W. Shi, B. Wu, et al., Influence of membrane thickness on membrane degradation and platinum agglomeration under long-term open circuit voltage conditions, Electrochim. Acta: 153; (2015) 254–262, https://doi.org/10.1016/ j. electacta.2014.12.024.

[15] S. Kreitmeier, P. Lerch, A. Wokaun, et al., Local degradation at membrane defects in polymer electrolyte fuel cells, Journal of Electrochem. Soc. 160 (4) (2013) F456–F463, https://doi.org/10.1149/1.023306jes.

[16] Tzelepis, S., Kavadias, K. A., Marnellos, G. E., & Xydis, G. A review study on proton exchange membrane fuel cell electrochemical performance focusing on anode and cathode catalyst layer modelling at macroscopic level. Renewable and Sustainable Energy Reviews.2021; 151, 111543. https://doi.org/10.1016/j.rser.2021.111543.

[17] Zhang, S., Xu, H., Qu, Z., Liu, S., & Talkhoncheh, F. K. Bio-inspired flow channel designs for proton exchange membrane fuel cells: A review. Journal of Power Sources.2022; 522, 231003. https://doi.org/10.1016/j.jpowsour.2022.231003

[18] Marappan, M., Palaniswamy, K., Velumani, T., Chul, K. B., Velayutham, R., Shivakumar, P., & Sundaram, S. Performance Studies of Proton Exchange Membrane Fuel Cells with Different Flow Field Designs – Review. Chemical Record.2021; 21(4), 663–714. https://doi.org/10.1002/tcr.202000138.

[19] Sauermoser, M., Kizilova, N., Pollet, B. G., & Kjelstrup, S. Flow Field Patterns for Proton Exchange Membrane Fuel Cells. Frontiers in Energy Research.2020; 8, 1–20. https://doi.org/10.3389/fenrg.2020.00013.

[20] Arif, M., Cheung, S. C. P., & Andrews, J. Different Approaches Used for Modeling and Simulation of Polymer Electrolyte Membrane Fuel Cells: A Review. Energy and Fuels.2020; 34(10), 11897–11915. https://doi.org/10.1021/acs.energyfuels.0c02414.

[21] Marappan, M., Palaniswamy, K., Velumani, T., Chul, K. B., Velayutham, R., Shivakumar, P., & Sundaram, S. Performance Studies of Proton Exchange Membrane Fuel Cells with Different Flow Field Designs – Review. Chemical Record.2021; 21(4), 663–714. https://doi.org/10.1002/tcr.202000138.

[22] Habib, M. S., Arefin, P., Salam, M. A., Ahmed, K., Uddin, M. S., Hossain, T. Islam, T. Proton Exchange Membrane Fuel Cell (PEMFC) Durability Factors, Challenges, and Future Perspectives: A Detailed Review. Material Science Research India. 2021; 18(2), 217–234. https://doi.org/10.13005/msri/180209.

[23] Faghri A, Guo Z. Challenges and opportunities of thermal management issues related to fuel cell technology and modeling. Int J Heat Mass Transfer. 2005; 48:3891–3920.
[24] Kandlikar SG, Lu Z. Thermal management issues in a PEMFC stack–A brief review of current status. Appl Therm Eng. 2009; 29:1276–1280.
[25] Polak A, Grzeczka G, Piłat T. Influence of cathode stoichiometry on operation of PEM fuel cells' stack supplied with pure oxygen. J Mar Eng Technol. 2017; 16(4):283–290.
[26] Bernardi DM, Verbrugge MW. Mathematical model of a gas diffusion electrode bonded to a polymer electrolyte. AIChE J 1991; 37:1151–63. https://doi.org/10.1002/aic.690370805.
[27] Ticianelli EA, Derouin CR, Redondo A, Srinivasan S. Methods to advance technology of proton exchange membrane fuel cells. J Electrochem Soc 1988; 2209:135. https://doi.org/10.1149/1.2096240.
[28] Springer TE, Wilson MS, Gottesfeld S. Modeling and Experimental Diagnostics In polymer electrolyte fuel cells. J Electrochem Soc 1993; 3513:140. https://doi.org/10.1149/1.2221120.
[29] Gloaguen F, Convert P, Gamburzev S, Velev OA, Srinivasan S. An evaluation of the macro-homogeneous and agglomerate model for oxygen reduction in PEMFCs. Electrochim Acta 1998; 43:3767–72. https://doi.org/10.1016/S0013-4686 (98)00136-4.
[30] Fukada S. Analysis of oxygen reduction rate in a proton exchange membrane fuel cell. Energy Convers Manag 2001:11.
[31] Ridge SJ, White RE, Tsou Y, Beaver RN, Eisman GA. Oxygen reduction in a proton exchange membrane test cell. J Electrochem Soc 1989; 136:1902–9. https://doi. org/10.1149/1.2097078.
[32] Hsuen H-K. Mechanistic approach to performance equations for cathodes in polymer electrolyte fuel cells. J Power Sources 2003; 123:26–36. https://doi.org/10.1016/S0378-7753 (03)00511-1.
[33] Jeng KT, Kuo CP, Lee SF. Modeling the catalyst layer of a PEM fuel cell cathode using a dimensionless approach. J Power Sources 2004; 128:145–51. https://doi. org/10.1016/j.jpowsour.2003.10.004.
[34] Song D, Wang Q, Liu Z, Navessin T, Eikerling M, Holdcroft S. Numerical optimization study of the catalyst layer of PEM fuel cell cathode. J Power Sources 2004; 126:104–11. https://doi.org/10.1016/j.jpowsour.2003.08.043.
[35] Qi Z, Kaufman A. Low Pt loading high performance cathodes for PEM fuel cells. J Power Sources 2003; 113:37–43. https://doi.org/10.1016/S0378-7753 (02) 00477-9.

[36] Du CY, Yang T, Shi PF, Yin GP, Cheng XQ. Performance analysis of the ordered and the conventional catalyst layers in proton exchange membrane fuel cells. Electrochim Acta 2006; 51:4934–41. https://doi.org/10.1016/j.electacta.2006.01.047.

[37] Broka K, Ekdunge P. Modelling the PEM fuel cell cathode n.d.:9.

[38] Gerteisen D, Hakenjos A, Schumacher JO. AC impedance modelling study on porous electrodes of proton exchange membrane fuel cells using an agglomerate model. J Power Sources 2007; 173:346–56. https://doi.org/10.1016/j.jpowsour.2007.04.071.

[39] Liu J, Oshima N, Kurihara E, Saha LK. Transport phenomena within the porous cathode for a proton exchange membrane fuel cell. J Power Sources 2010; 195:6342–8. https://doi.org/10.1016/j.jpowsour.2010.04.038.

[40] Hickner MA, Siegel NP, Chen KS, Hussey DS, Jacobson DL, Arif M. Situ high- resolution neutron radiography of cross-sectional liquid water profiles in proton exchange membrane fuel cells. Journal of Electrochemical Soc 2008; 155. https://doi.org/10.1149/1.2826287. B427.

[41] Eikerling M, Kornyshev AA. Electrochemical impedance of the cathode catalyst layer in polymer electrolyte fuel cells. Journal of Electroanal Chem 1999; 475:107–23. https://doi.org/10.1016/S0022-0728 (99)00335-6.

[42] S. J. Lee, S. Mukerjee, J. McBreen, Y. W. Rho R, Y. T. Kho, T. H.lee. Effects of nafion impregnation on performances of PEMFC electrodes. Electrochimical Acta 1997; 43:3693–701.

[43] Marr C, and Li X. Composition and performance modelling of catalyst layer in a proton exchange membrane fuel cell. 1999. p. 11.

[44] Rowe A, Li X. Mathematical modeling of proton exchange membrane fuel cells. J Power Sources 2001; 102:82–96. https://doi.org/10.1016/S0378-7753 (01)00798-4.

[45] Fan D, White RE. Modification of Newman's BAND (J) subroutine to multi-region systems containing interior boundaries: MBAND. J Electrochem Soc 1991; 138: 1688–91. https://doi.org/10.1149/1.2085854.

[46] Ticiauelli JzA, Derouin CR. valuation of plating in low catalyst loading electrodes to attain high power densities in SPE fuel cells n.d.:21.

[47] Ramousse J, Deseure J, Lottin O, Didierjean S, Maillet D. Modelling of heat, mass and charge transfer in a PEMFC single cell. J Power Sources 2005; 145:416–27. https://doi.org/10.1016/j.jpowsour.2005.01.067.

[48] Hu G, Li G, Zheng Y, Zhang Z, Xu Y. Optimization and parametric analysis of PEMFC based on an agglomerate model for catalyst layer. J Energy Inst 2014; 87:163–74. https://doi.org/10.1016/j.joei.2014.03.004.

[49] Sun W, Peppley BA, Karan K. An improved two-dimensional agglomerate cathode model to study the influence of catalyst layer structural parameters. Electrochim Acta 2005; 50:3359–74. https://doi.org/10.1016/j.electacta.2004.12.009.

[50] Acosta M, Merten C, Eigenberger G, Class H, Helmig R, Thoben B, et al. Modeling non-isothermal two-phase multicomponent flow in the cathode of PEM fuel cells. J Power Sources 2006; 159:1123–41. https://doi.org/10.1016/j.jpowsour.2005.12.068.

[51] Secanell M, Carnes B, Suleman A, Djilali N. Numerical optimization of proton exchange membrane fuel cell cathodes. Electrochim Acta 2007; 52:2668–82. https://doi.org/10.1016/j.electacta.2006.09.049.

[52] Kulikovsky AA, Divisel A and Kornyshev AA. Modeling the cathode compartment of polymer electrolyte fuel cells: dead and active reaction zones. Journal of Electrochem Soc 1999; 3981:146. https:// doi.org/10.1149/1.1392580.

[53] Kamarajugadda S, Mazumder S. Generalized flooded agglomerate model for the cathode catalyst layer of a polymer electrolyte membrane fuel cell. J Power Sources 2012; 208:328–39. https://doi.org/10.1016/j.jpowsour.2012.02.063.

[54] Kamarajugadda S, Mazumder S. On the implementation of membrane models in computational fluid dynamics calculations of polymer electrolyte membrane fuel cells. Comput Chem Eng 2008; 32:1650–60. https://doi.org/10.1016/j.compchemeng.2007.08.004.

[55] Roshandel R, Ahmadi F. Effects of catalyst loading gradient in catalyst layers on performance of polymer electrolyte membrane fuel cells. Renew Energy 2013; 50: 921–31. https://doi.org/10.1016/j.renene.2012.08.040.

[56] Fofana D, Hamelin J, Benard P. Modelling and experimental validation of high-performance low platinum multilayer cathode for polymer electrolyte membrane fuel cells (PEMFCs). Int J Hydrogen Energy 2013; 38:10050–62. https://doi.org/ 10.1016/j.ijhydene.2013.05.175.

[57] Cetinbas FC, Advani SG, Prasad AK. An improved agglomerate model for the PEM catalyst layer with accurate effective surface area calculation based on the sphere- packing approach. J Electrochem Soc 2014; 161: F803–13. https://doi.org/10.1149/2.116406jes.

[58] Secanell M, Karan K, Suleman A, Djilali N. Multi-variable optimization of PEMFC cathodes using an agglomerate model. Electrochim Acta 2007; 52:6318–37. https://doi.org/10.1016/j.electacta.2007.04.028.

[59] Xing L, Liu X, Alaje T, Kumar R, Mamlouk M, Scott K. A two-phase flow and non-isothermal agglomerate model for a proton exchange membrane (PEM) fuel cell. Energy 2014; 73:618–34. https://doi.org/10.1016/j.energy.2014.06.065.

[60] Gurau V, Liu H, Kakaç S. Two-dimensional model for proton exchange membrane fuel cells. AIChE J 1998; 44:2410–22. https://doi.org/10.1002/aic.690441109.

[61] Singh D, Lu DM, Djilali N. A two-dimensional analysis of mass transport in proton exchange membrane fuel cells. Int J Eng Sci 1999; 37:431–52. https://doi.org/ 10.1016/S0020-7225(98)00079-2.

[62] Bernardi DM and Verbrugge MW. A mathematical model of the solid-polymer-electrolyte fuel cell. J Electrochem Soc 1992; 2477:139. https://doi.org/10.1149/1.2221251.

[63] Siegel NP, Ellis MW, Nelson DJ, von Spakovsky MR. Single domain PEMFC model based on agglomerate catalyst geometry. J Power Sources 2003; 115:81–9. https://doi.org/10.1016/S0378-7753 (02) 00622-5.

[64] Sahraoui M, Kharrat C, Halouani K. Two-dimensional modeling of electrochemical and transport phenomena in the porous structures of a PEMFC. Int J Hydrogen Energy 2009; 34:3091–103. https://doi.org/10.1016/j.ijhydene.2008.11.012.

[65] Jung C-Y, Park C-H, Lee Y-M, Kim W-J, Yi S-C. Numerical analysis of catalyst agglomerates and liquid water transport in proton exchange membrane fuel cells. Int J Hydrogen Energy 2010; 35:8433–45. https://doi.org/10.1016/j.ijhydene.2010.05.035.

[66] Ameri M, Oroojie P. Two-dimensional PEM fuel cell modeling at different operation voltages. https://doi.org/10.3384/ecp110571166; 2011. 1166, 1173.

[67] Xing L, Mamlouk M, Scott K. A two-dimensional agglomerate model for a proton exchange membrane fuel cell. Energy. 2013; 61:196–210. https://doi.org/10.1016/j.energy.2013.08.026.

[68] Yan Q, Toghiani H, Causey H. Steady state and dynamic performance of proton exchange membrane fuel cells (PEMFCs) under various operating conditions and load changes. J Power Sources 2006; 161:492–502. https://doi.org/10.1016/j.jpowsour.2006.03.077.

[69] Liu JX, Guo H, Ye F, Ma CF. Two-dimensional analytical model of a proton exchange membrane fuel cell. Energy 2017; 119:299–308. https://doi.org/10.1016/j.energy.2016.12.075.

[70] Tao WQ, Min CH, Liu XL, He YL, Yin BH, Jiang W. Parameter sensitivity examination and discussion of PEM fuel cell simulation model validation Part I. Current status of modeling research and model development. J Power Sources 2006:15.
[71] Hosseini M, Afrouzi HH, Arasteh H, Toghraie D. Energy analysis of a proton exchange membrane fuel cell (PEMFC) with an open-ended anode using agglomerate model: a CFD study. Energy 2019; 116090:188. https://doi.org/ 10.1016/j.energy.2019.116090.

[72] Rao RM, Bhattacharyya D, Rengaswamy R, Choudhury SR. A two-dimensional steady state model including the effect of liquid water for a PEM fuel cell cathode. J Power Sources 2007; 173:375–93. https://doi.org/10.1016/j.jpowsour.2007.04.053.
[73] Gurau V, Liu H, Kakac. Two-dimensional model for proton exchange membrane fuel cells. AIChE J 1998; 44(NO. 11):2410e22.
[74] Qi R and Zhang L-Z. Multi-scale modelling on PEM-based electrolyte dehumidifier: Transient heat and mass transfer in anode catalyst layer with microstructures. 2021; https://doi.org/10.1016/j.ijheatmasstransfer.2021.121720
[75] Das PK, Li X, Liu Z-S. A three-dimensional agglomerate model for the cathode catalyst layer of PEM fuel cells. J Power Sources 2008; 179:186–99. https://doi.org/10.1016/j.jpowsour.2007.12.085.
[76] Das PK, Li X, Liu Z-S. Analytical approach to polymer electrolyte membrane fuel cell performance and optimization. Journal of Electroanalytical Chemistry 2007; 604:72–90. https:// doi.org/10.1016/j.jelechem.2007.02.028.
[77] Obut S, Alper E. Numerical assessment of dependence of polymer electrolyte membrane fuel cell performance on cathode catalyst layer parameters. J Power Sources 2011; 196:1920–31. https://doi.org/10.1016/j.jpowsour.2010.10.030.
[78] Chang WR, Hwang JJ, Weng FB, Chan SH. Effect of clamping pressure on the performance of a PEM fuel cell. Journal Power Sources 2007; 166:149–54. https://doi. org/10.1016/j.jpowsour.2007.01.015.
[79] Xie B, Zhang G, Xuan J, Jiao K. Three-dimensional multi-phase model of PEM fuel cell coupled with improved agglomerate sub-model of catalyst layer. Energy Convers Manag 2019; 112051:199. https://doi.org/10.1016/j.enconman.2019.112051.

[80] Owejan JP, Owejan JE, Gu W. Impact of platinum loading and catalyst layer structure on PEMFC performance. Journal of Electrochem Soc 2013; 160: F824–33. https:// doi.org/10.1149/2.072308jes.

[81] Natarajan D, Nguyen TV. Three dimensional effects of liquid water flooding in the cathode of a PEM fuel cell. J Power Sources 2003; 115:66e80.

[82] Berning T, Lu DM, Djilali N. Three-dimensional computational analysis of transport phenomena in a PEM fuel cell. Journal of Power Sources 2002; 106:284–94. https://doi.org/10.1016/S0378-7753 (01)01057-6.

[83] Berning T, Djilali N. Three-dimensional computational analysis of transport phenomena in a PEM fuel cell—a parametric study. J Power Sources 2003; 124: 440–52. https://doi.org/10.1016/S0378-7753 (03)00816-4.

[84] Wang L. Husar A, Zhou T, Liu H. A parametric study of PEM fuel cell performances. Int J Hydrogen Energy 2003; 28:1263–72. https://doi.org/10.1016/S0360-3199 (02)00284-7.

[85] Meng H, Wang C-Y. Large-scale simulation of polymer electrolyte fuel cells by parallel computing. Chem Eng Sci 2004; 59:3331–43. https://doi.org/10.1016/j.ces.2004.03.039.

[86] Um S, Wang CY. Three-dimensional analysis of transport and electrochemical reactions in polymer electrolyte fuel cells. J Power Sources 2004; 125:40–51. https://doi.org/10.1016/j.jpowsour.2003.07.007.

[87] Ju H, Meng H, Wang C-Y. A single-phase, non-isothermal model for PEM fuel cells. Int J Heat Mass Tran. 2005; 48:1303–15. https://doi.org/10.1016/j.ijheatmasstransfer.2004.10.004.

[88] Sivertsen B, Djilali N. CFD-based modelling of proton exchange membrane fuel cells. J Power Sources 2005; 141:65–78. https://doi.org/10.1016/j.jpowsour.2004.08.054.

[89] Chiang M-S, Chu H-S. Numerical investigation of transport component design effect on a proton exchange membrane fuel cell. J Power Sources 2006; 160:340–52. https://doi.org/10.1016/j.jpowsour.2006.01.086.

[90] Sadiq Al-Baghdadi MAR, Shahad Al-Janabi HAK. Parametric and optimization study of a PEM fuel cell performance using three-dimensional computational fluid dynamics model. Renew Energy 2007; 32:1077–101. https://doi.org/10.1016/j.renene.2006.04.018.

[91] Rismanchi B, Akbari M. Performance prediction of proton exchange membrane fuel cells using a three-dimensional model. Int J Hydrogen Energy 2008; 33: 439–48. https://doi.org/10.1016/j.ijhydene.2007.07.046.

[92] Wang L, Liu H. Performance studies of PEM fuel cells with interdigitated flow fields. J Power Sources 2004:12.

[93] Yuan W, Tang Y, Pan M, Li Z, Tang B. Model prediction of effects of operating parameters on proton exchange membrane fuel cell performance. Renew Energy 2010; 35:656–66. https://doi.org/10.1016/j.renene.2009.08.017.

[94] Rizvandi OB, Yesilyurt S. A pseudo three-dimensional, two-phase, non-isothermal model of proton exchange membrane fuel cell. Electrochim Acta 2019; 302:180–97. https://doi.org/10.1016/j.electacta.2019.02.018.

[95] Nandjou F, Poirot-Crouvezier J-P, Chandesris M, Bultel Y. A pseudo-3D model to investigate heat and water transport in large area PEM fuel cells – Part 1: model development and validation. Int J Hydrogen Energy 2016; 41:15545–61. https://doi.org/10.1016/j.ijhydene.2016.05.117.

[96] Peng Y, Mahyari HM, Moshfegh A, Javadzadegan A, Toghraie D, Shams M, et al. A transient heat and mass transfer CFD simulation for proton exchange membrane fuel cells (PEMFC) with a dead-ended anode channel. Int Commun Heat MassTran 2020; 104638:115. https://doi.org/10.1016/j.icheatmasstransfer.2020.104638.

[97] Berning T, Lu DM, Djilali N. Three-dimensional computational analysis of transport phenomena in a PEM fuel cell. J Power Sources 2002; 106:284e94.

[98] Ge SH, and Yi BL. A mathematical model for PEMFC in different flow mode. J Power Sources 2003; 124:1e11.

[99] Jourdani M, Mounir H, Marhani A. Three-Dimensional PEM fuel cells modeling using COMSOL Multiphysics. 2017. https://doi.org/10.21152/1750-9548.11.4.427.

[100] Abdulla S and Patnaikuni V.S. Performance evaluation of Enhanced Cross flow Split Serpentine Flow Field design for higher active area PEM fuel cells.2020. https://doi.org/10.1016/j.ijhydene.2020.01.199.

[101] You L, Liu H. A two-phase flow and transport model for the cathode of PEM fuel cells. Int J Heat Mass Transfer. 2002; 45:2277–2287.

[102] Cao TF, Mu YT, Ding J, et al. Modeling the temperature distribution and performance of a PEM fuel cell with thermal contact resistance. Int J Heat Mass Transfer. 2015; 87:544–556.

[103] Takalloo PK, Nia ES, Ghazikhani M. Numerical and experimental investigation on effects of inlet humidity and fuel flow rate and oxidant on the performance on polymer fuel cell. Energy Convers Manag. 2016; 114:290–302.

[104] Wang Y, Cho S, Thiedmann R, et al. Stochastic modeling and direct simulation of the diffusion media for polymer electrolyte fuel cells. Int J Heat Mass Transfer. 2010; 53:1128–1138.
[105] Yuan J, Sundén B. On continuum models for heat transfer in micro/nano-scale porous structures relevant for fuel cells. Int J Heat Mass Transfer. 2013; 58:441–456.
[106] Pant LM, Mitra SK, Secanell M. A generalized mathematical model to study gas transport in PEMFC porous media. Int J Heat Mass Transfer. 2013; 58:70–79.
[107] Becker J, Wieser C, Fell S, et al. A multi-scale approach to material modeling of fuel cell diffusion media. Int J Heat Mass Transfer. 2011; 54:1360–1368.
[108] Hwang JJ, Chen PY. Heat/mass transfer in porous electrodes of fuel cells. Int J Heat Mass Transfer. 2006; 49:2315–2327.
[109] Liu Z, Zeng X, Ge Y, et al., multi-objective optimization of operating conditions and channel structure for a proton exchange membrane fuel cell. Int J Heat Mass Transfer. 2017; 111:289–298.
[110] Guobin Z, Kui J. Multi-phase models for water and thermal management of proton exchange membrane fuel cell: a review. J Power Sources. 2018; 391:120–133.
[111] Molaeimanesh GR, Bamdezh MA, Nazemian M. Impact of catalyst layer morphology on the performance of PEM fuel cell cathode via lattice boltzmann simulation. Int J Hydrogen Energy. 2018; 43 (45):20959–20975.
[112] Ghasemi M, Ramiar A, Ranjbar AA, et al., numerical study on thermal analysis and cooling flow fields effect on PEMFC performance. Int J Hydrogen Energy. 2017; 42(38):24319–24337.
[113] Pourrahmani H, Moghimi M, Siavashi M. Thermal management in PEMFCs: the respective effects of porous media in the gas flow channel. Int J Hydrogen Energy. 2019; 44(5):3121–3137.
[114] Zhao J, Li X. Oxygen transport in polymer electrolyte membrane fuel cells based on measured electrode pore structure and mass transport properties. Energy Convers Manag. 2019; 186:570–585.
[115] Jithin M, Siddharth S, Das MK, et al. Simulation of coupled heat and mass transport with reaction in PEM fuel cell cathode using lattice boltzmann method. Therm Sci Eng Prog. 2017; 4:85–96.
[116] Havaej P, Kermani MJ, Abdollahzadeh M, et al. A numerical modeling study on the influence of catalyst loading distribution on the performance of polymer electrolyte membrane fuel cell. Int J Hydrogen Energy. 2018; 43(21):10031–10047.

[117] Xia L, Zhang C, Hu M, et al. Investigation of parameter effects on the performance of high-temperature PEM fuel cell. Int J Hydrogen Energy. 2018; 43(52):23441–23449.
[118] Kone JP, Zhang X, Yan Y, et al. CFD modeling and simulation of PEM fuel cell using OpenFOAM. Energy Procedia. 2018; 145:64–69.
[119] Omeiri D, Laouar A. Three dimensional simulations of transport phenomena in a single-phase isothermal proton exchange membrane fuel cell. Procedia Comput Sci. 2018; 130:736–743. DOI: 10.1016/j.procs.2018.04.128.
[120] Thosar AU, Lele AK. Analytical solutions of an isothermal two-dimensional model of a cathode flow channel in transport limited operational regimes of a proton exchange membrane fuel cell. Chem Eng Sci. 2019; 196:166–175.
[121] Li W, Zhang Q, Wang C, et al. Experimental and numerical analysis of a three-dimensional flow field for PEMFCs. Appl Energy. 2017; 195:278–288.
[122] Ozden E, Tari I. Proton exchange membrane fuel cell degradation: a parametric analysis using computational fluid dynamics. J Power Sources. 2016; 304:64–73.
[123] Sun H, Xie C, Chen H, et al. A numerical study on the effects of temperature and mass transfer in high temperature PEM fuel cells with ab-PBI membrane. Appl Energy. 2015; 160:937–944.
[124] Tai CC, Chen CL, Liu CW. Computer simulation to investigate proton transport and conductivity in perfluorosulfonate ionomeric membrane. Int J Hydrogen Energy. 2017; 42(7):3981–3986.
[125] Amirfazli A, Asghari S, Koosha M. Mathematical modeling and simulation of thermal management in polymer electrolyte membrane fuel cell stacks. J Power Sources. 2014; 268:533–545.
[126] Sarmiento-Carnevali M, Serra M, Batlle C. Distributed parameter model simulation tool for PEM fuel cells. Int J Hydrogen Energy. 2014; 39(8):4044–4052.
[127] Cai Q, Brett DJL, Browning D, et al. A sizing-design methodology for hybrid fuel cell power systems and itsapplication to an unmanned underwater vehicle. J Power Sources. 2010; 195:6559–6569.
[128] Boillot M, Bonnet C, Jatroudakis N, et al. Effect of gas dilution on PEM fuel cell performance and impedance response. Fuel Cells. 2006; 6(1):31–36.

[129] Kahveci EE, Taymaz I. Assessment of single serpentine PEM fuel cell model developed by computational fluid dynamics. Fuel. 2018; 217:51–58.
[130] Yadav MK, Sahu BR, Gupta B, et al. Effect of mass flow rate and temperature on the performance of PEM fuel cell: an experimental study. Int J Curr Eng Technol. 2013; 3(3):950–956.
[131] Faghri A, Guo Z. Challenges and opportunities of thermal management issues related to fuel cell technology and modeling. Int J Heat Mass Transfer. 2005; 48:3891–3920.
[132] Khazaee I, Ghazikhani M. Experimental investigation of operating parameters and control of the performance of a PEM fuel cell. Int J Energy Environ. 2012; 3 (3):461–470.
[133] Young AP, Stumper J, Knights S, Gyenge E, Ionomer Degradation in Polymer Electrolyte Membrane Fuel Cells. Journal of The Electrochemical Society, 157 (3) B425-B436 (2010). DOI: 10.1149/1.3281899.
[134] S. K. Babu., R. Mukundam., C. Wang., D. Langlois., D.A. Cullen., D. Papadias., K.L.More., R.Ahluwalia., J.Waldecker., and R. Borup. (2021). Effect of Catalyst and Catalyst Layer Composition on Catalyst Support Durability. Journal of the Electrochemical Society. 168; 044502. DOI: 10.1149/ 1945-7111/abf21f.
[135] Treybal R. (2017). Mass Transfer Operations. McGraw Hill Education; 3rd edition.
[136] Um S., Wang C.Y., (2004). Three-dimensional analysis of transport and electrochemical reactions in polymer electrolyte fuel cells. Journal of Power Sources. 125; 40-51. doi: 10.1016/j.jpowsour.2003.07.007.
[137] L. Fan, G. Zhang, K. Jiao. (2017). Characteristics of PEMFC operating at high current density with low external humidification. Energy Conversion and Management. 150; 763-774.https://doi.org/10.1016/j.enconman.2017.08.034.
[138] M. Jourdani, H. Mounir, A. Marjani., (2017). Three-Dimensional PEM Fuel Cells Modeling using COMSOL Multiphysics. International Journal of Multiphysics.11; 4.
[139] https://www.christinedemerchant.com/carbon_characteristics_heat_conductivity.html
[140] Yu S.H., Sohn S., Nam J.H., Kim C-J., (2009). Numerical study to examine the performance of multi-pass serpentine flow-fields for cooling plates in polymer electrolyte membrane fuel cells. Journal of Power Sources.194; 697-703. doi: 10.1016/j.jpowsour.2009.06.025.

[141] Limjeerajarus N, Charoen-Amornkitt P. (2015). Effect of different flow field designs and number of channels on performance of a small PEFC. Int J Hydrogen Energy; 40:7144-58. https://doi.org/10.1016/j.ijhydene.2015.04.007.

[142] Alex Martin B, "Experimental and analytical study of an open cathode polymer electrolyte membrane fuel cell, " Electronic Theses and Dissertations, 2015, Paper 1658.

[143] PEM Fuel Cells Fundamentals (Gurbinder Kaur) Chapter 5 - Gas diffusion layer for proton exchange membrane fuel cells.

[144] Oliver T. Holton and Joseph W. Stevenson. The role of platinum in proton exchange membrane fuel cells. Platinum Metals Rev., 2013, 57, (4), 259–271. http://dx.doi.org/10.1595/147106713X671222.

[145] Qinghe Li, Zhiqiang Liu, Yi Sun, Sheng Yang, and Chengwei Deng. A Review on Temperature Control of Proton Exchange Membrane Fuel Cells. Processes 2021, 9, 235. https://doi.org/10.3390/pr9020235.

[146] Chinannai MF, Lee J, Ju H. Study of the characteristics of temperature rise and coolant flow rate control during malfunction of PEM fuel cells.International journal of hydrogen energy 2020. https://doi.org/10.1016/j.ijhydene.2020.04.221.

[147] Y. Wang, C.-Y. Wang, K.S. Chen, Elucidating differences between carbon paper and carbon cloth in polymer electrolyte fuel cells, Electrochim. Acta 52; 12.2007: 3965-3975. https://doi.org/10.1016/j.electacta.2006.11.012.

[148] Ahmad E-K., Thomas J.M., Dan J.L.B., Bruno G.P., (2012). Ex-situ characterisation of gas diffusion layers for proton exchange membrane fuel cells. Journal of Power Sources 218; 393-404.

[149] VanshMalik, Siddharth Srivastava, Mudit K.Bhatnagar, MohitVishnoi. Comparative study and analysis between solid oxide fuel cells (SOFC) and proton exchange membrane (PEM) fuel cell- A review. Materials today: proceedings; 47, (10), 2021, 2270-2275. https://doi.org/10.1016/j.matpr.2021.04.203.

[150] Ya-lu Fu, Biao Zhang, Xun Zhu, Ding-ding Ye, Pang-Chieh Sui, Ned Djilali, Qiang Liao. Pore-scale modeling of mass transport in the air-breathing cathode of membraneless microfluidic fuel cells. International Journal of Heat and Mass Transfer; 188:2022, 122590. https://doi.org/10.1016/j.ijheatmasstransfer.2022.122590.

[151] Hao Hu, Xiaoming Xu, Nan Mei, Chen Li .Numerical study on the influence of waveform channel and related design parameters on the cold start of proton exchange membrane fuel cell. Solid State Ionics. 373; 2021:115794. https://doi.org/10.1016/j.ssi.2021.115794.

[152] Zhang G, Kandlikar SG. A critical review of cooling techniques in proton exchange membrane fuel cell stacks. Int J Hydrogen Energy 2012; 37(3):2412-29.

[153] Suresh PV and Jayanti S. CFD Simulation of Flow Through the Reconstructed Microstructure of Fibrous Gas Diffusion Layer in a Polymer Electrolyte Membrane Fuel Cell. Chemical Product and Process Modeling. 2017; 20170008. DOI: 10.1515/cppm-2017-0008.

[154] Jayakumar A, Sethu SP, Ramos M, Robertson J, Al-Jumaily A., (2015). A technical review on gas diffusion, mechanism and medium of PEM fuel cell. Ionics (Kiel). 2015; 21:1–18. https://doi.org/10.1007/s11581-014-1322-x.

[155] Bock R., Shum A D., Xiao X., Karoliussen H., Seland F., Zenyuk I V., Burheim O S., (2018). Thermal Conductivity and Compaction of GDL-MPL interfacial composite material. Journal of the Electrochemical Society. 165(7), F514-F525. https://doi.org/10.1149/2.0751807jes.

[156] Kunze-Liebhäuser, J., Paschos, O., Pethaiah, S. S., & Stimming, U. (2019). Fuel Cell Comparison to Alternate Technologies. Fuel Cells and Hydrogen Production (Vol. i). https://doi.org/10.1007/978-1-4939-7789-5157.

[157] Hu, H., Xu, X., Mei, N., Li, C. (2021). Numerical study on the influence of waveform channel and related design parameters on the cold start of proton exchange membrane fuel cell. Solid State Ionics, 373, 115794. https://doi.org/10.1016/j.ssi.2021.115794.

RESUME

Name: Ramakant Gadhewal

Gender: Male

Nationality: Indian

Date of Birth:

Email: ramakantgadhewal@gmail.com

Academic Profile:

- Pursuing **Ph.D** from Department of Chemical Engineering at National Institute of Technology, Warangal, Telangana, India, (2022)
- **Senior Research Fellow (SRF) at** DAE-BRNS I.I.T. Mandi (H.P.), India, 2016
- **M.Tech**: Environmental Science and Engineering from Indian Institute of Technology, Dhanbad, Jharkhand, India, (2011)
- **P.G.D** in Petroleum & Natural Gas Flow Measurement & Control Technique from Fluid Control Research Institute (FCRI), Kerala, India, (2007)
- **B.E.** Chemical Engineering from Guru Ghasidas Vishwavidyalaya (Central University), Bilaspur, Chhattisgarh, India, (2005)

Computational Skills:

- **CAD Software**: SOLIDWORKS 2017, SALOME, ANSYS Design Modeler, Blender Meshing **Meshing skills**: HyperMesh, STAR- CCM+, PointWise,
- **CFD Software**: FLUENT, OpenFOAM, STAR-CCM+, COMSOL, ParaView
- **Linux OS**: Ubuntu 16.04:
- **Engineering Software**: MATLAB, EES
- **Language**: C/C++, FORTRAN-77, Python, Bash Scripting